F36 experiment update August 2021

Wavefront Analysis with a Shack-Hartmann Sensor using a modern CMOS imager

THE MOST IMPORTANT IN A NUTSHELL

The lab experiment F36 is an experiment from the field of optics.
The first task (task #1) is to determine the system gain of the used CMOS detector from the statistical properties of photons. This procedure is commonly referred to as the determination/measurement of the so-called photon transfer curve. The result is the system gain in units of electrons per ADU (analog-digital unit). To perform task #1, an adjustable flat-field lamp is used.

As the main part of the experiment, a Shack-Hartmann sensor will be set up on an optical bench and put into operation. Subsequently, the optical quality of an eyeglass lens will be determined. From the determined Shack-Hartmann gradients (task #2a), the wavefront for the correction of a typical eye defect will be calculated. Zernike polynomials are to be fitted to the measured Shack-Hartmann gradients (task #2b for the long report only).

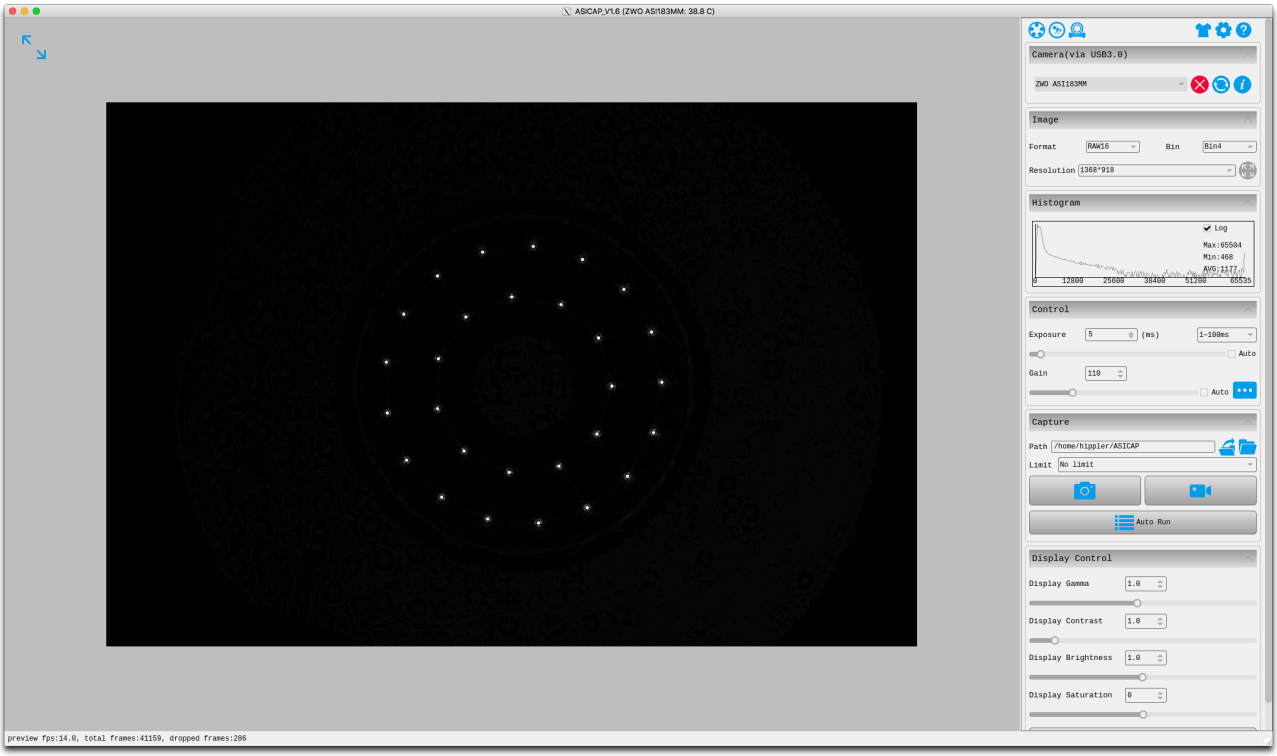

Figure 1: Shack-Hartmann spots recorded with the CMOS imager.

The CMOS camera can be operated with the supplied asicap software.

To run this software just type asicap in the command-line shell. A screenshot of the asicap GUI is shown in fig. 1.

Alternatively, python3 scripts are available, which are based on the INDI software (https://indilib.org). The Instrument Neutral Distributed Interface (INDI) is a protocol designed for astronomical equipment control.

After login with the user name fprakt, three special commands (bash shell aliases) are available: py3, kindi, and sindi. The first one starts the private (virtual environment) python3 environment. The second and third alias stop and start the web-indi interface. To use the web-indi commands you have to be in the python3 environment, i.e. use py3.

After starting the web-indi interface with sindi, please open a web browser and enter http://localhost:8624 as web address, e.g. type firefox http://localhost:8624 & in the command-line shell.

Within the browser GUI you can now start the indi server and connect it to the CMOS camera (see fig. 2).

Once started, python3 scripts can be used to record camera images. Example scripts are available in the directory F36examples.

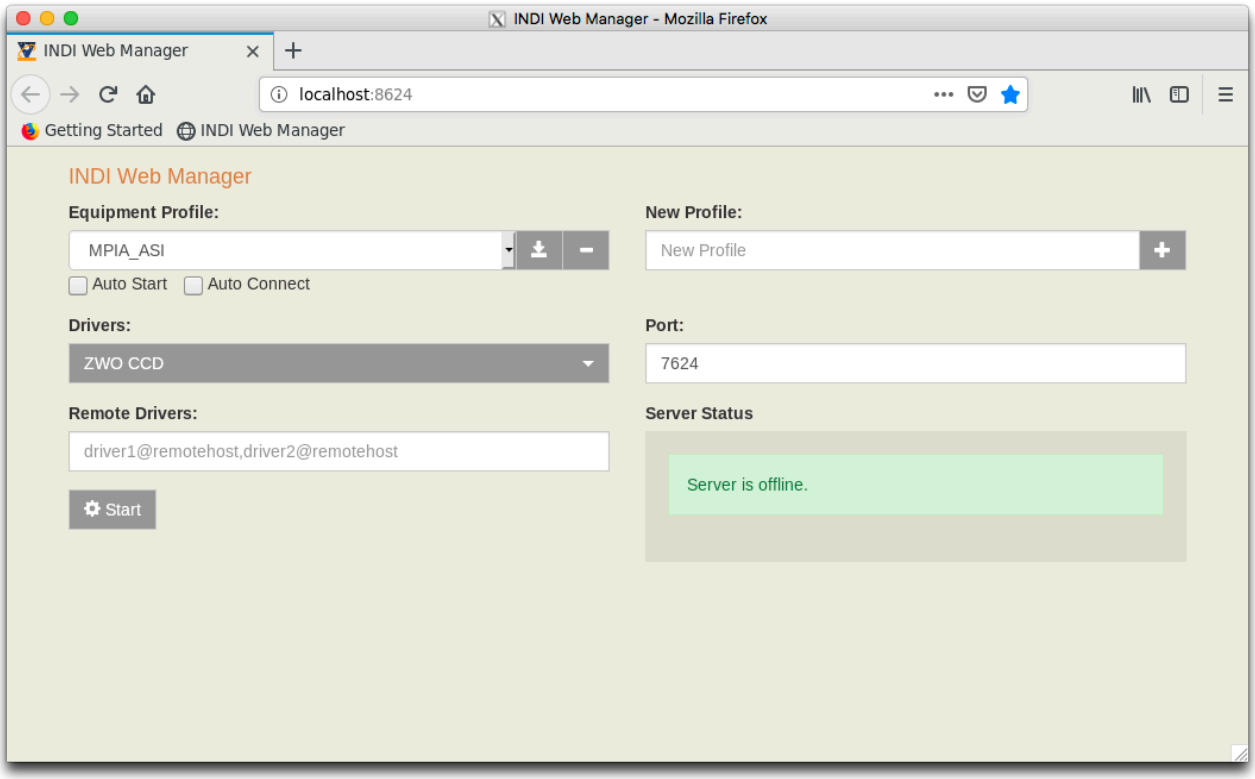

Figure 2: Screenshot of firefox browser connected to the local INDI Web Manager.

End of the F36 experiment in a nutshell.

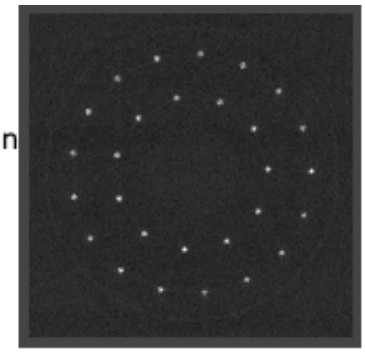

Wavefront analysis with a Shack-Hartmann wavefront sensor
Wellenfrontanalyse mit einem Shack-Hartmann Wellenfrontsensor

Advanced lab course for physics and astronomy students of the University of Heidelberg at MPIA - lab course F36
Fortgeschrittenen-Praktikum für Studierende der Physik und Astronomie der Universität Heidelberg am MPIA - Versuch F36

Download/view course materials (note last update **August 2021**).
Schedule overview and available dates during the semester break.

Further materials

Adaptive Optik für die Astronomie, Augenheilkunde, Hochenergielaser und mehr, von Stefan Hippler, Markus Kasper, Ric Davies und Roberto Ragazzoni. In german language.

Adaptive Optics on Large Telescopes, by Andreas Glindemann, Stefan Hippler, Thomas Berkefeld, and Wolfgang Hackenberg.

Adaptive Optics on Extremely Large Telescopes, Stefan Hippler, 2019

Contacts and directions

Responsible: Dr. Stefan Hippler.

Current tutors.

Directions to MPIA.

Questions

Guess the Zernike function number shown at the right.

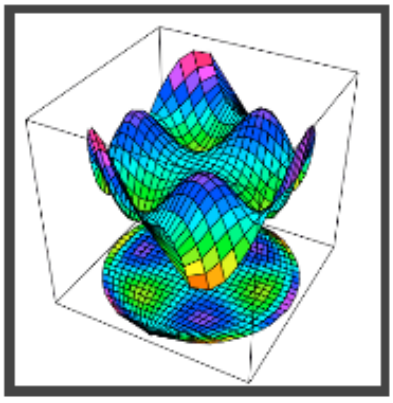

More questions / weitere Fragen.

Miscellaneous

Photos #1, #2. Interactive display of Shack-Hartmann spots for Seidel aberrations. Interactive display of Zernike functions (Java).
Advanced Physics Lab for Physicists University Heidelberg webpage.

https://www.mpia.de/~hippler/fprakt

Wavefront Analysis Experiment F36 – Starter

Version August 26, 2021

1. Login to lnx-d-0010 as user fprakt with password: please ask your supervisor.

2. Open 2 terminal windows, one to control the CMOS camera, and one to inspect and analyse the saved image data.

3. Please follow the notes in document F36 experiment update August 2021.

Figure 1: F36 set-up in lab 034. The F36 control computer lnx-d-0010 (small red stripe on the housing) with its monitor is shown on the right side.

Experiment[1] F36

» Wavefront analysis with a Shack-Hartmann sensor «

of the Advanced Physics Lab for Physicists
of the University of Heidelberg

Dr. Stefan Hippler
Heidelberg, April 2021

Introduction

Astronomical observations from the ground are limited in their quality by the turbulence of the Earth's atmosphere. Regardless of the size of the telescope, the real resolving power corresponds to that of a 10-20 cm telescope. In the past, the construction of ever larger telescopes mainly led to the collection of more light and thus to looking deeper into the universe. The spatial/angular resolving power, on the other hand, could only be significantly improved by so-called adaptive optics (AO). At the beginning of the 21st century, it can be stated that optical and infrared astronomy can hardly progress from the ground without AO. All next generation extremely large telescopes like the ELT, GMT, and TMT have adaptive optics so to say built-in.
The idea of AO was developed in the 1950s by Horace Babcock. However, the topic "The possibility of compensating atmospheric seeing" was technically not feasible at that time. In the 1970s and 1980s the American military worked on AO systems for observing satellites and focusing high-energy laser beams. In the early 1990s, the world's first civilian telescope, the 3.6-m telescope of the ESO on La Silla in Chile, was equipped with adaptive optics. Currently, every large telescope in the 8-10 m class has an AO.
A central component of each AO system is the so-called wavefront sensor, which can be used to measure the disturbances caused by the Earth's atmosphere on the flat optical waves arriving from space. In astronomy, the Shack-Hartmann sensor is one of the most commonly used sensor in AO systems, along with the Curvature Sensor and Pyramid wavefront sensor.

Overview of the tasks

With the help of a Shack-Hartmann wavefront sensor optical aberrations are to be determined. On an optical bench, a wavefront sensor according to the Shack-Hartmann principle is to be built up from individual optical components - these are a monochromatic light source with optical fibre, a collimator, a micro-lens mask, a relay lens, and a CMOS camera. The gain (gain = number of electrons per digital unit in the CMOS detector image) of the CMOS detector shall be determined. Finally some elementary phase errors of the wavefront (defocus, coma, astigmatism, tilt) shall be generated, measured and calculated.

List of tasks

Part 1: determination of the system gain of a CMOS detector; optical set-up and data reduction including linear plot of signal vs variance. For the **short report**, please add a chapter that describes the readout scheme of the used CMOS imager. Additionally, for the **long report**, a detailed error discussion has to be included.

---

[1] This document was mostly created with the help of the free translator DeepL and the German version of the script

Part 2: wavefront measurement of an astigmatic lens; optical set-up and data reduction including plot of Shack-Hartmann gradients. For the **short report**, please add a chapter about possible errors in determination of the Shack-Hartmann gradients. Additionally, for the long report, a detailed wavefront reconstruction has to be included, e.g. a fit of Zernike polynomials to the measured Shack-Hartmann gradients.

Things to know (things you should know and familiar with …)

1. Optical aberrations, imaging errors, point spread function (PSF), diffraction limited imaging.
2. Methods for the determination of wavefronts (wavefront phases).
3. Basics of the Hartmann test, extension by Shack.
4. Phase reconstruction with a Shack-Hartmann sensor.
5. Modal decomposition of optical aberrations using Zernike polynomials.
6. Application in astronomy: what are the most relevant properties of the optically turbulent atmosphere in order to design an astronomical AO system.

References

1. Stefan Hippler und Andrei Tokovinin: *Adaptive Optik Online Tutorial in German and English:* https://www.mpia.de/homes/hippler/AOonline/ao_online.html http://www.ctio.noao.edu/~atokovin/tutorial/index.html

2. John. W. Hardy: *Adaptive Optics for Astronomical Telescopes*, Oxford University Press, 1998

3. F. Roddier: *Adaptive Optics in Astronomy*, Cambridge University Press, 1999

4. Ben C. Platt, Roland Shack: *History and Principal of Shack-Hartmann Wavefront Sensing*, 2nd Intgernational Congress of Wavefront Sensing and Aberration-free Refractive Correction, Monerey, Journal of Refractive Surgery 17, 2001 (attached to the full F36 manual)

5. M.E. Kasper: *Optimierung einer adaptiven Optik und ihre Anwendung in der ortsaufgelösten Spektroskopie von T Tauri*, Dissertation Universität Heidelberg, 2000, https://www.MPIA.de/ALFA/TEAM/MEK/Download/diss.pdf

6. Glindemann, S. Hippler, T. Berkefeld, W. Hackenberg: *Adaptive Optics on Large Telescopes*, Experimental Astronomy 10, 2000, https://link.springer.com/article/10.1023%2FA%3A1008116831367

7. Stefan Hippler: *Adaptive Optics for Extremely Large Telescopes*, Journal of Astronomical Instrumentation, Vol. 08, No. 02, 1950001, 2019, https://www.worldscientific.com/doi/full/10.1142/S2251171719500016

Support

Responsible: Dr. Stefan Hippler
As a rule, the experiment is supervised by doctoral students at MPIA or the State Observatory (ZAH-LSW).

Further documents and scripts are available on the F36 webpages:
https://www.mpia.de/homes/hippler/fprakt

Script for experiment F36 (part I)

»Wavefront analysis with a Shack-Hartmann sensor«

of the Advanced Physics Lab for Physicists
of the University of Heidelberg

Measurement of the gain of a CMOS camera

Dr. Stefan Hippler

Heidelberg, August 2021

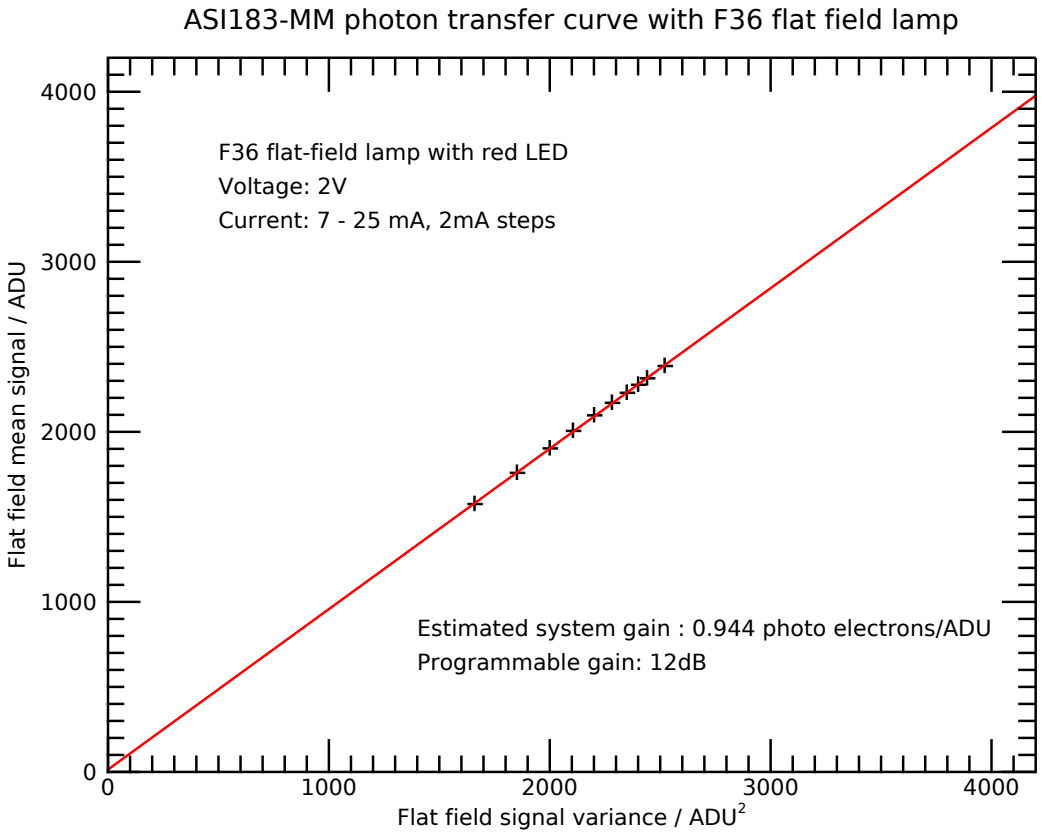

Contents

1 The CMOS camera of the Shack-Hartmann wavefront sensor

The Shack-Hartmann wavefront sensor to be set-up in the experiment has a central optical element a micro-lens mask (so called lenslet array).

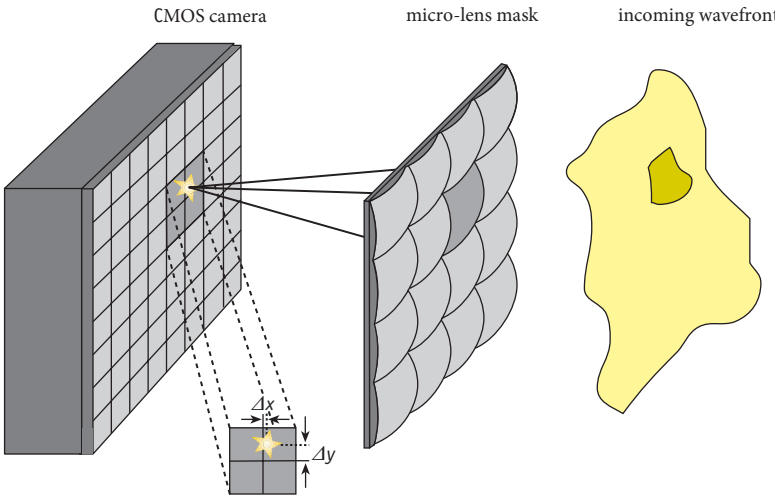

Fig.1: Measuring principle of the Shack-Hartmann wavefront sensor. The incoming wavefront, which is disturbed by the atmosphere, is divided into smaller areas by a micro-lens mask. Each micro-lens generates an image with its center shifted from a reference position according to the inclination of the wavefront over the micro-lens area.

Figure 1: A non-planar wavefront falling on a micro-lens mask causes a shift of the light spots on the CMOS detector. Credit: Sterne & Weltraum October 2004.

To record the spots that each lens of the lens array creates in its focal plane (see figure 1) we use a CMOS camera of the type ZWO ASI183 MM. This camera comes with an IMX183CLK CMOS detector from Sony with 5640 x 3694 active pixels. Each camera pixel has a size of 2.4 μm x 2.4 μm.

Further data and specifications of the camera and the detector built into it are given in the documents in the appendix.

Please note that there are many similarities but also differences between CCD (charge coupled device) and CMOS (complementary metal oxide semiconductor) detectors. However, the method for determining the system gain of those detectors is the same for both.

2 Features of the CMOS camera

2.1 Introduction and explanation of terms

A CMOS camera is usually a camera which is equipped with a CMOS detector. A CMOS camera or CMOS sensor is an image detector with active pixels, i.e. each pixel is a photon detector with active amplifier. The generic category of such sensors is often referred to as Active Pixel Sensor (APS). The Sony chip used in our experiment is manufactured in the Complementary metal-oxide-semiconductor technology, hence the name CMOS.

A CMOS camera is distinguished from other optical detectors, such as Eye, film or photo-multiplier, by two characteristics, in particular:

Excellent sensitivity The quantum efficiency (QE) is around 50% - for some wavelengths even up to 90% - and is thus one order of magnitude larger than in the human eye or in film, where the QE is only a few percent.

Linearity between measurement signal and quantity of light collected Unlike photographic plates, which only cover a comparatively small range of linear response, the CMOS detector behaves linearly over a range starting from zero noise levels to saturation levels. This makes a CMOS camera particularly suitable for photometric applications.

For the development of the CCD, Willard Boyle and George E. Smith received the 2009 Nobel Prize in Physics.

The CMOS detector is further characterized by the following values, **of which some shall be determined during the internship**.

quantum efficiency, QE determines the sensitivity of the detector to incident electromagnetic radiation. The quantum efficiency is defined as the number of processes that an absorbed photon creates on average. The QE is determined by the energy of the photon and thus from the wavelength of light or the electromagnetic radiation. The QE indicates the probability with which the inner photoelectric effect releases a photo-electron, which can be measured.

The quantum yield of the Sony IMX183 CMOS detector can be determined from the following figure.

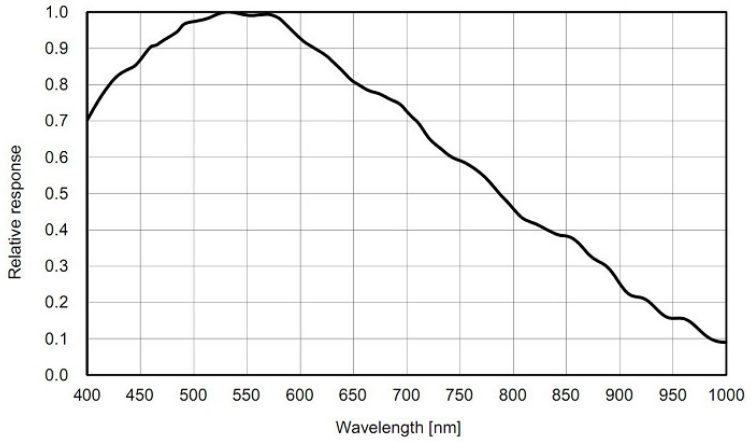

Figure 2: Relative QE of the IMX183 detector. The maximum value is ≈ 0.84. Source: ZWO ASI183 manual.

bias level is the average pixel value that the camera electronics reads out at shortest exposure time and without flux on the detector; this is ideally a dark image with an exposure time of 0 s. Since it is an electronic offset, this value is usually subtracted from the measured data.

readout noise consists of fluctuations of the signal, which are caused by the electronics during readout, i.e. analog to digital conversion.The readout noise can be expressed as standard deviation in analog to digital units (ADU) per pixel or electrons per pixel. For the conversion from ADU to electrons the camera amplification factor is needed (see below).

dark current consists of electrons which are generated by the temperature of the detector (i.e. thermal noise, Fermi distribution, Boltzmann distribution), i.e. electrons that move from the valence band to the conduction band and thus add to the measured signal.

flat-field is an image where the pixels are all equally illuminated with either monochromatic light or white light. The flag-field image shows the differences in sensitivity of the individual pixels. Especially in astronomy, with its very low-contrast objects, the flat-field image often shows additional features. These can be caused by dust on optical elements in front of the detector or on the detector itself.

camera system gain describes the relationship between the photo-electrons measured and the signal in ADU, that you get on the computer. The system gain is not identical to the programmable gain amplifier (PGA) of the CMOS camera. This programmable gain is used to match the maximum amplitude of the CMOS signal to the full voltage range of the analog to digital converter (ADC).

signal-to-noise ratio SNR characterizes the quality of an image.

The last two values are particularly important. The camera's system gain represents the connection between a pure number resulting from the ADC and the physically interesting number of photo-electrons. In addition, if you know the quantum efficiency of the detector and the wavelength at which it was observed, the number of photons absorbed by a pixel is known. The signal-to-noise ratio, SNR, should be kept as high as possible, because it reduces the measurement noise of the Shack-Hartmann sensor.

3 Characteristics of the CMOS camera to be determined

3.1 CMOS camera system gain

The camera gain, also known as system gain, indicates how many electrons one ADU represents. For example, if the camera has a 12-bit analog-to-digital converter (ADC), the system gain is set such that the analog range of a pixel (full well capacity, full well depth in electrons) is covered digitally to the fullest extent possible.

Example: If the readout noise of the CMOS detector is around 3 electrons/pixel and a 12-bit ADC is available, the system gain is set to 1–3 electrons per ADU to avoid too fine noise sampling. Thus the analog measuring range per pixel is between 4000 and 12000 electrons.

To determine the system gain the photon transfer curve is used. The photon transfer curve represents the measured detector signal vs. the variance of the signal for different illumination levels. Flat-field effects are usually corrected. The system gain is the slope of the linear part of the curve. More about system gain - especially the mathematical and physical basics - can be found in the article by Michael Newberry in the appendix.

Many measurements made with the CMOS camera should be done in the dark because the camera reacts very sensitively to all light levels. As light sources a diode laser and a special LED flat-field lamp are available. The supervisor will tell you how these are controlled and used.

Warning: do not look directly into the laser light with your eyes.

3.2 Quick guide to photon transfer curve recording

Place the flat-field lamp directly in front of the CMOS camera. Operate the flat-field lamp with a red (or yellow or green) LED at a voltage of about 2 V and max. 25 mA. Select the exposure time such that the detector is not saturated (< 65000 ADU) under any circumstances. With the above settings and **without pixel binning**, the exposure time is approx. 60ms (note that this can vary a lot depending on the used LED). It is recommended to use a pixel binning of 4. In this case please make a short investigation what the effect of pixel binning is on images taken with the same set-up. Set the programmable gain to 12dB (note that this corresponds to the number 120 in the asicap GUI). Take two pictures at this light intensity. Then set a lower light intensity (2 mA less) and take two pictures again with the same exposure time. Repeat this as often as necessary and with appropriate light levels that in the photon transfer curve one can later see the saturation effect as well as the linearity of the Poisson noise and the effect of the system noise.

Designate each pair of shots with the same light intensity as image A and B.

Consider beforehand whether a dark current and offset/bias correction should be taken into account.

Now take each picture - or an area that looks evenly illuminated - and calculate the average signal S from each picture there. Correct for differences between the pairs of images in the mean signal, by multiplying

image B with the ratio $S(A)/S(B)$. Subtract B from A. Which effects fall out here? What is the variance of the resulting image? Create the photon transfer curve, i.e. plot the determined mean values against the variance. Calculate the system gain in electrons per ADU. Explain the non-linear parts of the curve, if available.

4 Software to operate the CMOS camera

The camera can be operated with different programs. The program of the camera manufacturer is called `asicap`. It is started from the command line. A graphical user interface gives you easy control over the CMOS camera.

Another method to readout the camera is based on the open source software INDI (https://indilib.org). In combination with a python interface, python3 scripts can be used to read the camera. Example scripts can be found in the *F36examples* directory.

Script[1] for experiment F36 (part II)

» Wavefront analysis with a Shack-Hartmann sensor «

of the Advanced Physics Lab for Physicists
of the University of Heidelberg

Set-up of a Shack-Hartmann wavefront sensor. Measurement of simple optical aberrations. Wavefront reconstruction using Zernike functions.

Heidelberg, April 2021

Dr. Stefan Hippler, Dr. Wolfgang Brandner, Prof. Dr. Thomas Henning

Introduction and motivation: The influence of the atmosphere on the image quality of a telescope

If you look at the starry sky with the naked eye, the first thing you notice is the sparkling of the stars, the scintillation. This effect is caused by atmospheric turbulence, which ensures that cold and warm layers of air are constantly mixed. The temperature dependence of the refractive index of air leads to an optical inhomogeneity, albeit very weak. This causes the atmosphere to break up into many randomly distributed turbulence cells with diameters of 10 to 20 cm, which act like weak lenses. Due to their light-collecting effect, they cause intensity fluctuations over areas of a few centimetres near the ground. When observing with a telescope several meters in diameter, the turbulence is less noticeable as a result of intensity fluctuations than as a disturbance due to the granular structure (speckles) of the images of individual stars. Since many of these turbulence cells are captured simultaneously by the telescope aperture, the image fragments into many randomly distributed single images, the speckles. The number of speckles corresponds approximately to the number of turbulence cells over the telescope aperture, and the size of the star image made by those speckles is about one arcsecond under good atmospheric conditions.

The shape and position of the speckle patterns change depending on how fast the turbulence passes over the telescope aperture. In general, the exposure time must be less than 1/10 second to see a »sharp« speckle image. If several exposures with short exposure times are strung together like in a film, the temporal change of the turbulences can be seen as a teeming movement of the individual speckles and as the star image moving sideways left and right as well as up and down. At exposure times of a few seconds, both effects contribute to the blurring of the speckle image, and a uniformly illuminated image »disc« is created, whose width FWHM (Full Width Half Maximum) is called »seeing« in astronomical terminology. Depending on the observation site and meteorological conditions, the seeing is 0.5 to 2.5 arcseconds.

The definition of the resolving power of a telescope can be used to establish a relationship between the seeing and the size of the turbulence cells. For the diffraction limited resolving power α (in radians) of a telescope with diameter D at the wavelength λ the following holds:

$$\alpha = \lambda / D$$

In the visible, at a wavelength of 500 nm, a 3.5 m telescope, for example, has a theoretical resolving power of 1.43E-7 rad or about 0.03 arcseconds. This means that two point-like stars that are 0.03 arcseconds apart can just about be resolved as single stars. The seeing limited angular resolution

[1] This document was mostly created with the help of the free translator DeepL and the German version of the script

of 1 arcsecond, corresponds to the diffraction limited angular resolution of a telescope with a diameter of 10 cm at 500 nm; this is just about the relevant size of the turbulence cells in the atmosphere.

In the context of describing turbulence as a statistical phenomenon, instead of turbulence cells, one speaks of the *coherence length* r_0, which is also called the *Fried parameter* after an American physicist. This parameter denotes the diameter of the wavefront over which the wavefront disturbance, i.e. the deviation from the plane wave, is negligible (standard deviation < 1 rad). Therefore, the vivid picture of turbulence cells with the diameter r_0, within which the light can propagate undisturbed, is absolutely correct. The greater the coherence length becomes, i.e. the more r_0 approaches the telescope diameter D, the closer the resolving power comes to the diffraction limit α. Note that r_0 is wavelength dependant.

The wavefront can be imagined as a mountain and valley landscape created by the turbulence, whose typical height difference is in the range of 3-6 μm, regardless of the wavelength. Relevant for the image quality is the ratio of the deviation of the wavefront from the plane wave to the observation wavelength; for example, a numerical value of 3-6 μm at a wavelength of 10 μm is a relatively insignificant value of 0.3 to 0.6 wavelengths units. On the other side, in the visible at a wavelength of 0.5 μm, the deviation is 6 - 12 wavelengths units, a much stronger effect. A formula for the coherence length r_0 describes this effect quantitatively.
The Fried parameter depends on the wavelength as $r_0 \sim \lambda^{6/5}$. This means that the range over which wavefront distortions are negligible increases with wavelength. A r_0 of typically 10 cm at 0.5 μm is then equivalent to an r_0 of 360 cm at 10 μm!

Accordingly, the speckle patterns at 0.5 μm and at 10 μm look completely different under identical atmospheric conditions (see Figure 1). On a 3.5 m telescope, there is a cloud of $(D/r_0)^2 \approx 1000$ speckles in the visible at 0.5 μm, which are in a wild swarming movement and whose envelope has a FWHM of 1 arcsecond. Each speckle has the size of the diffraction disk of the telescope, i.e. 0.036 arcseconds. In the infrared at 10 μm there is only one speckle with a FWHM of 0.6 arcseconds, the size of the diffraction disk at 10 μm, because r_0 is larger than the telescope diameter D. The only effect of the turbulence is that the image moves relatively slowly back and forth, and up and down.

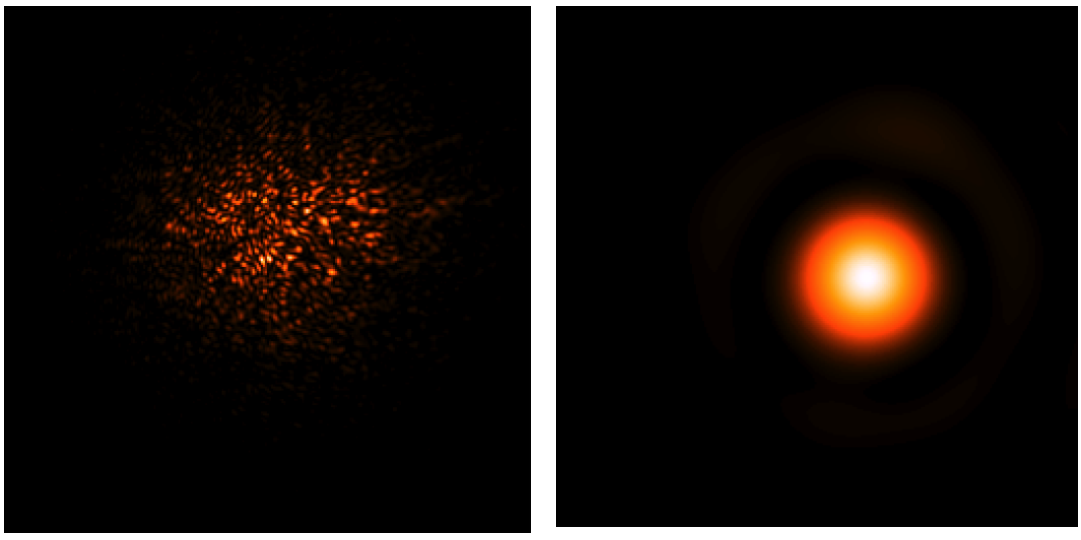

Figure 1: Star images simulated at λ=0.5 µm (left) and λ=10 µm (right) for identical atmospheric conditions on a 3.5 m telescope. While at λ=0.5 µm there is a speckle pattern with about 1000 single speckles and an envelope of one arcsecond, at λ=10 µm one can already see the diffraction disk with only slightly deformed diffraction rings.

This numerical example already gives an impression of how different the requirements for adaptive optics (AO) are at λ=0.5 μm and at λ=10 μm. While at 10 μm it is sufficient to freeze the image motion to produce a diffraction-limited image, at 0.5 μm all 1000 speckles must be combined into a single diffraction disk with the help of a deformable mirror to achieve the physically possible imaging performance of the telescope. Due to the technical requirements of an adaptive optics system in the visible spectral range, the observation is usually limited to the near infrared range at 1-2 μm, where the smaller number of 50-200 speckles also reduces the requirements.

Measure and correct wavefronts: The components of an adaptive optics system

Adaptive optics typically includes a tip-tilt mirror and a deformable mirror, which continuously compensate for atmospheric wavefront deformations. The compensated deformations are measured with a wavefront sensor. A real-time control system (real-time computer) converts the signals from the wavefront sensor into control signals for the correcting element. A part of the light is decoupled and sent to the observation, which is usually an infrared camera.

Figure 2 shows a scheme of an adaptive optics system often used in astronomy and its components. There are a number of methods to measure wavefront disturbances. The most common in astronomy are the curvature wavefront sensing method, the Shack-Hartmann wavefront analysis and the analysis with pyramid wavefront sensors.

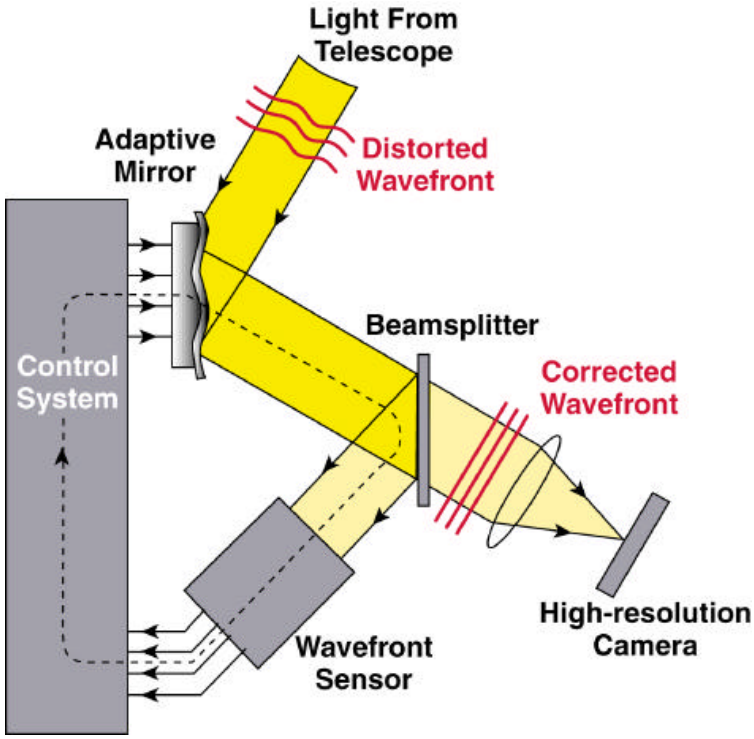

Figure 2: Schematic representation of an adaptive optics system in astronomy (image credit: Jerry Nelson)

Wavefront measurements with the Shack-Hartmann sensor

The Shack-Hartmann measurement principle will now be briefly explained. The aperture of a telescope is divided into sub-apertures by a micro-lens mask. In each sub-aperture the relative position of a star – and thus the local wavefront tilt – is measured. This allows the deformation of the light wave to be determined.

An array of micro-lenses divides the aperture of the light beam to be measured into sub-apertures. Each micro-lens creates a focal point at a distance of the focal length of the lens. A local tilt of the wavefront within the sub-aperture causes a shift of the focal point from position x_1 to x_2 by the amount Δx. In a first approximation this displacement is exactly proportional to the tilt of the wavefront across the micro-lens.
Fig. 3 shows this displacement. A Shack-Hartmann wavefront sensor detects this displacement (gradient) and thus concludes the amount of tilt of the wavefront across the micro-lens. After appropriate detection of a two-dimensional matrix of focal point shifts, the complete wavefront can be reconstructed. Possible errors in the reconstruction of the wavefront tilt across a micro-lens arise from the uncertainties in the determination of the focal point shift. The determination of the shift is discussed in more detail below.

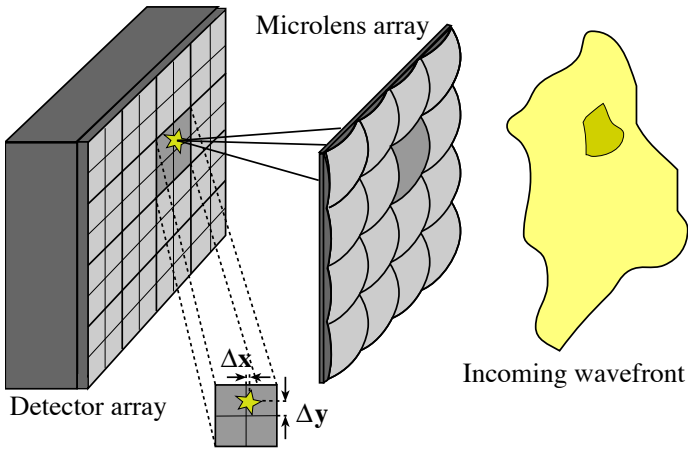

Figure 3: Schematic representation of the Shack-Hartmann measuring principle

Applying simplifications of paraxial optics, the following one-dimensional relationship can be defined:

$$\Delta x = f\theta$$

Here θ is the tilt angle in radians of the wavefront over a micro-lens, and Δx is the shift of the focal point on the detector (gradient). In the practical experiment, a so-called relay optic (an Apo-Rodagon-N f/2.8 objective with 50 mm focal length) is located between the lens array with the focal length f = 45 mm, which images the focal plane of the micro-lenses onto the CMOS detector and additionally causes an optical magnification / reduction M. The micro-lens array used in the practical course has a diameter of 5 mm and has 28 micro-lenses arranged in two rings (keystone arrangement). The horizontal distance between two adjacent micro-lenses is therefore approximately equal to the diameter of a sub-aperture (approximately 755 microns). One pixel of the CMOS detector has a size of 2.4μm x 2.4μm. With this information the magnification M of the relay optics can be determined.

For the optical path length difference OPD applies:

$$OPD = \theta \cdot d_{sub}$$

In a one-dimensional case, this results in a simple relationship between the measured variable of the Shack-Hartmann sensor Δx and the gradient of the wavefront over the sub-aperture or the optical path length difference OPD in units of the used wavelength λ:

$$\Delta x = f \cdot M \cdot \lambda \cdot OPD / d_{sub}$$

The Shack-Hartmann sensor uses several lenses to reconstruct the wavefront. These lenses are usually placed equidistantly in a two-dimensional lateral arrangement in the optical beam path. This lens array creates a matrix of focal points. The displacement of each focal point is a measure of the tilt of the wavefront within the associated lens, and from the measurements of the individual displacements, the entire wavefront can be reconstructed using an approximation algorithm.

To detect the images of a Shack-Hartmann lens array, a CCD or CMOS camera is usually used. For the detection of the image of each individual sub-aperture, a square section of at least 2 x 2 pixels is required. To avoid optical crosstalk between the sub-apertures, a safety distance of at least one pixel width is inserted between the sub-apertures. According to this principle, some Shack-Hartmann systems work with 3 x 3 pixels per sub-aperture. A common alternative is 4 x 4 to 8 x 8 pixels per sub-aperture (for example at Starfire Optical Range or the adaptive optics system ALFA at the Calar Alto observatory).
The larger the number of pixels, the higher the dynamic range of the wavefront sensor (i.e. stronger tilts can be measured) and the objects may have a larger extension. However, this is associated with more noise, because the number of pixels to be read out and the readout time increase. To increase the readout speed and reduce the readout noise, the 8 x 8 pixels can be "binned" to so-called super-pixels, which creates/simulates a smaller number of (larger) pixels.

From Shack-Hartmann gradients to wavefronts

As can be seen from the previous description, for each sub-aperture *i*, the mean path length differences can be determined by

$$\frac{d_{sub}\Delta x_i}{fM\lambda} = OPD_{x_i} \text{ und } \frac{d_{sub}\Delta y_i}{fM\lambda} = OPD_{y_i}$$

With this information, it is possible to reconstruct the wavefront across the entire micro-lens mask.

In general, a wavefront can be represented as a sum of higher order polynomials with respective coefficients. A representation frequently used in optics was developed by Frits Zernike in 1934 to describe the quality of concave mirrors. The Zernike polynomials have orthogonality and represent typical forms of optical aberrations such as $Z_{3,5}$ = astigmatism, Z_4 = defocus, or $Z_{7,8}$ = coma (see Table 1). The Zernike representation of a wavefront *W(x,y)* is the sum of the products of these polynomials $Z_n(x,y)$ with the respective coefficients C_n

$$W(x,y) = \sum_0^\infty C_n Z_n(x,y)$$

$Z_j(x,y)$	n, m	$Z_n^m(x,y)$	Name
$Z_0(x,y)$	0, 0	1	piston
$Z_1(x,y)$	1, -1	y	tilt
$Z_2(x,y)$	1, 1	x	tip
$Z_3(x,y)$	2, -2	2xy	astigmatism
$Z_4(x,y)$	2, 0	$2x^2+2y^2-1$	defocus
$Z_5(x,y)$	2, 2	x^2-y^2	astigmatism
$Z_6(x,y)$	3, -3	$3x^2y-y^3$	trefoil
$Z_7(x,y)$	3, -1	$3x^2y+3y^3-2y$	coma
$Z_8(x,y)$	3, 1	$3x^3+3xy^2-2x$	coma
$Z_9(x,y)$	3, 3	x^3-3xy^2	trefoil
$Z_{10}(x,y)$	4, -4	$4x^3y-4xy^3$	secondary astigmatism
$Z_{11}(x,y)$	4, -2	$8x^3y+8xy^3-6xy$	secondary astigmatism
$Z_{12}(x,y)$	4, 0	$6x^4+12x^2y^2+6y^4-6x^2-6y^2+1$	spherical aberration

Table 1: Some Zernike polynomials in Cartesian coordinates (Jim Schwiegerling 2016, https://wp.optics.arizona.edu/visualopticslab/wp-content/uploads/sites/52/2016/08/Zernike-Notes-15Jan2016.pdf)

Experiment execution and measurements

The following set-ups, adjustments, and measurements will be carried out during the course:

1. Assembly of a Shack-Hartmann sensor from the individual components provided on an optical bench
2. Recording of Shack-Hartmann images (Shack-Hartmann Spot images) taken with a laser light source. See exemplary figure 4
3. Find the best focus as a function of the position of the relay optics on the optical bench
4. Measurement of Shack-Hartmann gradients for various optical aberrations
5. Determination of a wavefront from the measured data (Shack-Hartmann gradient image)

For the long report additionally:

6. Reconstruction of wavefronts using the Zernike polynomials
7. Alternatively to item 6: local reconstruction of the wavefronts using a suitable 2D surface fit

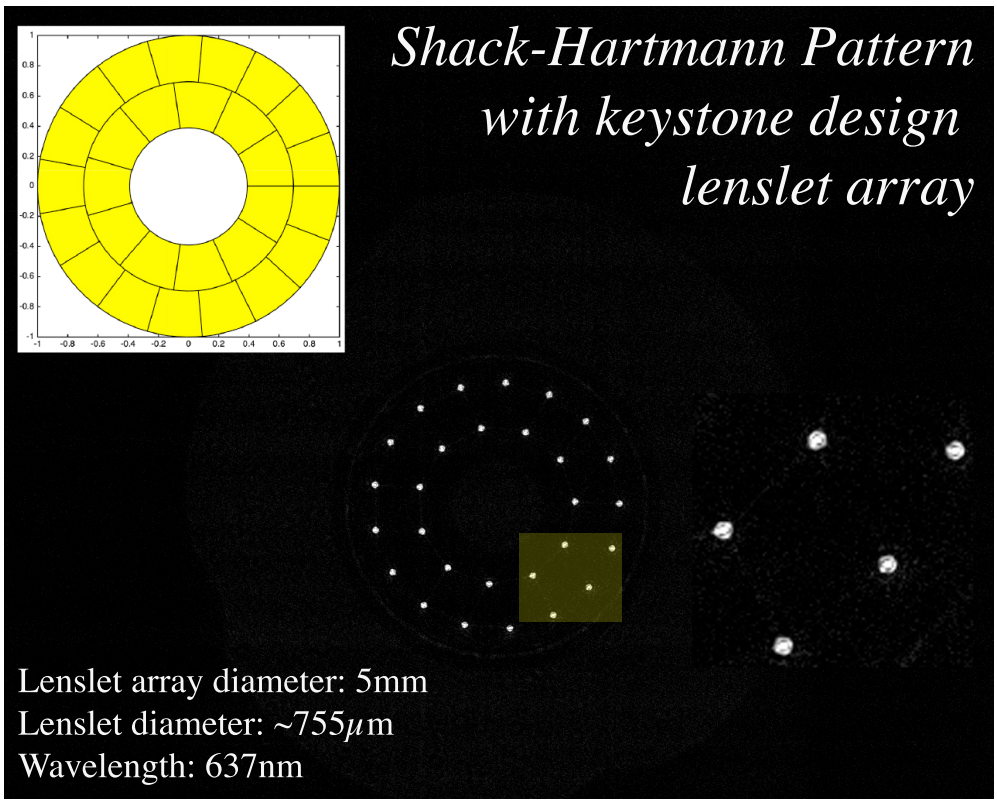

Figure 4: Example of a Shack-Hartmann spots image; the yellowish square is magnified on the lower right

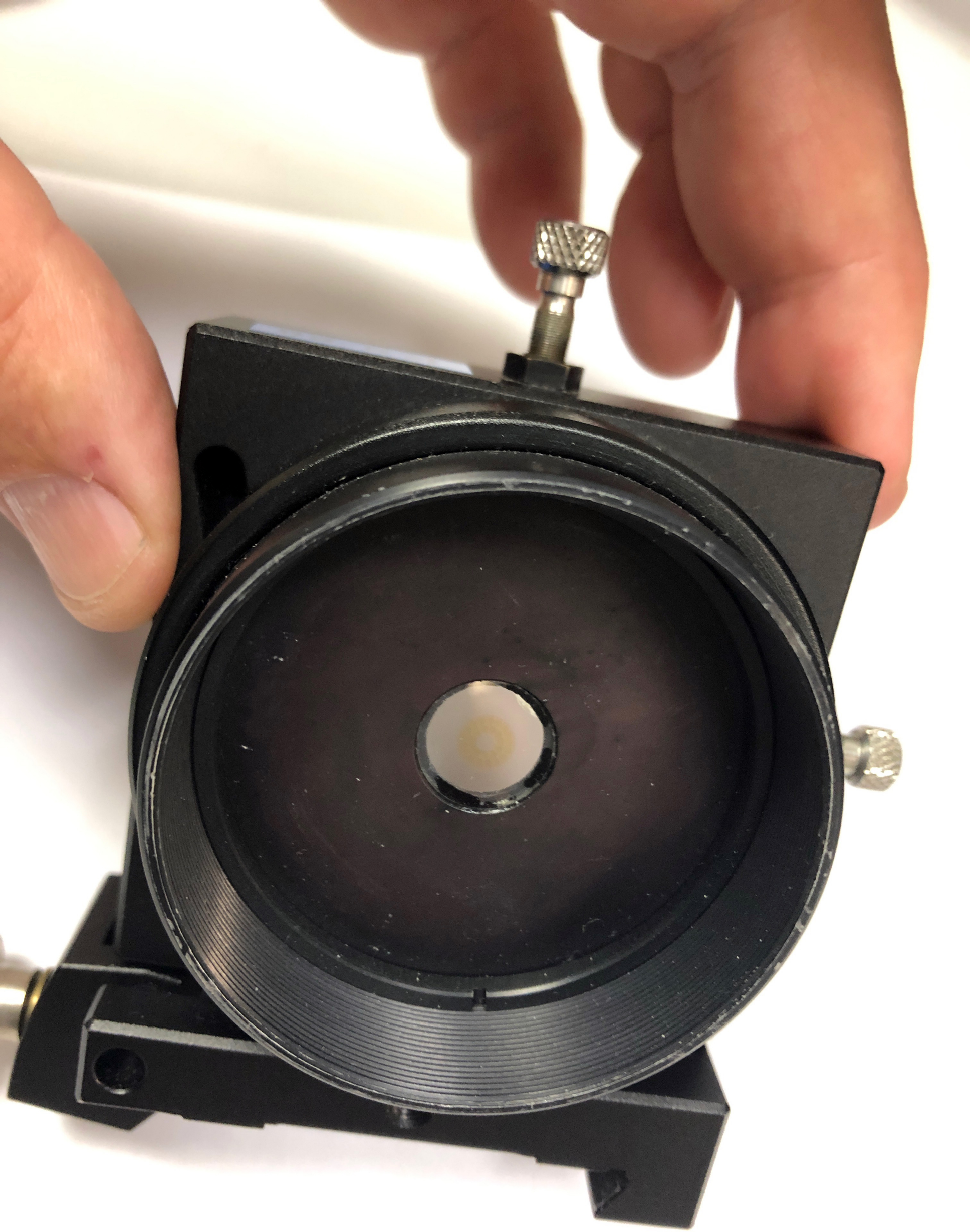

Keystone design lenslet mask with mount

Advanced Lab Course F36

Procedure to determine Shack-Hartmann Spot locations with python3, Astropy, and Photutils

Dr. Stefan Hippler, April 2021

This note describes the example python3 script to find Shack-Hartmann spot positions in the observed image.

Photutils documentation is available online at https://photutils.readthedocs.io/en/stable/

1) Login as user fprakt on lnx-d-0010

2) To work with the available example scripts, please copy the entire directory "/home/fprakt/F36examples" into your work directory. Then change your active directory to "YOUR_WORK_DIRECTORY/F36examples/F36_task2_scripts". Activate the virtual python3 environment with the shell command py3. Now you can (modify and) run the sample scripts, e.g. **python find_centroids_and_save_results.py** and **python display_gradients.py**. The figures shown below will appear on your screen together with further information about the image and the spot locations.

More details about the used centroid finder is available at:

https://photutils.readthedocs.io/en/stable/api/photutils.detection.DAOStarFinder.html

```
(py3_sandbox) fprakt@lnx-d-0010:~/F36examples/F36_task2_scripts$ python find_centroids_and_save_results.py

---> find_centroids_and_save_results.py, Stefan Hippler, April 30, 2021

---> Reading file: ./F36_reference_SHspots.fits

---> Converting data to 12-bit ...

---> Image mean: 641.79, median: 637, sigma: 38.00, find threshold: 826.98

---> Found 28 spots in image

 id xcentroid ycentroid sharpness   roundness1    roundness2  npix sky  peak    flux      mag
--- --------- --------- ---------- ------------ ------------ ---- --- ----- --------- ----------
  1 720.08177 123.56882 0.40409799  0.066538861    0.11010063   25   0 26539 22.274935 -3.3695411
  2 840.70366 135.55985 0.40461666  0.042710531   -0.17590734   25   0 31072 27.646855 -3.6041143
  3 603.10322 156.59675 0.40233711  -0.16080653  -0.051547893   25   0 27492 25.130628 -3.5005083
  4 949.00752 189.92142 0.39294921    0.1073487  -0.058660734   25   0 32818  29.31153 -3.6675962
  5 505.99478 229.36473 0.40082322  -0.14501806    0.10780836   25   0 25091 22.162555 -3.3640495
  6 794.07869 246.01619 0.38996849  0.008280169     -0.101368   25   0 29004 25.584968 -3.5199622
  7 675.53902 254.62887 0.39632474  -0.16485004  -0.097554931   25   0 25837 22.066673 -3.3593422
  8 1030.7577 280.07905 0.40523574    0.1623673   0.088867701   25   0 32573 28.340654 -3.6310247
  9 898.51423 303.13899  0.4097248    0.0589246   -0.0644976   25   0 29496 25.003196 -3.4949888
 10 580.18701  326.1156 0.40224904   -0.1387513  -0.050410844   25   0 24957 21.188419 -3.3152464
 11 441.38839 332.29406 0.40300285 -0.021678245   0.008996143   25   0 23100 20.351147 -3.2714722
 12 1073.7061 393.45148 0.41088001  0.062060971    0.14720669   25   0 37349 32.487645 -3.7792956
 13 955.95771 407.67658 0.41127137   0.15497422   0.083781814   25   0 33442 28.762587 -3.6470699
 14 538.08435 438.15048 0.40290838  0.053038455    0.11949138   25   0 27050 23.581338 -3.4314211
 15   419.683 451.41954 0.39565889  0.036503705    0.21885485   25   0 27229 24.670916 -3.4804632
 16 1073.4942 514.86387 0.40581228  0.044588678    0.13120185   25   0 36340 32.375875 -3.7755538
 17 947.27311 526.69672 0.40844275 -0.015956012  -0.038167057   25   0 29158 24.305328 -3.4642537
 18 563.53326 554.19912 0.39332839  0.038569455 0.00054343175   25   0 27300 23.611906 -3.4328276
 19 441.37902 570.90864 0.40518349  0.093080566   0.030859327   25   0 27267 23.808355 -3.4418235
 20 876.03191 622.07348  0.4161373 -0.069642993  -0.018393197   25   0 30247 25.691481 -3.5244728
 21 1029.2172 627.79225 0.40875433 -0.092141743   0.060193028   25   0 34694 30.580925 -3.7136265
 22 647.99955 638.44133 0.39192978   0.13957713  -0.017149401   25   0 28428 24.747785 -3.4838408
 23 764.22195 663.72146 0.38797877  0.048178882   0.014037077   25   0 27750 22.672896 -3.3887675
 24 504.43542 674.00359 0.40493888  0.043182619  -0.033521309   25   0 27630 24.159709 -3.4577293
 25 947.06627  716.7948 0.38761677  -0.28431296  -0.095125962   25   0 33015 29.575883 -3.6773443
 26 600.90194 747.30487 0.40697688   0.10182691  -0.056714402   25   0 30479 27.446505 -3.5962176
 27 838.21599 770.45629 0.40054669  -0.14464381   0.059495501   25   0 26279  22.79199 -3.3944556
 28 717.75088 781.20952  0.4035489 -0.039909521  -0.057787147   25   0 30385 26.762283 -3.5688079

 ---> Output graphics created in file: Figure_1_reference.pdf

 ---> Results saved in file: spots_saved_reference.npy

---> press Enter to quit and close all windows.
```

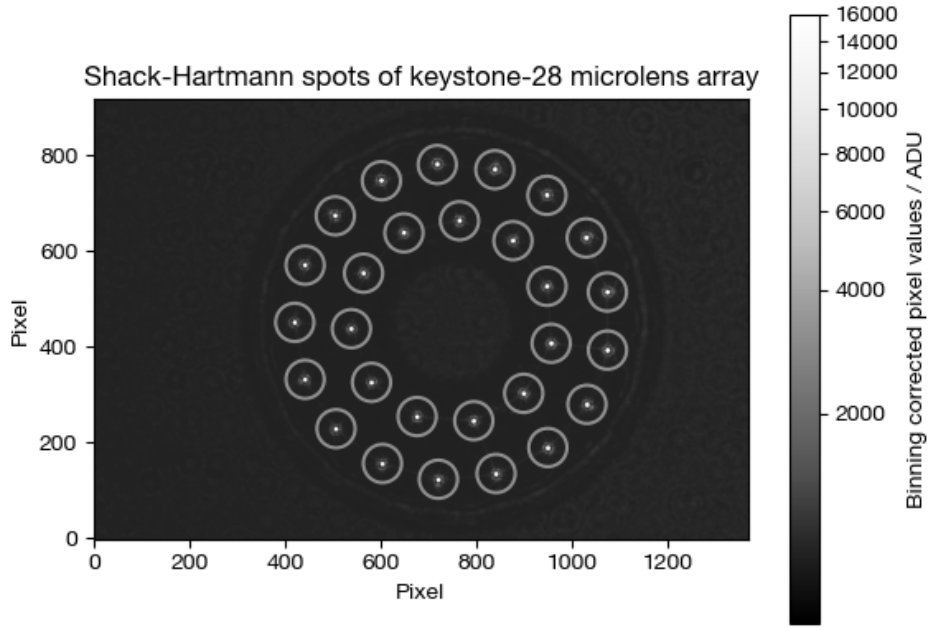

Figure 1: graphical output after running the script find_centroids_and_save_results.py

3) Modify the script find_centroids_and_save_results.py such that it analyses different input files. Note the search parameters used in DAOStarFinder.

4) Once you have analyzed the reference image as well as the “eyeglass” image use the script **display_gradients.py** to visually inspect the Shack-Hartmann gradient image. The output should look similar to figure 2 below.

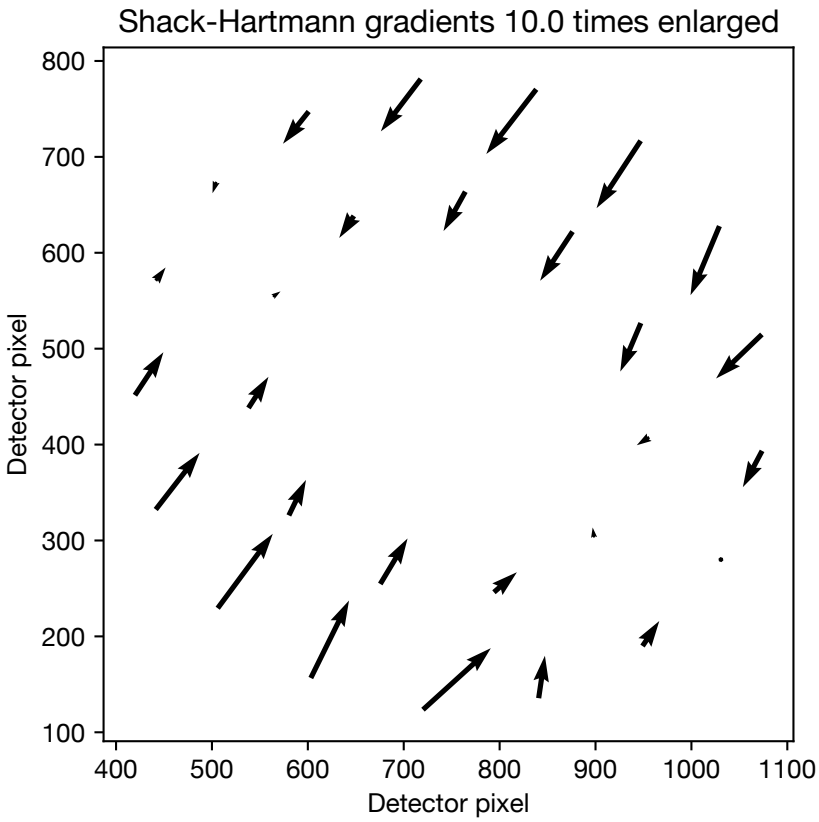

Figure 2: Plot of Shack-Hartmann gradients.

```
#
# find_centroids_and_save_results.py, Stefan Hippler, April 30, 2021
#
# the KS28 lenslet array should produce 28 nice diffraction limited spots...
#
# template taken from: https://photutils.readthedocs.io/en/stable/detection.html
#

import numpy as np

from astropy.stats import sigma_clipped_stats
from astropy.visualization import SqrtStretch
from astropy.visualization import AsinhStretch
from astropy.visualization.mpl_normalize import ImageNormalize

from photutils import datasets
from photutils import DAOStarFinder
from photutils import CircularAperture
from photutils import find_peaks

import matplotlib.pyplot as plt
from matplotlib.backends.backend_pdf import PdfPages

import astropy.io.fits as fits

print("")
print("---> find_centroids_and_save_results.py, Stefan Hippler, April 30, 2021")
print("")

#
# select used binning
# conv_factor for pixel binning = 1
# conv_factor = 1./16.
# conv_factor for pixel binning = 2
# conv_factor = 1./4.
# conv_factor for pixel binning = 4
conv_factor = 1.

#
# read SH data with and without (=reference) aberrations ...
# change file names here
#

# select input files here ...

F36_SHspots_file = './F36_reference_SHspots.fits'
pdf_out_file     = 'Figure_1_reference.pdf'
pdf_out          = PdfPages(pdf_out_file)
data_out         = 'spots_saved_reference.npy'
ptitle           = 'Shack-Hartmann spots of keystone-28 microlens array \n Reference positions'

# F36_SHspots_file = './F36_eyeglass_SHspots.fits'
# pdf_out_file     = 'Figure_2_eyeglass.pdf'
# pdf_out          = PdfPages(pdf_out_file)
# data_out         = 'spots_saved_eyeglass.npy'
# ptitle           = 'Shack-Hartmann spots of keystone-28 microlens array \n Eyeglass positions'

#
# daophot parameters used for finding/centroiding spots
# adapt to set-up
#

spots_FWHM          = 4.0
thresh_fact         = 5.0
roundlow            = -0.5
roundhi             = 0.5
spot_circles_radius = 40.
spot_circles_color  = 'white'
nbrightest          = 28

#
# turn on interactive mode
#
```

```
plt.ion()
print('---> Reading file: %s' % F36_SHspots_file)
F36_fits = fits.open(F36_SHspots_file)
F36_data = F36_fits[0].data

print("")
print('---> Converting data to 12-bit ...')
F36_data = F36_data * conv_factor

mean, median, std = sigma_clipped_stats(F36_data, sigma=3.0)
find_threshold = median + (thresh_fact * std)

print("")
print("---> Image mean: %.2f, median: %d, sigma: %.2f, find threshold: %.2f" % (mean,

median, std, find_threshold))
daofind = DAOStarFinder(fwhm=spots_FWHM, threshold=find_threshold, brightest=nbrightest)
sources = daofind(F36_data - median)

#
# filter out sources depending on roundness1...
#
round_mask = ((sources['roundness1'] > roundlow) & (sources['roundness1'] < roundhi) &
(sources['roundness2'] > roundlow) & (sources['roundness2'] < roundhi))
sources_filtered = sources[round_mask]

for col in sources_filtered.colnames:
    sources_filtered[col].info.format = '%.8g' # for consistent table output
spots_found = len(sources_filtered)

print("")
print("---> Found %d spots in image" % spots_found)
print("")
print(sources_filtered)

positions = (sources_filtered['xcentroid'], sources_filtered['ycentroid'])
apertures = CircularAperture(positions, r=spot_circles_radius)
norm1     = ImageNormalize(stretch=SqrtStretch())
norm2     = ImageNormalize(stretch=AsinhStretch())
vvmin     = 35.
vvmax     = 16000.

plt.imshow(F36_data, cmap='Greys_r', origin='lower', norm=norm2, vmin=vvmin, vmax=vvmax,
 aspect='equal')

apertures.plot(color=spot_circles_color, lw=1.5, alpha=0.5)
cbar = plt.colorbar()
cbar.set_label('Binning corrected pixel values / ADU')

plt.title(ptitle)
plt.xlabel('Pixel')
plt.ylabel('Pixel')

#plt.xlim((400., 1000))
#plt.ylim((200., 800))
pdf_out.savefig()
pdf_out.close()

print("")
print(" ---> Output graphics created in file: " + pdf_out_file)

# the end
#

np.save(data_out, sources_filtered)

print("")
print(" ---> Results saved in file: " + data_out)

print("")
input("---> press Enter to quit and close all windows.\n")
```

History and Principles of Shack-Hartmann Wavefront Sensing

Ben C. Platt, PhD; Roland Shack, PhD

The Shack-Hartmann wavefront sensor was developed out of a need to solve a problem. The problem was posed, in the late 1960s, to the Optical Sciences Center (OSC) at the University of Arizona by the US Air Force. They wanted to improve the images of satellites taken from earth. The earth's atmosphere limits the image quality and exposure time of stars and satellites taken with telescopes over 5 inches in diameter at low altitudes and 10 to 12 inches in diameter at high altitudes.

Dr. Aden Mienel was director of the OSC at that time. He came up with the idea of enhancing images of satellites by measuring the Optical Transfer Function (OTF) of the atmosphere and dividing the OTF of the image by the OTF of the atmosphere. The trick was to measure the OTF of the atmosphere at the same time the image was taken and to control the exposure time so as to capture a snapshot of the atmospheric aberrations rather than to average over time. The measured wavefront error in the atmosphere should not change more than $\lambda/10$ over the exposure time. The exposure time for a low earth orbit satellite imaged from a mountaintop was determined to be about 1/60 second.

Mienel was an astronomer and had used the standard Hartmann test (Fig 1), where large wooden or cardboard panels were placed over the aperture of a large telescope. The panels had an array of holes that would allow pencils of rays from stars to be traced through the telescope system. A photographic plate was placed inside and outside of focus, with a sufficient separation, so the pencil of rays would be separated from each other. Each hole in the panel would produce its own blurry image of the star. By taking two images a known distance apart and measuring the centroid of the images, one can trace the rays through the focal plane. Hartmann used these ray traces to calculate figures of merit for large telescopes. The data can also be used to make ray intercept curves (H'- tan U').

When Mienel could not cover the aperture while taking an image of the satellite, he came up with the idea of inserting a beam splitter in collimated space behind the eyepiece and placing a plate with holes in it at the image of the pupil. Each hole would pass a pencil of rays to a vidicon tube (this was before CCD arrays and image intensifiers). The two major problems with this idea were the weak intensity of the projected ray spots and the accuracy of measuring the centroid of the blurry pencil of rays. A tradestudy was performed using the diameter of the holes, distance between the hole plate and the vidicon, and angular measurement accuracy as variables.

Dr. Roland Shack was involved in the study and soon came to the conclusion that the only workable solution was to replace the holes in the plate with lenses. For the first time, the idea of measuring the wavefront error, at the same time an image is taken of the satellite or star, seemed to be feasible. The configuration for the first Shack-Hartmann sensor

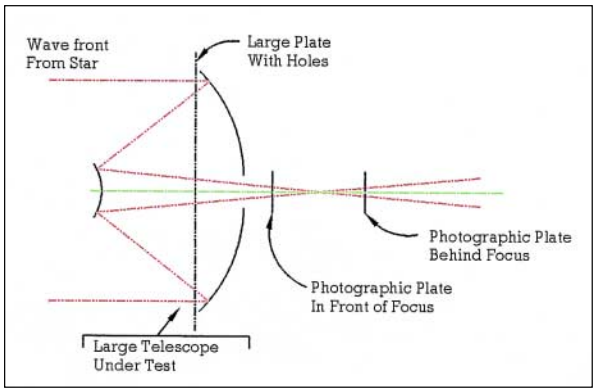

Figure 1. Optical schematic for an early Hartmann test.

From Calhoun Vision, Inc, Pasadena, CA (Platt) and the Optical Science Center, University of Arizona, Tucson, AZ (Shack).

Presented at the 2nd International Congress of Wavefront Sensing and Aberration-free Refractive Correction, in Monterey, CA, on February 9-10, 2001.

Correspondence: Ben C. Platt, PhD, Calhoun Vision, Inc, 2555 E. Colorado Blvd, Suite 400, Pasadena, CA 91107. Tel: 626.395.5215; Fax: 626.685.2003; E-mail: BPlatt@calhounvision.com

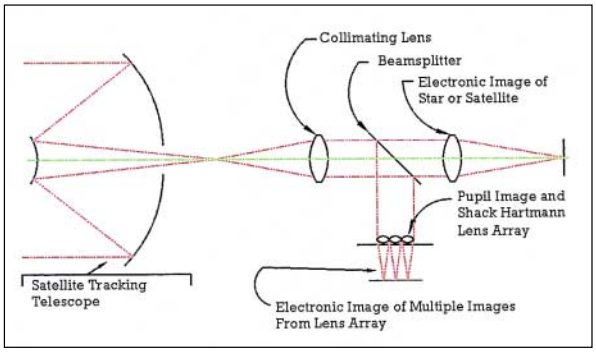

Figure 2. Optical schematic for first Shack-Hartmann sensor.

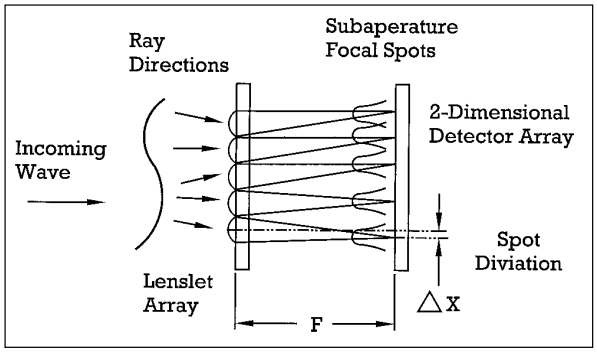

Figure 3. Illustration shows how displacements of focused spots from the lens array represent wavefront tilt.

is illustrated in Figure 2. The concept of measuring displacements of the spots formed by the lens array to calculate wavefront tilt is shown in Figure 3. Just as the derivative of the wavefront optical path difference (OPD) map produces wavefront slopes, the integration of wavefront slopes produces wavefront OPD maps.

At that time, Dr. Ben Platt was a Research Associate working in the Infrared Materials Lab at the Optical Sciences Center, University of Arizona, for Professor William Wolfe. Part of his time was spent helping Shack set up the Optical Testing Lab. He was given the task of purchasing an array of lenses to test the concept. The semiconductor industry was making arrays of lenses with short focal lengths, ~6 mm, and relatively large diameters, ~6 mm. Lenses with a diameter of 1 mm and focal length of 100 to 150 mm were required for the design. No one could be found to fabricate these lenses. Platt tried about six different methods before developing one that worked. Some of the methods tried included the following:

1. The end of a steel rod was polished with the correct radius and pressed into a metal surface in a square pattern. Epoxy and thermal plastic were used to mold a lens array from the indented surface.
2. Commercial arrays of short focal length lenses were used with index fluids where the difference in refractive index produced the desired focal length.
3. Lenticular lens screens from 3-D pictures were tried with index fluids.
4. Thin cylindrical lenses were fabricated and assembled into crossed arrays.
5. Thick cylindrical lenses were purchased, ground into thin slabs, and glued together.

Dr. Platt finally decided that the only way to produce the long focal lengths with 1 mm center-to-center distances was to use crossed cylindrical lenses and to polish the surfaces into a very flat low expansion optical flat. The optical shop at the university was asked to polish the lenses. They had no experience in this area and could not provide support. Platt designed and fabricated a polishing machine that used a cylindrical rod of nylon about 120 mm in diameter and about 150 mm long with a hole through the center so it could slide back and forth on a steel rod. The rod was supported from two arms that allowed the nylon roll to be lowered and raised over the optical blank. The optical blank was attached to a tilt table and translating stage for aligning the optical blank to the nylon polishing tool and for translating the blank to the next cylindrical lens location. A mechanical counter was attached to the steel arm supporting the rod to keep track of the number of polishing strokes at each lens location. After several weeks of trial and error, the system was ready to be transfered to an optician. The optician started with a 150-mm-diameter, 25-mm-thick disk of Cervet, polished to λ/20. Fifty grooves were polished across the center of the blank. Two square pieces were cut from the grooved area.

Platt made a mount for compression, molding a 1-mm-thick square plate of optical grade thermal plastic (Plexiglass) between the two Cervet squares. Many attempts were made to produce good quality lens arrays. Two sets of molds were also broken in the process. Each heating and cooling cycle in the molding process took several hours. So, Platt decided to work all day and most of the night in his wife's kitchen. His wife's electric knife sharpener was used to trim the Plexiglass plates. Her apron and oven mittens were also used to remove the molds from the oven. After a few weeks, the process was perfected and good quality lens arrays were being produced. For at least the next 5 years, all lens arrays used in Shack-Hartmann wavefront sensors were

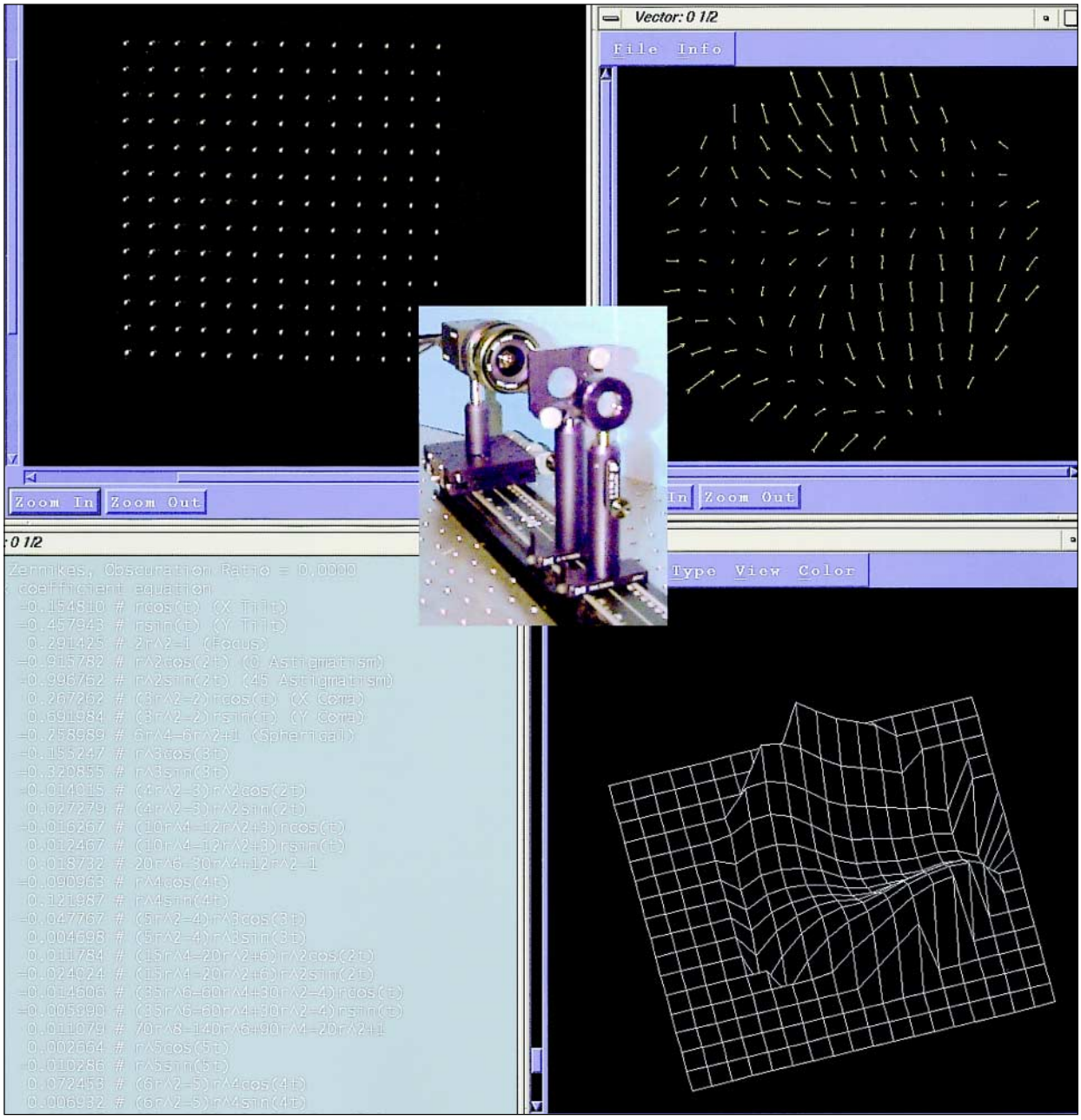

Figure 4. Recent image from Adaptive Optics Associates (AOA) shows the optical set-up used to test the first Shack-Hartmann sensor. **Upper left)** Array of images formed by the lens array from a single wavefront. **Upper right)** Graphical representation of the wavefront tilt vectors. **Lower left)** Zernike polynomial terms fit to the measured data. **Lower right)** 3-D plot of the measured wavefront.

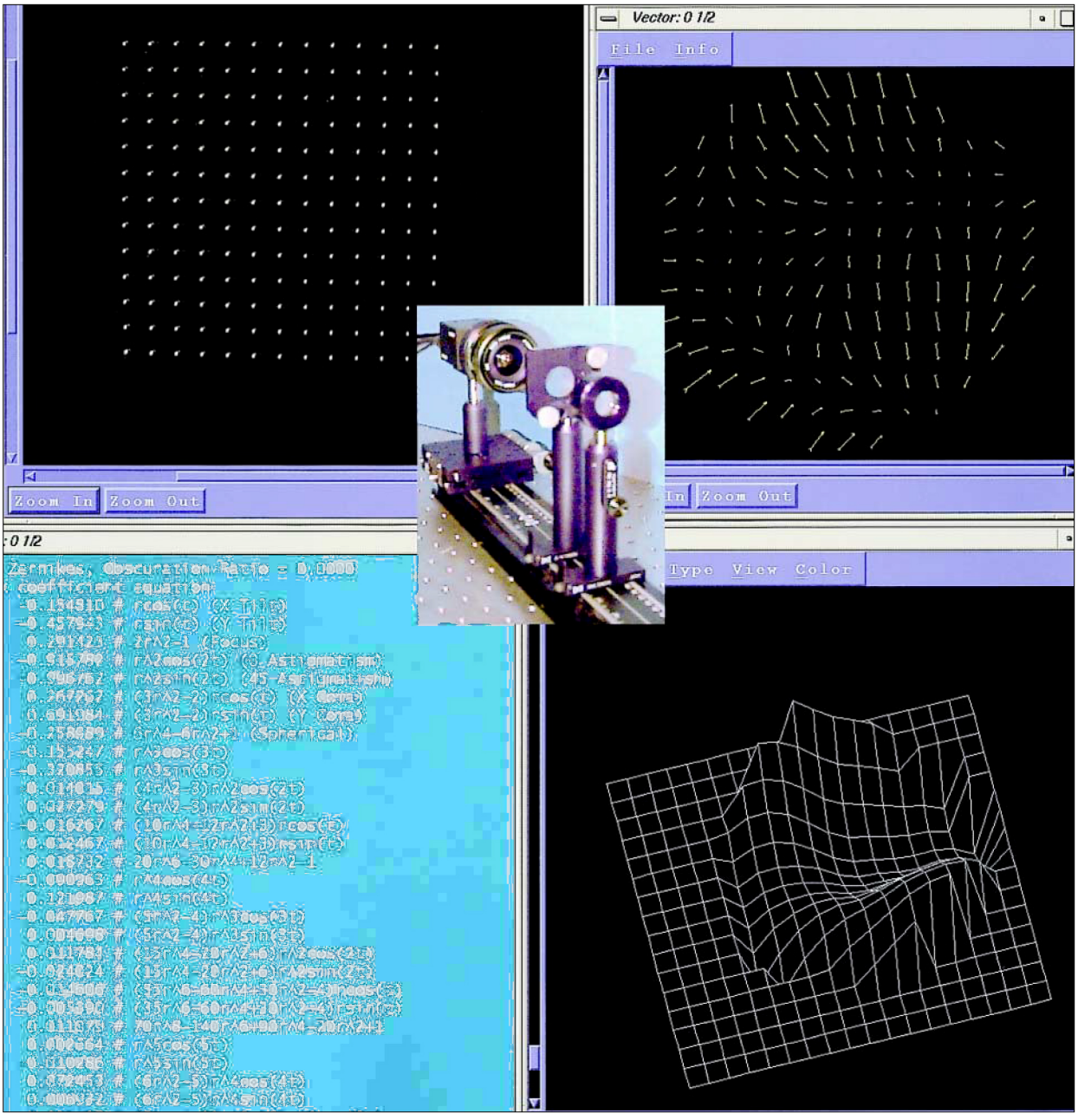

Figure 4. Recent image from Adaptive Optics Associates (AOA) shows the optical set-up used to test the first Shack-Hartmann sensor. **Upper left)** Array of images formed by the lens array from a single wavefront. **Upper right)** Graphical representation of the wavefront tilt vectors. **Lower left)** Zernike polynomial terms fit to the measured data. **Lower right)** 3-D plot of the measured wavefront.

made by Platt in his wife's kitchen. Because of the high risk of breaking the molds, Platt took the molds with him when he left the university and made lens arrays, on request, for Shack, without charge. Several students used the arrays in their research projects.

The Air Force project was simulated in the laboratory. The target was a scaled photograph of a satellite using the correct angle of illumination. A 35-mm reflex camera was used to record the focused spots from the lens array. The focused patterns were low-resolution images of the satellite and not just spots. All images were identical so this did not affect the ability to determine centroids of the images. Atmospheric aberrations were simulated with a static phase plate. A pinhole was later used for a test target. Figure 4, provided by Adaptive Optics Associates (AOA), shows a recent set-up that illustrates the set-up used in 1971. The upper left image shows what the spot pattern looked like. The upper right image shows a vector representation of the wavefront tilts. The length of the arrow illustrates the magnitude of the tilt and the direction of the arrow illustrates the angle of the tilt. The lower left image is the Zernike polynomial fit to the calculated wavefront. The lower right image is the plot of the measured wavefront.

A reference set of spots were taken with a calibrated wavefront in order to make accurate measurements. This was necessary because of residual aberrations in the optical set-up. To account for shrinkage in the film, both sets of dots were taken on the same slide of film. We tried two methods of generating the reference set of spots: one method offset the reference set of spots by introducing a tilt in the wavefront, and the other method used color film and no offset. This method requires optics with an acceptable amount of chromatic aberrations. The color separation method was easiest to work with. Two methods of separating the two sets of spots were used. One method used a measuring microscope and color filters over the eyepiece. The other method used color filters over a slide projector and a Vernier caliper. Both methods produced results that were repeatable to $\lambda/50$. Accuracy was determined by a tolerance analysis and by comparing the measured results of an aberration plate, using the Shack-Hartmann sensor, to the measured results of a commercial Zygo interferometer. Accuracy was determined to be at least $\lambda/20$.

An article was written on the Lenticular Hartmann Screen in March 1971 for the Optical Sciences Center newsletter at the University of Arizona. In that same year, Platt presented a paper on the Shack-Hartmann Sensor at an OSA meeting in San Diego, CA. An attempt was made to file for a patent through the University of Arizona. The application was never filed.

A complete system was designed, fabricated, and delivered to the Air Force in the early 1970s to be used on the satellite-tracking telescope at Cloudcroft, NM. The system was never installed and the facility was later decommissioned.

Shack also worked with astronomers in Europe. He gave lens arrays to any astronomer that wanted one. During that time, Ray Wilson was responsible for the alignment and testing of all large telescopes at the European Southern Observatories (ESO). Wilson fabricated a wavefront sensor with one of the lens arrays he received from Shack and tested all the large telescopes at the ESO. He discovered that they were all misaligned and that he could properly align them with the data from the new tester. Wilson published a paper on this work in April of 1984. He sent a copy of the paper to Shack, thanking him for introducing this new tester to him and coining the name "Shack-Hartmann sensor." In 1974, Platt received a telephone call from Europe and was asked to build Shack-Hartmann wavefront sensors. Platt was not able to build them at that time because the start-up company he was working for would not allow him to work on any other project or to work on the side.

The military and the astronomers had parallel wavefront sensor and adaptive optics programs. Both groups also developed the laser guide star concept at nearly the same time. The military was always one or two steps ahead of the astronomers because they had better funding and higher technology hardware.

Platt later left the start-up company and went to work for the University of Dayton Research Institute on a contract at the Air Force Weapons Center. While there, he proposed a Shack-Hartmann wavefront sensor to test the beam quality of the laser on the Airborne Laser Lab. He also proposed a scanning Hartmann tester. Both instruments were fabricated and used in the laboratory. Several copies of the scanning Hartmann sensor were fabricated and used in several field tests. They received very little attention because of the classification of the program. During the late 1970s, Platt also proposed to use the scanning and non-scanning Shack-Hartmann sensors to measure the flatness of semiconductor disks.

During the same time period, Adaptive Optics Associates (AOA) was developing (for the Air Force) adaptive optics that would compensate for the earth's atmosphere. They started out with a scanning Hartmann system and ended up with a standard Shack-Hartmann wavefront sensor using lens arrays. AOA developed their own lens arrays and eventually sold them commercially. Massachusetts Institute of Technology (MIT) developed methods for making lens arrays using binary optics. Soon afterward, other organizations started making lens arrays using binary optics. When the lens arrays became easily available, more and more people started experimenting with the Shack-Hartmann sensor. Now, several companies are selling Shack-Hartmann sensors commercially.

Software to convert the 2-D tilt data into 2-D wavefront data is another major part of the wavefront sensor. The first software program was written at the University of Arizona. They had developed a program for reducing interferograms. This program was later modified to reduce shearing interferograms. Since shearing interferograms represent wavefront tilt, it was easy to modify this program to reduce Shack-Hartmann data. This program was made available to the public for the cost of copying. AOA developed its own software package for commercial and military applications. Most of the astronomical groups also developed their own software. Soon, the software was easily available.

In the mid 1980s, Dr. Josef Bille, from the University of Erlangen-Nurnberg, started working with Shack to use the lens array for measuring the profile of the cornea. Bille was the first to use the sensor in ophthalmology. He used it first to measure the profile of the cornea and later to measure aberrations in the eye, by projecting a point source onto the retina. His first published paper was in 1989.

In 1985, Platt formed a company to provide optical instruments and consulting support to the government and commercial organizations. One of the instruments he wanted to produce commercially was the Shack-Hartmann sensor. He wrote several proposals for different applications, including an application to the National Eye Institute (NEI) of the National Institutes of Health (NIH) for corneal topography. By the time the proposal was resubmitted, photorefractive keratectomy (PRK) was replacing radial keratotomy, and NEI was looking only at corneal topography instruments that could measure the profile of a diffuse surface.

The next major milestone in the United States for using the Shack-Hartmann sensor in ophthalmology occurred with the work of David Williams at the University of Rochester. He was the first (in the United States) to use the Shack-Hartmann sensor for measuring aberrations in the eye. He also demonstrated improved imaging of the retina by coupling the Shack-Hartmann wavefront sensor to a deformable mirror, generating the first adaptive optics system used in ophthalmology.

The United States military started using the Shack-Hartmann sensor in 1974 to test lasers, and in the early 1980s, in adaptive optical systems. From 1974 to 1996, Platt wrote proposals to use the Shack-Hartmann sensor for applications ranging from aligning telescopes, testing lasers, testing semiconductor disks, to measuring the profile of the cornea. Current applications for the Shack-Hartmann sensor in ophthalmology, astronomy, adaptive optics, optical alignment, and commercial optical testing are too numerous to list. Hundreds of programs using the Shack-Hartmann sensor can be found on the Internet. It is currently the most popular wavefront sensor in the world for applications other than standard optical testing of optical components. Although the Shack-Hartmann sensor is being used to test optical components, it is not expected to replace the interferometer—only to complement it.

A Appendix A - SONY product information IMX183CLK

SONY

[Product Information]

Ver.1.0

IMX183CLK

Diagonal 15.86 mm (Type 1) CMOS Image Sensor with Square Pixel for Monochrome Cameras

Description

The IMX183CLK is a diagonal 15.86 mm (Type 1) CMOS image sensor with a monochrome square pixel array and approximately 20.48 M effective pixels. 12-bit digital output makes it possible to output the signals of approximately 20.48 M effective pixels with high definition for shooting still picture. In addition, this sensor enables output effective approximately 9.03 M effective pixels (aspect ratio approx.17:9) signal performed horizontal and vertical cropping at 59.94 frame/s in 10-bit digital output format for high-definition moving picture. Furthermore, it realizes 12-bit digital output for shooting high-speed and high-definition moving pictures by horizontal and vertical addition and subsampling. Realizing high-sensitivity, low dark current, this sensor also has an electronic shutter function with variable storage time.
In addition, this product is designed for use in consumer use digital still camera and consumer use camcorder. When using this for another application, Sony Semiconductor Solutions Corporation does not guarantee the quality and reliability of product. Therefore, don't use this for applications other than consumer use digital still camera and consumer use camcorder.
In addition, individual specification change cannot be supported because this is a standard product.
Consult your Sony Semiconductor Solutions Corporation sales representative if you have any questions.

Features

- ◆ Input clock frequency 72 MHz
- ◆ All-pixel scan mode
  Various readout modes (*)
- ◆ High-sensitivity, low dark current, no smear, excellent anti-blooming characteristics
- ◆ Variable-speed shutter function (minimum unit: 1 horizontal sync signal period (1XHS))
- ◆ Low power consumption
- ◆ H driver, V driver and serial communication circuit on chip
- ◆ CDS/PGA on chip. Gain +27 dB (step pitch 0.1 dB)
- ◆ 9-bit/10-bit/12-bit A/D conversion on chip
- ◆ All-pixel simultaneous reset supported (use with mechanical shutter)
- ◆ 118-pin high-precision ceramic package

* Please refer to the datasheet for binning/subsampling details of readout modes.

Device Structure

◆CMOS image sensor

◆Image size — Diagonal 15.86 mm (Type 1)

◆Total number of pixels — 5640 (H) × 3710 (V) approx. 20.92 M pixels

◆Number of effective pixels
- Type1 approx. 20.48 M pixels use — 5544 (H) × 3694 (V) approx. 20.48 M pixels
- Type 1/1.4 approx. 9.03 M pixels use — 4152 (H) × 2174 (V) approx. 9.03 M pixels

◆Number of active pixels
- Type1 approx. 20.48 M pixels use — 5496 (H) × 3672 (V) approx. 20.18 M pixels diagonal 15.86 mm
- Type 1/1.4 approx. 9.03 M pixels use — 4128 (H) × 2168 (V) approx. 8.95 M pixels diagonal 11.19 mm

◆Number of recommended recording pixels
- Type1 approx. 20.48 M pixels use — 5472 (H) × 3648 (V) approx. 19.96 M pixels aspect ratio 3:2
- Type 1/1.4 approx. 9.03 M pixels use — 4096 (H) × 2160 (V) approx. 8.85 M pixels aspect ratio approx. 17:9

◆Chip size — 16.05 mm (H) × 12.61 mm (V)

◆Unit cell size — 2.40 µm (H) × 2.40 µm (V)

◆Optical black — Horizontal (H) direction : Front 48 pixels, rear 0 pixel
Vertical (V) direction : Front 16 pixels, rear 0 pixel

◆Package — 118 pin LGA

Image Sensor Characteristics

(Tj = 60 °C)

Item		Value	Remarks
Sensitivity (F8)	Typ.	1576 digit	1/30 s integration
Saturation signal	Min.	3824 digit	

Basic Drive Mode

Type 1 Approx. 20.48 M Pixels (3:2)

Drive mode	Number of recording pixels	Max frame rate [frame/s]	Output data bit length [bit]
Readout mode 0	5472 (H) × 3648 (V) approx. 19.96 M pixels	21.98	12
Readout mode 1	5472 (H) × 3648 (V) approx. 19.96 M pixels	24.98	10
Readout mode 2	2736 (H) × 1538 (V) approx. 4.21 M pixels	59.94	12
Readout mode 2A	2736 (H) × 1824 (V) approx. 4.99 M pixels	49.95	12
Readout mode 3	1824 (H) × 1216 (V) approx. 2.22 M pixels	59.94	12
Readout mode 4	1824 (H) × 370 (V) approx. 0.67 M pixels	239.76	12
Readout mode 5	1824 (H) × 404 (V) approx. 0.74 M pixels	29.97	12
Readout mode 6	1824 (H) × 190 (V) approx. 0.35 M pixels	449.55	12
Readout mode 7	2736 (H) × 1538 (V) approx. 4.21 M pixels	59.94	10

Type 1/1.4 Approx. 9.03 M Pixels (Approx. 17:9)

Drive mode	Number of recording pixels	Max frame rate [frame/s]	Output data bit length [bit]
Readout mode 1	4096 (H) × 2160 (V) approx. 8.85 M pixels	59.94	10

B Appendix B - ZWO ASI183 manual

ASI183 Manual

Revision 1.1

Mar, 2018

Table of Contents

1. Instruction

Congratulations and thank you for buying one of our ASI Cameras！This manual will give you a brief introduction to your ASI camera. Please take the time to read it thoroughly and if you have any other questions, feel free to contact us. info@zwoptical.com

ASI183 Cameras are designed for astronomical photography. This is another great camera from ZWO not only suitable for DSO imaging but also planetary imaging. The excellent performance and multifunctional usage will impress you a lot!

For software installation instructions and other technical information please refer to “ASI USB3.0 Cameras software Manual”

https://astronomy-imaging-camera.com/

2. Camera Models and Sensor Type

There are 4 types of ASI183 models:

Models	Mono or Color	Regulated TEC Cooling	Sensor
ASI183MM	Mono	No	Sony IMX183CLK-J
ASI183MC	Color	No	Sony IMX183CQJ-J
ASI183MM Pro	Mono	Yes	Sony IMX183CLK-J
ASI183MC Pro	Color	Yes	Sony IMX183CQJ-J

Which camera to choose:

Monochrome camera sensors are capable of higher detail and sensitivity than is possible with color sensors, but you need additional accessories such as filter wheel and filters. The post-processing is more complicated too, so a color camera is often recommended for the beginner of astrophotographer.

TEC cooling will help to reduce dark current noise for long exposures. For short exposures, such as under one second, the dark current noise is very low, however cooling is recommended for DSO imaging when long exposures are required.

3. What's in the box?

ASI183MM or ASI183MC

ASI183MM Pro or ASI183MC Pro

4. Camera technical specifications

Sensor	1″ CMOS IMX183CLK-J/CQJ-J
Diagonal	15.9mm
Resolution	20.18Mega Pixels 5496*3672
Pixel Size	2.4μm
Image area	13.2mm*8.8mm
Max FPS at full resolution	19FPS
Shutter	Rolling shutter
Exposure Range	32μs-2000s
Read Noise	1.6e @30db gain
QE peak	84%
Full well	15ke
ADC	12 bit or 10 bit
DDR3 buffer	256MB(Cooled)
Interface	USB3.0/USB2.0
Adapters	2″ / 1.25″ / M42X0.75 Uncooled 2″ / M42X0.75 Cooled
Protect window	AR window
Dimensions	Uncooled 62mm/Cooled 78mm
Weight	Uncooled 140g/Cooled 410g
Back Focus Distance	6.5mm
Cooling:	Regulated Two Stage TEC
Delta T	40°C -45°C below ambient
Cooling Power consumption	12V at 3A Max
Supported OS	Windows, Linux & Mac OSX
Working Temperature	-5°C—45°C
Storage Temperature	-20°C—60°
Working Relative Humidity	20%—80%
Storage Relative Humidity	20%—95%

5. QE Graph & Read Noise

QE and Read noise are the most important parts to measure the performance of a camera. Higher QE and Lower read noise are needed to improve the SNR of an image.

For the Mono 183 Sensor, the peak value for QE is around 84%

Relative QE

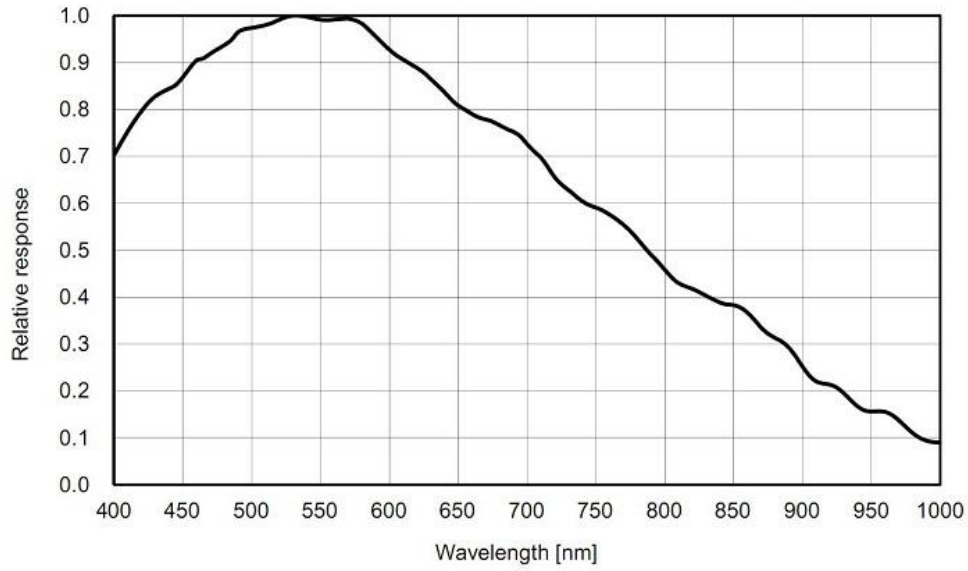

Color 183 sensor

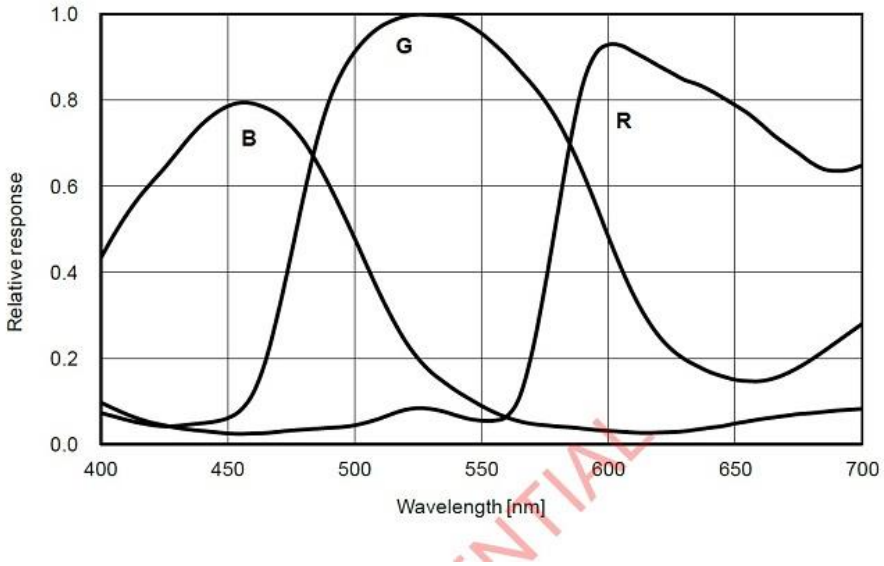

Read noise includes pixel diode noise, circuit noise and ADC quantization error noise, and the lower the better.

The Read Noise of the ASI183 cameras is extremely low when compared with traditional CCD cameras and it is even lower when the camera is used at a higher gain.

Depending on your target, you can set the gain lower for higher dynamic range (longer exposure) or set the gain higher for lower noise (such as short exposure or lucky imaging).

Read noise, full well, gain & dynamic range for ASI183

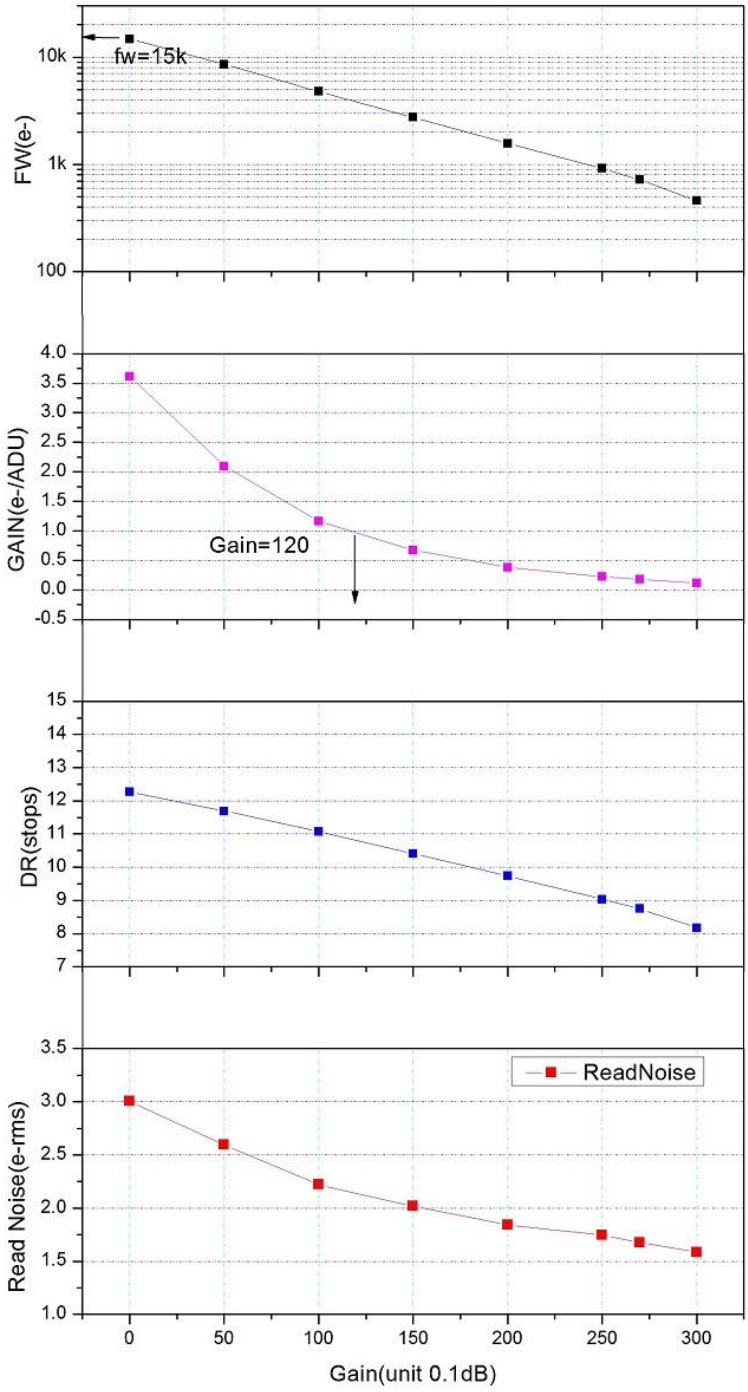

6. Getting to know your camera

6.1 External View

The first generation of cooled camera we used a ST4 port instead of USB2.0 hub

You can order the holder ring from us or our dealer to mount the cooled camera to tripod. There is 1/4″ screw under the holder

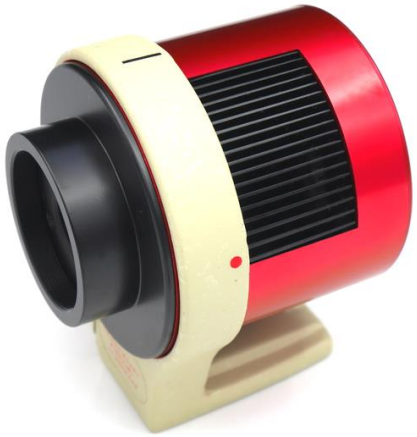

6.2 Power consumption

ASI cameras are designed to have very low power consumption which is around 300ma@5V. You only need the USB cable to power up the camera. However, you will need a separate power supply to activate the cooler. We recommend 12V at 3A or more AC-DC adapter for cooler power supply (2.1mm*5.5mm, center positive). You may also use a battery supply from 9 to 15V to power the cooler.

Here is a test result of the cooler power consumption of our cooled camera. It only needs 0.5A to cool the camera to 30℃ below ambient.

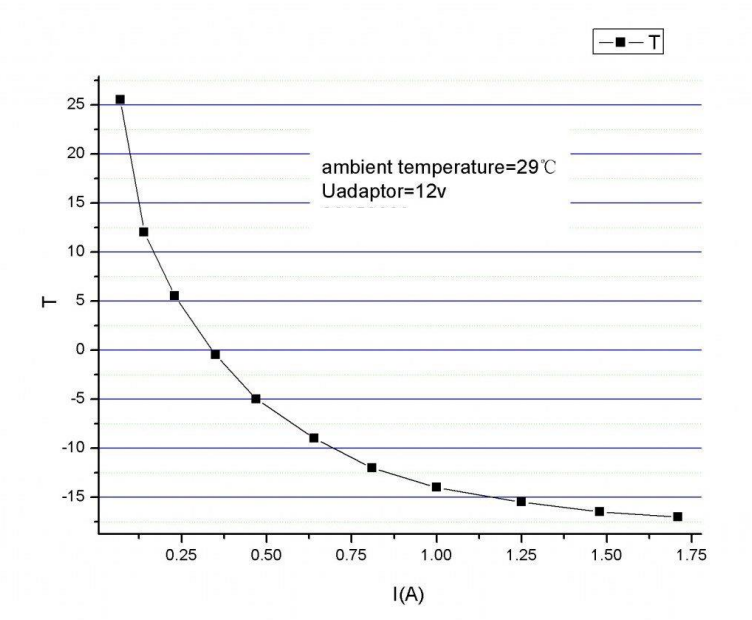

6.3 Cooling system

The cooled ASI183 cameras have a robust, regulated cooling system, which means that the camera sensor can be kept at the desired temperature throughout your imaging session. The super low readout noise, combined with efficient cooling and adjustable gain setting, allows you to do short or lucky DSO imaging unlike the traditional CCD cameras which need very long exposures for each frame. However, keep in mind that cooling won't help with very short exposures such as less than 100ms. The lowest temperature that can be set is -40℃~-45℃ below ambient.

Here is a dark current test result of 183 sensor at various temperatures.

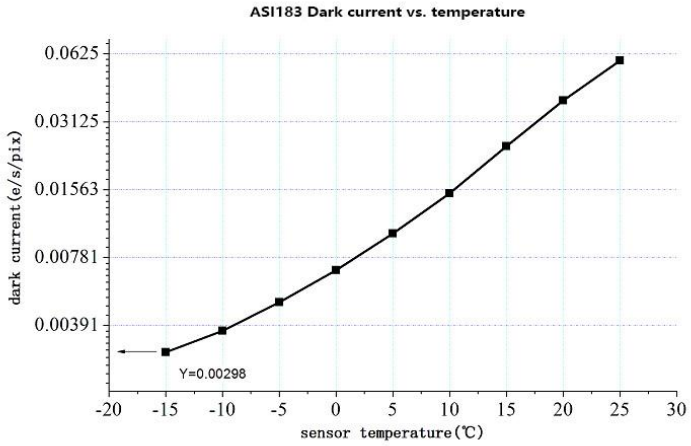

6.4 Back focus distance

When the attached 11mm T2 Extender is removed the optical distance from the sensor to the camera body is reduced to 6.5mm.

6.5 Protect Window

There is a protect window before the sensor of ASI183 camera.

It's an AR-AR coated BK7 glass, diameter is 32mm and 2mm thick.

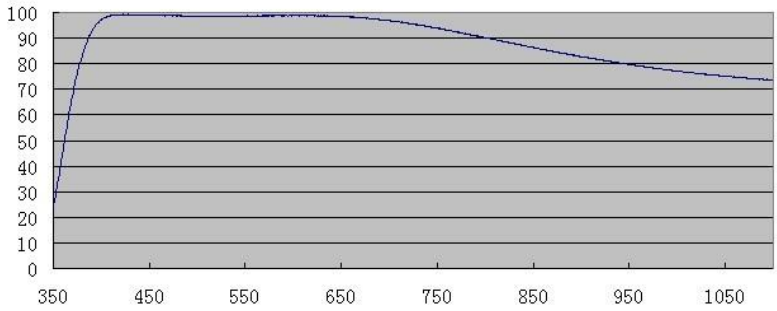

6.6 Analog to Digital Converter (ADC)

The ASI183 camera records in 12bit ADC and 10bit ADC. You can image at a faster fps rate if you choose to use 10bit ADC (high speed mode). This camera also supports ROI (region of interest) shooting, and this smaller ROI has faster fps. You can uncheck “high speed” and choose 8bit output on software to enable 10bit ADC output, otherwise this camera will use 12bit ADC.

Here is the maximum speed of ASI183 running at 10bit ADC or 12bit ADC at 8bit mode.

Resolution	USB3.0	
	10Bit ADC	12Bit ADC
5496×3672	19fps	19fps
3840x2160	41fps	36fps
1920x1680	80fps	70fps
1280x720	117fps	103fps
640x480	170fps	150fps
320x240	308.fps	271fps

6.7 Binning

The ASI183 camera supports hardware bin2 and software bin2, bin3 and bin4 mode. Hardware binning is supported by sensor but is done in digital domain like software binning and use 10bit ADC. The only advantage of hardware binning is faster fps. We recommend customer to use software binning if you don’t care speed.

6.8 DDR Buffer

The ASI183 Pro camera includes a 256MB DDR3 memory buffer to help improve data transfer reliability. Additionally, the use of a memory buffer minimizes amp-glow, which is caused by the slow transfer speeds when the camera is used with a USB 2.0 port. DDR memory buffer is the main difference between ASI “Cool” and “Pro” cameras.

7. How to use your camera

There are many adapters available for this camera for connecting to your scope or lens. Some are included with the camera and others you can order from our site:

Color camera connecting drawing:

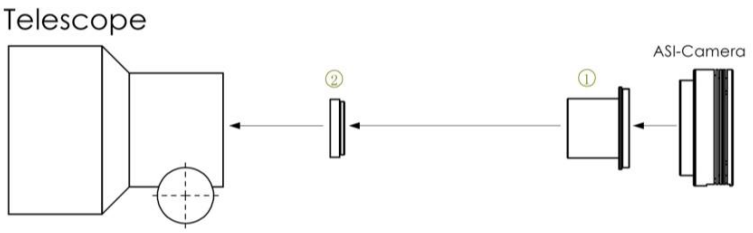

1. 1.25” T-Mount
2. 1.25”filter(optional)

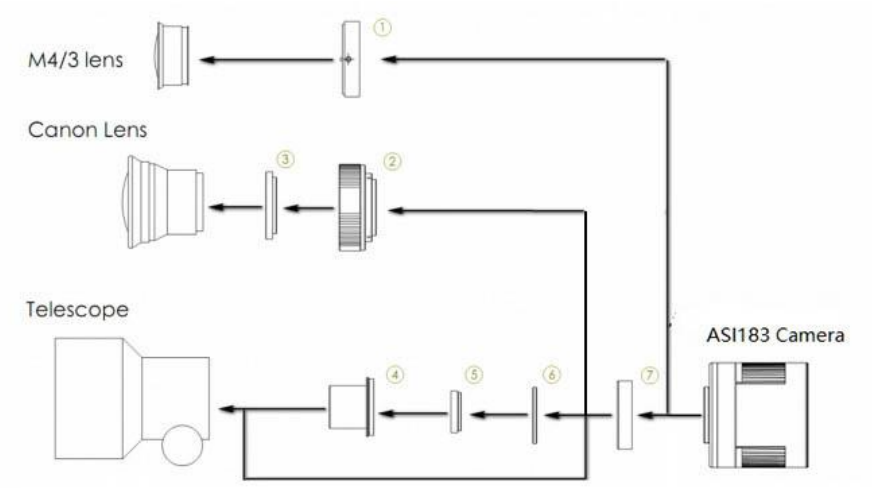

1. M43-T2 adapter
2. EOS-T2 adapter
3. 2”Filter (optional)
4. 1.25” T-Mount
5. 1.25” Filter (optional)
6. M42-1.25” Filter (optional)
7. T2 extender 11mm

Mono camera connecting drawing:

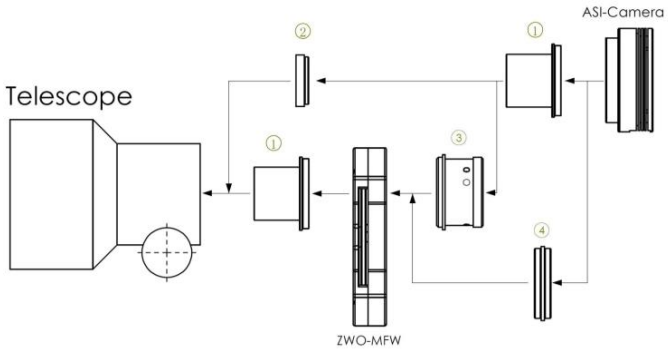

1. 1.25” T-Mount
2. 1.25” filter(optional)
3. M42-1.25” adapter
4. M42-M42（Male screw thread）

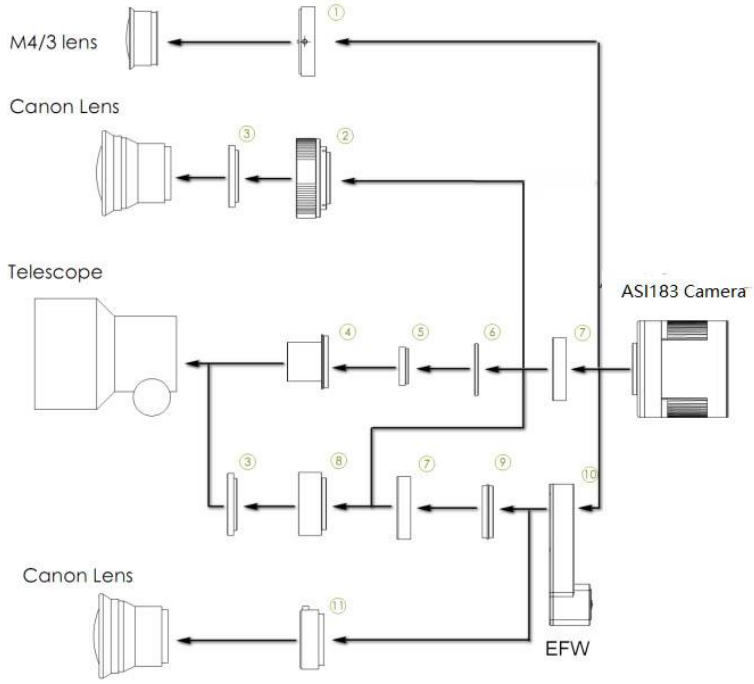

1. M43-T2 adapter
2. EOS-T2 adapter
3. 2”Filter (optional)
4. 1.25” T-Mount
5. 1.25” Filter (optional)
6. M42-1.25” Filter (optional)
7. T2 extender 11mm
8. M42-M48 extender 16.5mm
9. T2-T2 adapter
10. EFW mini
11. EOS adapter for EFW

Here are the steps to show you how to connect mono 183 and our EFW mini to your scopes. Benefiting from the short back focus design, 1.25” filter is big enough for ASI183 camera.

<table>
<tr>
<td> 

EFW Mini & ASI183MM cooled camera</td>
<td> 
Unscrew the six screws.</td>
</tr>
<tr>
<td> 
Take the back cover off.</td>
<td> 
Screw on all the filters.</td>
</tr>
<tr>
<td> 
Tighten back the screws.</td>
<td> 

Screw off the T2-1.25” holder on the EFW, screw off the T2 ring on the 183 camera.</td>
</tr>
</table>

Attached the camera to the EFW as shown.

Take out the 1.25” T-Mount form the T2-1.25” holder.

Install the T-mount to the back of the EFW.

Attach it to your telescope.

Here is the sideways view.

T2 extender can be used for attaching the telescope with 2” interface.

Here is an example of the whole setup including an OAG and guider camera.

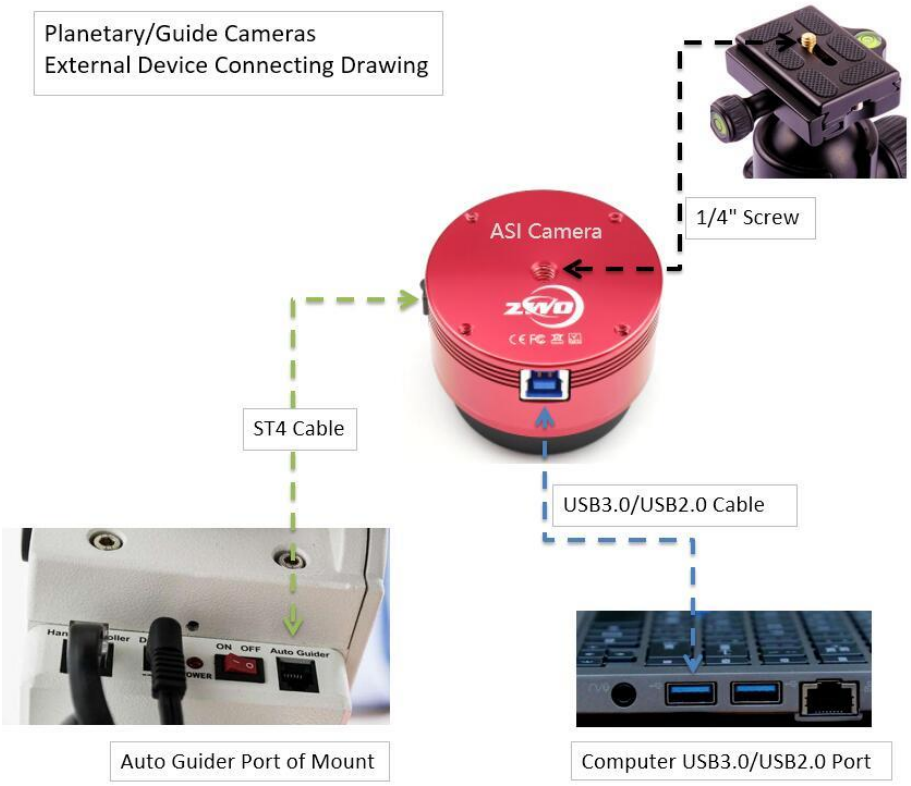


Cooled Cameras
External Device Connecting Drawing
USB Hub For accessaries
12V Power Adapter
USB2.0 OUT
USB3.0 IN
DC 12V⎓3A
ASI Pro/Cool Camera
USB2.0 Cable
USB3.0/USB2.0 Cable
EFW mini
Accessaries
Computer USB3.0/USB2.0 Port

8. Cleaning

The camera comes with an AR protect window, which can protect the sensor from dust and humidity. Should you need to clean the sensor, it's better to do so during the daytime. To see the dust, you just need to setup your telescope and point it to a bright place. A Barlow is required to see these dusts clear. Then attach the camera and adjust the exposure to make sure not over exposed. You can see an image like below if it's dirty.

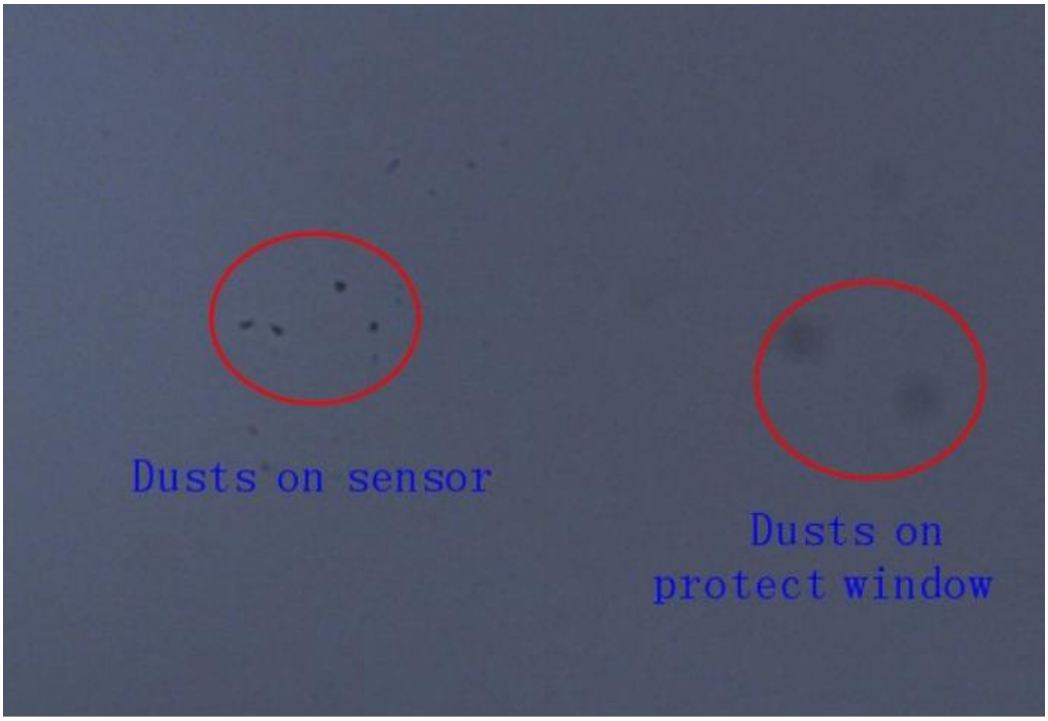

The big dim spot on the image (at right) are the shadows of dust on the protect window.

The very small but very dark spot in the image (at left) are the shadows of the dusts on the sensor.

The suggested way to clean them is try to blow them away with a manual air pump. To clean the dust on the sensor you will need to open the camera chamber.

We have a very detailed instruction on our website:
https://astronomy-imaging-camera.com/manuals/

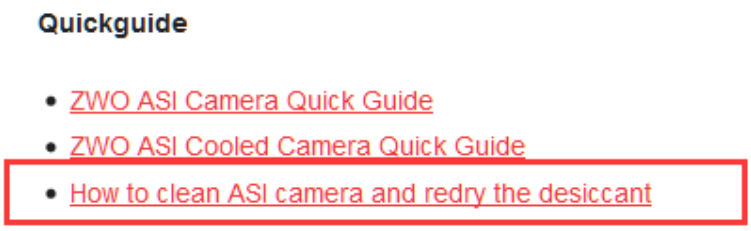

9. Mechanical drawing

ASI183MM/ASI183MC

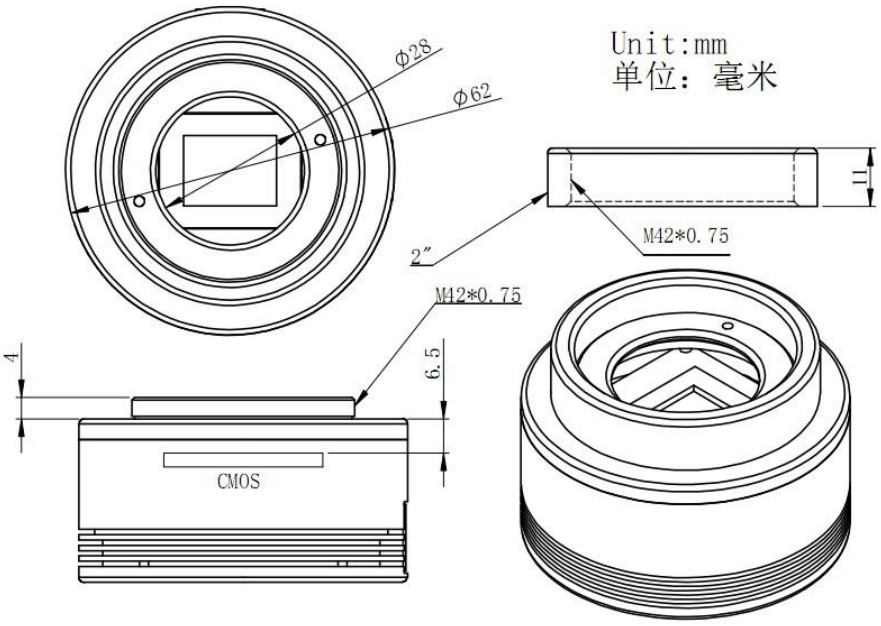

ASI183MM Pro /ASI183MC Pro

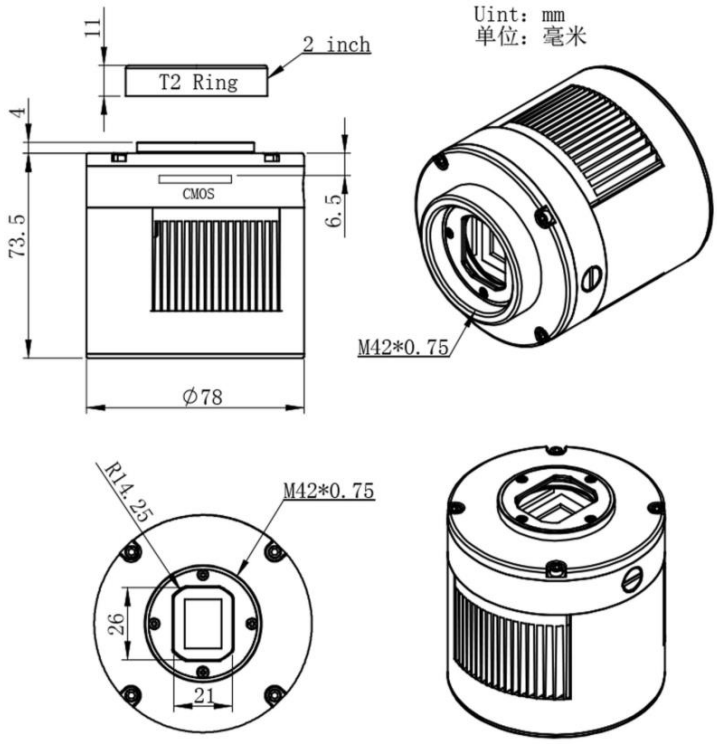

10. Servicing

Repairs, servicing and upgrades are available by emailing info@zwoptical.com

For customers who bought the camera form your local dealer, dealer is responsible for the customer service.

11. Warranty

We provide 2-year warranty for our products, we will offer repair service for free or replace for free if the camera doesn't work within warranty period.

After the warranty period, we will continue to provide repair support and service on a charged basis.

This warranty does not apply to damage that occurred as a result of abuse or misuse, or caused by a fall or any other transportation failures after purchase.

Customer must pay for shipping when shipping the camera back for repair or replacement.

C Appendix C - Measuring the gain of a CCD camera

Measuring the Gain of a CCD Camera

Michael Newberry
Axiom Research, Inc.

1. Introduction

The gain of a CCD camera is the conversion between the number of electrons ("e-") recorded by the CCD and the number of digital units ("counts") contained in the CCD image. It is useful to know this conversion for evaluating the performance of the CCD camera. Since quantities in the CCD image can only be measured in units of counts, knowing the gain permits the calculation of quantities such as readout noise and full well capacity in the fundamental units of electrons. The gain value is required by some types of image de-convolution such as Maximum Entropy since, in order to do properly the statistical part of the calculation, the processing needs to convert the image into units of electrons. Calibrating the gain is also useful for detecting electronic problems in a CCD camera, including gain change at high or low signal level, and the existence of unexpected noise sources.

This Axiom Tech Note develops the mathematical theory behind the gain calculation and shows how the mathematics suggests ways to measure the gain accurately. This note does not address the issues of basic image processing or CCD camera operation, and a basic understanding of CCD bias, dark and flat field correction is assumed. Developing the mathematical background involves some algebra, and readers who do not wish to read through the algebra may wish to skip Section 3.

2. Overview

The gain value is set by the electronics that read out the CCD chip. Gain is expressed in units of electrons per count. For example, a gain of 1.8 e-/count means that the camera produces 1 count for every 1.8 recorded electrons. Of course, we cannot split electrons into fractional parts, as in the case for a gain of 1.8 e-/count. What this number means is that 4/5 of the time 1 count is produced from 2 electrons, and 1/5 of the time 1 count is produced from 1 electron. This number is an average conversion ratio, based on changing large numbers of electrons into large numbers of counts. Note: This use of the term "gain" is in the opposite sense to the way a circuit designer would use the term since, in electronic design, gain is considered to be an increase in the number of output units compared with the number of input units.

It is important to note that every measurement you make in a CCD image uses units of counts. Since one camera may use a different gain than another camera, count units do not provide a straightforward comparison to be made. For example, suppose two cameras each record 24 electrons in a certain pixel. If the gain of the first camera is 2.0 and the gain of the second camera is 8.0, the same pixel would measure 12 counts in the image from the first camera and 3 counts in the image from the second camera. Without knowing the gain, comparing 12 counts against 3 counts is pretty meaningless.

Before a camera is assembled, the manufacturer can use the nominal tolerances of the electronic components to estimate the gain to within some level of uncertainty. This calculation is based on resistor values used in the gain stage of the CCD readout electronics. However, since the actual resistance is subject to component tolerances, the gain of the assembled camera may be quite different from this estimate. The actual gain can only be determined by actual performance in a gain calibration test. In addition, manufacturers

sometimes do not perform an adequate gain measurement. Because of these issues, it is not unusual to find that the gain of a CCD camera differs substantially from the value quoted by the manufacturer.

3. Mathematical Background

The signal recorded by a CCD and its conversion from units of electrons to counts can be mathematically described in a straightforward way. Understanding the mathematics validates the gain calculation technique described in the next section, and it shows why simpler techniques fail to give the correct answer.

This derivation uses the concepts of "signal" and "noise". CCD performance is usually described in terms of signal to noise ratio, or "S/N", but we shall deal with them separately here. The signal is defined as the quantity of information you measure in the image—in other words, the signal is the number of electrons recorded by the CCD or the number of counts present in the CCD image. The noise is the uncertainty in the signal. Since the photons recorded by the CCD arrive in random packets (courtesy of nature), observing the same source many times records a different number of electrons every time. This variation is a random error, or "noise" that is added to the true signal. You measure the gain of the CCD by comparing the signal level to the amount of variation in the signal. This works because the relationship between counts and electrons is different for the signal and the variance. There are two ways to make this measurement:

1. Measure the signal and variation within the same region of pixels at many intensity levels.
2. Measure the signal and variation in a single pixel at many intensity levels.

Both of these methods are detailed in section 6. They have the same mathematical foundation.

To derive the relationship between signal and variance in a CCD image, let us define the following quantities:

S_C	The signal measured in count units in the CCD image
S_E	The signal recorded in electron units by the CCD chip. This quantity is unknown.
N_C	The total noise measured in count units in the CCD image.
N_E	The total noise in terms of recorded electrons. This quantity is unknown.
g	The gain, in units of electrons per count. This will be calculated.
R_E	The readout noise of the CCD chip, measured in electrons. This quantity is unknown.
? $_E$	The photon noise in the signal N_E
? $_o$	An additional noise source in the image. This is described below.

We need an equation to relate the number of electrons, which is unknown, to quantities we measure in the CCD image in units of counts. The signals and noises are simply related

through the gain factor as

$$S_E = gS_C \text{ and } N_E = gN_C$$

These can be inverted to give

$$S_C = \frac{1}{g}S_E \text{ and } N_C = \frac{1}{g}N_E$$

The noise is contributed by various sources. We consider these to be readout noise, R_E, photon noise attributable to the nature of light, σ_E, and some additional noise, σ_o, which will be shown to be important in Section 5. Remembering that the different noise sources are independent of each other, they add in quadrature. This means that they add as the square their noise values. If we could measure the total noise in units of electrons, the various noise sources would combine in the following way:

$$N_E^2 = R_E^2 + \sigma_E^2 + \sigma_{o,E}^2$$

The random arrival rate of photons controls the photon noise, σ_E. Photon noise obeys the laws of Poissonian statistics, which makes the square of the noise equal to the signal, or $\sigma_E^2 = S_E$. Therefore, we can make the following substitution:

$$N_E^2 = R_E^2 + S_E + \sigma_{o,E}^2.$$

Knowing how the gain relates units of electrons and counts, we can modify this equation to read as follows:

$$g^2 N_C^2 = g^2 R_C^2 + gS_C + g^2 \sigma_{o,C}^2$$

which then gives

$$N_C^2 = R_C^2 + \frac{1}{g}S_C + \sigma_{o,C}^2$$

We can rearrange this to get the final equation:

$$N_C^2 = \frac{1}{g}S_C + (R_C^2 + \sigma_{o,C}^2).$$

This is the equation of a line in which N_C^2 is the y axis, S_C is the x axis, and the slope is 1/g. The extra terms $(R_C^2 + \sigma_{o,C}^2)$ are grouped together for the time being. Below, they will be separated, as the extra noise term has a profound effect on the method we use to measure

gain. A better way to apply this equation is to plot our measurements with S_C as the y axis and N_C^2 as the x axis, as this gives the gain directly as the slope. Theoretically, at least, one could also calculate the readout noise, R_C^2, from the point where the line hits the y axis at $S_C = 0$. Knowing the gain then allows this to be converted to a Readout Noise in the standard units of electrons. However, finding the intercept of the line is not a good method, because the readout noise is a relatively small quantity and the exact path where the line passes through the y axis is subject to much uncertainty.

With the mathematics in place, we are now ready to calculate the gain. So far, I have ignored the "extra noise term", $\sigma_{o,C}$. In the next 2 sections, I will describe the nature of the extra noise term and show how it affects the way we measure the gain of a CCD camera.

4. Crude Estimation of the Gain

In the previous section we derived the complete equation that relates the signal and the noise you measure in a CCD image. One popular method for measuring the gain is very simple, but it is not based on the full equation I have derived above. The simple can be described as follows:

1. Obtain images at different signal levels and subtract the bias from them. This is necessary because the bias level adds to the measured signal but does not contribute noise.
2. Measure the signal and noise in each image. The mean and standard deviation of a region of pixels give these quantities. Square the noise value to get a variance at each signal level.
3. For each image, plot Signal on the y axis against Variance on the x axis.
4. Find the slope of a line through the points. The gain equals the slope.

Is measuring the gain actually this simple? Well, yes and no. If we actually make the measurement over a substantial range of signal, the data points will follow a curve rather than a line. Using the present method we will always measure a slope that is too shallow, and with it we will always underestimate the gain. Using only low signal levels, this method can give a gain value that is at least "in the ballpark" of the true value. At low signal levels, the curvature is not apparent, though present. However, the data points have some amount of scatter themselves, and without a long baseline of signal, the slope might not be well determined. The curvature in the Signal - Variance plot is caused by the extra noise term which this simple method neglects.

The following factors affect the amount of curvature we obtain:

- The color of the light source.
  Blue light is worse because CCD's show the greatest surface irregularity at shorter wavelengths. These irregularities are described in Section 5.
- The fabrication technology of the CCD chip.
  These issues determine the relative strength of the effects described in item 1.
- The uniformity of illumination on the CCD chip.
  If the Illumination is not uniform, then the sloping count level inside the pixel region used to measure it inflates the measured standard deviation.

Fortunately, we can obtain the proper value by doing just a bit more work. We need to change the experiment in a way that makes the data plot as a straight line. We have to devise a way to account for the extra noise term, $\sigma_{o,C}$. If $\sigma_{o,C}$ were a constant value we could combine it with the constant readout noise. We have not talked in detail about readout noise, but we have assumed that it merges together all constant noise sources that do not change with the signal level.

5. Origin of the Extra Noise Term in the Signal - Variance Relationship

The mysterious extra noise term, $\sigma_{o,C}$, is attributable to pixel-to-pixel variations in the sensitivity of the CCD, known as the flat field effect. The flat field effect produces a pattern of apparently "random" scatter in a CCD image. Even an exposure with infinite signal to noise ratio ("S/N") shows the flat field pattern. Despite its appearance, the pattern is not actually random because it repeats from one image to another. Changing the color of the light source changes the details of the pattern, but the pattern remains the same for all images exposed to light of the same spectral makeup. The importance of this effect is that, although the flat field variation is not a true noise, unless it is removed from the image it contributes to the noise you actually measure.

We need to characterize the noise contributed by the flat field pattern in order to determine its effect on the variance we measure in the image. This turns out to be quite simple: Since the flat field pattern is a fixed percentage of the signal, the standard deviation, or "noise" you measure from it is always proportional to the signal. For example, a pixel might be 1% less sensitive than its left neighbor, but 3% less sensitive than its right neighbor. Therefore, exposing this pixel at the 100 count level produces the following 3 signals: 101, 100, 103. However, exposing at the 10,000 count level gives these results: 10,100, 10,000, 10,300. The standard deviation for these 3 pixels is $\sigma_{o,C} = 2.333$ counts for the low signal case but is $\sigma_{o,C} = 233.3$ counts for the high signal case. Thus the standard deviation is 100 times larger when the signal is also 100 times larger. We can express this proportionality between the flat field "noise" and the signal level in a simple mathematical way:

$$\sigma_{o,C} = kS_C$$

In the present example, we have k=0.02333. Substituting this expression for the flat field variation into our master equation, we get the following result:

$$N_C^2 = \frac{1}{g} S_C + R_C^2 + k^2 S_C^2 .$$

With a simple rearrangement of the terms, this reveals a nice quadratic function of signal:

$$N_C^2 = R_C^2 + \frac{1}{g} S_C + k^2 S_C^2 .$$

When plotted with the Signal on the x axis, this equation describes a parabola that opens upward. Since the Signal - Variance plot is actually plotted with Signal on the y axis, we

need to invert this equation to solve for S_C:

$$S_C = \frac{-1 + \sqrt{1 + 4g^2k^2(N_C^2 - R_C^2)}}{2gk^2}$$

This final equation describes the classic Signal - Variance plot. In this form, the equation describes a family of horizontal parabolas that open toward the right. The strength of the flat field variation, k, determines the curvature. When k = 0, the curvature goes away and it gives the straight line relationship we desire. The curvature to the right of the line means that the stronger the flat field pattern, the more the variance is inflated at a given signal level. This result shows that it is impossible to accurately determine the gain from a Signal - Variance plot unless we know one of two things: Either 1) we know the value of k, or 2) we setup our measurements to avoid flat field effects. Option 2 is the correct strategy. Essentially, the weakness of the method described in Section 4 is that it assumes that a straight line relationship exists but ignores flat field effects.

To illustrate the effect of flat field variations, mathematical models were constructed using the equation above with parameters typical of commonly available CCD cameras. These include readout noise R_E = 15e- and gain g = 2.0 e- / Count. Three models were constructed with flat field parameters k = 0, k = 0.005, and k = 0.01. Flat field variations of this order are not uncommon. These models are shown in the figure below.

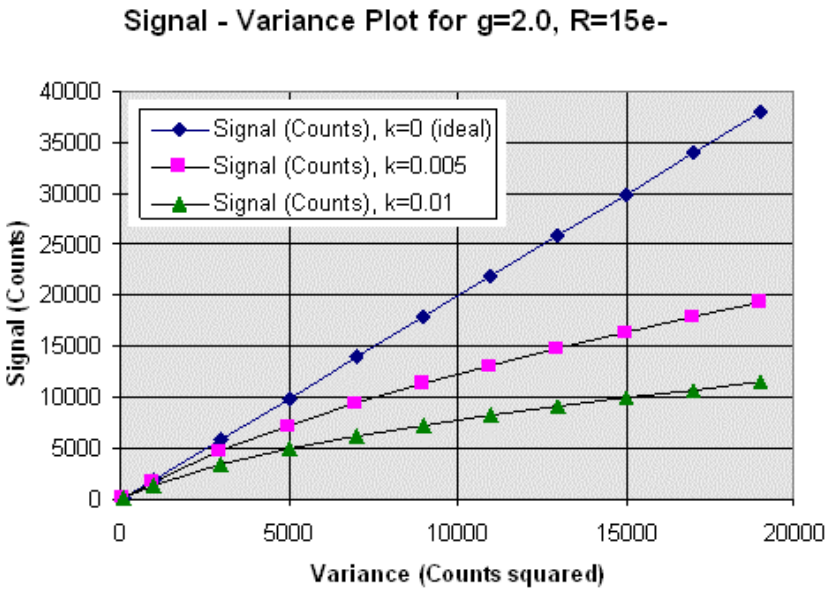

Increasing values of k correspond to progressively larger flat field irregularities in the CCD chip. The amplitude of flat field effects, k, tends to increase with shorter wavelength, particularly with thinned CCD's (this is why Section 4 recommends using a redder light source to illuminate the CCD). The flat field pattern is present in every image exposed to light. Clearly, it can be seen from the models that if one simply obtains images at different signal levels and measures the variance in them, then fitting a line through any part of the curve yields a slope lower than its true value. Thus the simple method of section 4 always underestimates the gain.

The best strategy for doing the Signal - Variance method is to find a way to produce a straight line by properly compensating for flat field effects. This is important by the "virtue of straightness": Deviation from a straight line is completely unambiguous and easy to detect. It avoids the issue of how much curvature is attributable to what cause. The electronic design of a CCD camera is quite complex, and problems can occur, such as gain change at different signal levels or unexplained extra noise at high or low signal levels. Using a "robust" method for calculating gain, any significant deviation from a line is a diagnostic of possible problems in the camera electronics. Two such methods are described in the following section.

6. Robust Methods for Measuring Gain

In previous sections, the so-called simple method of estimating the gain was shown to be an oversimplification. Specifically, it produces a Signal - Variance plot with a curved relationship resulting from flat field effects. This section presents two robust methods that correct the flat field effects in the Signal - Variance relationship to yield the desired straight-line relationship. This permits an accurate gain value to be calculated. Adjusting the method to remove flat field effects is a better strategy than either to attempt to use a low signal level where flat field effects are believed not to be important or to attempt to measure and compensate for the flat field parameter k.

When applying the robust methods described below, one must consider some procedural issues that apply to both:

- Both methods measure sets of 2 or more images at each signal level. An image set is defined as 2 or more successive images taken under the same illumination conditions. To obtain various signal levels, it is better to change the intensity received by the CCD than to change the exposure time. This may be achieved either by varying the light source intensity or by altering the amount of light passing into the camera. The illumination received by the CCD should not vary too much within a set of images, but it does not have to be truly constant.
- Cool the CCD camera to reduce the dark current to as low as possible. This prevents you from having to subtract dark frames from the images (doing so adds noise, which adversely affects the noise measurements at low signal level). In addition, if the bias varies from one frame to another, be sure to subtract a bias value from every image.
- The CCD should be illuminated the same way for all images within a set. Irregularities in illumination within a set are automatically removed by the image processing methods used in the calibration. It does not matter if the illumination pattern changes when you change the intensity level for a different image set.
- Within an image set, variation in the light intensity is corrected by normalizing the images so that they have the same average signal within the same pixel region. The process of normalizing multiplies the image by an appropriate constant value so that its mean value within the pixel region matches that of other images in the same set. Multiplying by a constant value does not affect the signal to noise ratio or the flat field structure of the image.
- Do not estimate the CCD camera's readout noise by calculating the noise value at zero signal. This is the square root of the variance where the gain line intercepts the y axis. Especially do not use this value if bias is not subtracted from every frame. To calculate the readout noise, use the "Two Bias" method and apply the gain value determined from this test. In the Two Bias Method, 2 bias frames are taken in succession and then subtracted from each other. Measure the standard deviation inside a region of, say 100x100 pixels and divide by 1.4142. This gives the readout noise in units of counts. Multiply this by the gain factor to get the Readout Noise in

units of electrons. If bias frames are not available, cool the camera and obtain two dark frames of minimum exposure, then apply the Two Bias Method to them.

A. METHOD 1: Correct the flat field effects at each signal level

In this strategy, the flat field effects are removed by subtracting one image from another at each signal level. Here is the recipe:

For each intensity level, do the following:

1. Obtain 2 images in succession at the same light level. Call these images A and B.
2. Subtract the bias level from both images. Keep the exposure short so that the dark current is negligibly small. If the dark current is large, you should also remove it from both frames.
3. Measure the mean signal level S in a region of pixels on images A and B. Call these mean signals S_A and S_B. It is best if the bounds of the region change as little as possible from one image to the next. The region might be as small as 50x50 to 100x100 pixels but should not contain obvious defects such as cosmic ray hits, dead pixels, etc.
4. Calculate the ratio of the mean signal levels as $r = S_A / S_B$.
5. Multiply image B by the number r. This corrects image B to the same signal level as image A without affecting its noise structure or flat field variation.
6. Subtract image B from image A. The flat field effects present in both images should be cancelled to within the random errors.
7. Measure the standard deviation over the same pixel region you used in step 3. Square this number to get the Variance. In addition, divide the resulting variance by 2.0 to correct for the fact that the variance is doubled when you subtract one similar image from another.
8. Use the Signal from step 3 and the Variance from step 7 to add a data point to your Signal - Variance plot.
9. Change the light intensity and repeat steps 1 through 8.

B. METHOD 2: Avoid flat field effects using one pixel in many images.

This strategy avoids the flat field variation by considering how a single pixel varies among many images. Since the variance is calculated from a single pixel many times, rather than from a collection of different pixels, there is no flat field variation.

To calculate the variance at a given signal level, you obtain many frames, measure the same pixel in each frame, and calculate the variance among this set of values. One problem with this method is that the variance itself is subject to random errors and is only an estimate of the true value. To obtain a reliable variance, you must use 100's of images at each intensity level. This is completely analogous to measuring the variance over a moderate sized pixel region in Method A; in both methods, using many pixels to compute the variance gives a more statistically sound value. Another limitation of this method is that it either requires a perfectly stable light source or you have to compensate for light source variation by adjusting each image to the same average signal level before measuring its pixel. Altogether, the method requires a large number of images and a lot of processing. For this reason, Method A is preferred. In any case, here is the recipe:

Select a pixel to measure at the same location in every image. Always measure the same pixel in every image at every signal level.

For each intensity level, do the following:

1. Obtain at least 100 images in succession at the same light level. Call the first image A and the remaining images i. Since you are interested in a single pixel, the images may be small, of order 100x100 pixels.
2. Subtract the bias level from each image. Keep the exposure short so that the dark current is negligibly small. If the dark current is large, you should also remove it from every frame.
3. Measure the mean signal level S in a rectangular region of pixels on image A. Measure the same quantity in each of the remaining images. The measuring region might be as small as 50x50 to 100x100 pixels and should be centered on the brightest part of the image.
4. For each image S_i other than the first, calculate the ratio of its mean signal level to that of image A. This gives a number for each image, $r_i = S_A / S_i$.
5. Multiply each image i by the number r_i. This corrects each image to the same average intensity as image A.
6. Measure the number of counts in the selected pixel in every one of the images. From these numbers, compute a mean count and standard deviation. Square the standard deviation to get the variance.
7. Use the Signal and Variance from step 6 to add a data point to your Signal - Variance plot.
8. Change the light intensity and repeat steps 1 through 7.

7. Summary

In Section 3 we derived the mathematical relationship between Signal and Variance in a CCD image. The resulting equation includes flat field effects that are later shown to weaken the validity of the gain unless they are compensated. Section 4 describes a simple, commonly employed method for estimating the gain of a CCD camera. This method does not compensate for flat field effects and can lead to large errors in the gain calculation. The weakness of this method is described and mathematically modeled in section 5. In Section 6, two methods are proscribed for eliminating the flat field problem. Method A, which removes the flat field effect by subtracting two images at each signal level requires far less image processing effort and is the preferred choice.

Zernike Polynomials

1 Introduction

Often, to aid in the interpretation of optical test results it is convenient to express wavefront data in polynomial form. Zernike polynomials are often used for this purpose since they are made up of terms that are of the same form as the types of aberrations often observed in optical tests (Zernike, 1934). This is not to say that Zernike polynomials are the best polynomials for fitting test data. Sometimes Zernike polynomials give a poor representation of the wavefront data. For example, Zernikes have little value when air turbulence is present. Likewise, fabrication errors in the single point diamond turning process cannot be represented using a reasonable number of terms in the Zernike polynomial. In the testing of conical optical elements, additional terms must be added to Zernike polynomials to accurately represent alignment errors. The blind use of Zernike polynomials to represent test results can lead to disastrous results.

Zernike polynomials are one of an infinite number of complete sets of polynomials in two variables, ρ and θ, that are orthogonal in a continuous fashion over the interior of a unit circle. It is important to note that the Zernikes are orthogonal only in a continuous fashion over the interior of a unit circle, and in general they will not be orthogonal over a discrete set of data points within a unit circle.

Zernike polynomials have three properties that distinguish them from other sets of orthogonal polynomials. First, they have simple rotational symmetry properties that lead to a polynomial product of the form

$$r[\rho]\ g[\theta],$$

where g[θ] is a continuous function that repeats self every 2π radians and satisfies the requirement that rotating the coordinate system by an angle α does not change the form of the polynomial. That is

$$g[\theta + \alpha] = g[\theta]\ g[\alpha].$$

The set of trigonometric functions

$$g[\theta] = e^{\pm i m \theta},$$

where m is any positive integer or zero, meets these requirements.
The second property of Zernike polynomials is that the radial function must be a polynomial in ρ of degree 2n and contain no power of ρ less than m. The third property is that r[ρ] must be even if m is even, and odd if m is odd.

The radial polynomials can be derived as a special case of Jacobi polynomials, and tabulated as $r[n, m, \rho]$. Their orthogonality and normalization properties are given by

$$\int_0^1 r[n, m, \rho]\ r[n', m, \rho]\ \rho\, d\rho = \frac{1}{2\,(n+1)}\ \text{KroneckerDelta}[n - n']$$

and

$$r[n,\ m,\ 1] = 1.$$

As stated above, r[n, m, ρ] is a polynomial of order 2n and it can be written as

$$\mathbf{r[n\_,\ m\_,\ \rho\_] := \sum_{s=0}^{n-m} (-1)^s \frac{(2\,n-m-s)!}{s!\,(n-s)!\,(n-m-s)!}\,\rho^{2\,(n-s)-m}}$$

In practice, the radial polynomials are combined with sines and cosines rather than with a complex exponential. It is convenient to write

```
rcos[n_, m_, ρ_] := r[n, m, ρ] Cos[m θ]
```

and

```
rsin[n_, m_, ρ_] := r[n, m, ρ] Sin[m θ]
```

The final Zernike polynomial series for the wavefront opd Δw can be written as

$$\mathbf{\Delta w[\rho\_,\ \theta\_] := \overline{\Delta w} + \sum_{n=1}^{nmax} \left(a[n]\ r[n,\ 0,\ \rho] + \sum_{m=1}^{n} (b[n,\ m]\ rcos[n,\ m,\ \rho] + c[n,\ m]\ rsin[n,\ m,\ \rho]) \right)}$$

where Δw[ρ, θ] is the mean wavefront opd, and a[n], b[n,m], and c[n,m] are individual polynomial coefficients. For a symmetrical optical system, the wave aberrations are symmetrical about the tangential plane and only even functions of θ are allowed. In general, however, the wavefront is not symmetric, and both sets of trigonometric terms are included.

2 Calculating Zernikes

For the example below the degree of the Zernike polynomials is selected to be 6. The value of nDegree can be changed if a different degree is desired.

The array zernikePolar contains Zernike polynomials in polar coordinates (ρ, θ), while the array zernikeXy contains the Zernike polynomials in Cartesian, (x, y), coordinates. zernikePolarList and zernikeXyList contains the Zernike number in column 1, the n and m values in columns 2 and 3, and the Zernike polynomial in column 4.

```
nDegree = 6;


i = 0;
Do[If[m == 0, {i = i + 1, temp[i] = {i - 1, n, m, r[n, m, ρ]}},
              {i = i + 1, temp[i] = {i - 1, n, m, Factor[rcos[n, m, ρ]]},
    i = i + 1, temp[i] = {i - 1, n, m, Factor[rsin[n, m, ρ]]}}], {n, 0, nDegree}, {m, n, 0, -1}];
```

```
zernikePolarList = Array[temp, i];
Clear[temp];
Do[zernikePolar[i - 1] = zernikePolarList[[i, 4]], {i, 1, Length[zernikePolarList]}];
```

$$\text{zernikeXyList} = \text{Map[TrigExpand, zernikePolarList]} /. \left\{\rho \to \sqrt{x^2 + y^2},\ \text{Cos}[\theta] \to \frac{x}{\sqrt{x^2 + y^2}},\ \text{Sin}[\theta] \to \frac{y}{\sqrt{x^2 + y^2}}\right\};$$

```
Do[zernikeXy[i - 1] = zernikeXyList[[i, 4]], {i, 1, Length[zernikeXyList]}]
```

2.1 Tables of Zernikes

In the tables term # 1 is a constant or piston term, while terms # 2 and # 3 are tilt terms. Term # 4 represents focus. Thus, terms # 2 through # 4 represent the Gaussian or paraxial properties of the wavefront. Terms # 5 and # 6 are astigmatism plus defocus. Terms # 7 and # 8 represent coma and tilt, while term # 9 represents third-order spherical and focus. Likewise terms # 10 through # 16 represent fifth-order aberration, terms # 17 through # 25 represent seventh-order aberrations, terms # 26 through # 36 represent ninth-order aberrations, and terms # 37 through # 49 represent eleventh-order aberrations.

Each term contains the appropriate amount of each lower order term to make it orthogonal to each lower order term. Also, each term of the Zernikes minimizes the rms wavefront error to the order of that term. Adding other aberrations of lower order can only increase the rms error. Furthermore, the average value of each term over the unit circle is zero.

2.1.1 Zernikes in polar coordinates

```
TableForm[zernikePolarList, TableHeadings -> {{}, {"#", "n", "m", "Polynomial"}}]
```

#	n	m	Polynomial
0	0	0	1
1	1	1	$\rho \text{Cos}[\theta]$
2	1	1	$\rho \text{Sin}[\theta]$
3	1	0	$-1 + 2\rho^2$
4	2	2	$\rho^2 \text{Cos}[2\theta]$
5	2	2	$\rho^2 \text{Sin}[2\theta]$
6	2	1	$\rho\ (-2 + 3\rho^2)\ \text{Cos}[\theta]$
7	2	1	$\rho\ (-2 + 3\rho^2)\ \text{Sin}[\theta]$
8	2	0	$1 - 6\rho^2 + 6\rho^4$
9	3	3	$\rho^3 \text{Cos}[3\theta]$
10	3	3	$\rho^3 \text{Sin}[3\theta]$

11	3	2	$\rho^2 (-3 + 4 \rho^2) \text{Cos}[2 \theta]$
12	3	2	$\rho^2 (-3 + 4 \rho^2) \text{Sin}[2 \theta]$
13	3	1	$\rho (3 - 12 \rho^2 + 10 \rho^4) \text{Cos}[\theta]$
14	3	1	$\rho (3 - 12 \rho^2 + 10 \rho^4) \text{Sin}[\theta]$
15	3	0	$-1 + 12 \rho^2 - 30 \rho^4 + 20 \rho^6$
16	4	4	$\rho^4 \text{Cos}[4 \theta]$
17	4	4	$\rho^4 \text{Sin}[4 \theta]$
18	4	3	$\rho^3 (-4 + 5 \rho^2) \text{Cos}[3 \theta]$
19	4	3	$\rho^3 (-4 + 5 \rho^2) \text{Sin}[3 \theta]$
20	4	2	$\rho^2 (6 - 20 \rho^2 + 15 \rho^4) \text{Cos}[2 \theta]$
21	4	2	$\rho^2 (6 - 20 \rho^2 + 15 \rho^4) \text{Sin}[2 \theta]$
22	4	1	$\rho (-4 + 30 \rho^2 - 60 \rho^4 + 35 \rho^6) \text{Cos}[\theta]$
23	4	1	$\rho (-4 + 30 \rho^2 - 60 \rho^4 + 35 \rho^6) \text{Sin}[\theta]$
24	4	0	$1 - 20 \rho^2 + 90 \rho^4 - 140 \rho^6 + 70 \rho^8$
25	5	5	$\rho^5 \text{Cos}[5 \theta]$
26	5	5	$\rho^5 \text{Sin}[5 \theta]$
27	5	4	$\rho^4 (-5 + 6 \rho^2) \text{Cos}[4 \theta]$
28	5	4	$\rho^4 (-5 + 6 \rho^2) \text{Sin}[4 \theta]$
29	5	3	$\rho^3 (10 - 30 \rho^2 + 21 \rho^4) \text{Cos}[3 \theta]$
30	5	3	$\rho^3 (10 - 30 \rho^2 + 21 \rho^4) \text{Sin}[3 \theta]$
31	5	2	$\rho^2 (-10 + 60 \rho^2 - 105 \rho^4 + 56 \rho^6) \text{Cos}[2 \theta]$
32	5	2	$\rho^2 (-10 + 60 \rho^2 - 105 \rho^4 + 56 \rho^6) \text{Sin}[2 \theta]$
33	5	1	$\rho (5 - 60 \rho^2 + 210 \rho^4 - 280 \rho^6 + 126 \rho^8) \text{Cos}[\theta]$
34	5	1	$\rho (5 - 60 \rho^2 + 210 \rho^4 - 280 \rho^6 + 126 \rho^8) \text{Sin}[\theta]$
35	5	0	$-1 + 30 \rho^2 - 210 \rho^4 + 560 \rho^6 - 630 \rho^8 + 252 \rho^{10}$
36	6	6	$\rho^6 \text{Cos}[6 \theta]$
37	6	6	$\rho^6 \text{Sin}[6 \theta]$
38	6	5	$\rho^5 (-6 + 7 \rho^2) \text{Cos}[5 \theta]$
39	6	5	$\rho^5 (-6 + 7 \rho^2) \text{Sin}[5 \theta]$
40	6	4	$\rho^4 (15 - 42 \rho^2 + 28 \rho^4) \text{Cos}[4 \theta]$
41	6	4	$\rho^4 (15 - 42 \rho^2 + 28 \rho^4) \text{Sin}[4 \theta]$
42	6	3	$\rho^3 (-20 + 105 \rho^2 - 168 \rho^4 + 84 \rho^6) \text{Cos}[3 \theta]$
43	6	3	$\rho^3 (-20 + 105 \rho^2 - 168 \rho^4 + 84 \rho^6) \text{Sin}[3 \theta]$
44	6	2	$\rho^2 (15 - 140 \rho^2 + 420 \rho^4 - 504 \rho^6 + 210 \rho^8) \text{Cos}[2 \theta]$
45	6	2	$\rho^2 (15 - 140 \rho^2 + 420 \rho^4 - 504 \rho^6 + 210 \rho^8) \text{Sin}[2 \theta]$

46	6	1	$\rho\,(-6+105\,\rho^2-560\,\rho^4+1260\,\rho^6-1260\,\rho^8+462\,\rho^{10})\,\mathrm{Cos}[\theta]$
47	6	1	$\rho\,(-6+105\,\rho^2-560\,\rho^4+1260\,\rho^6-1260\,\rho^8+462\,\rho^{10})\,\mathrm{Sin}[\theta]$
48	6	0	$1-42\,\rho^2+420\,\rho^4-1680\,\rho^6+3150\,\rho^8-2772\,\rho^{10}+924\,\rho^{12}$

2.1.2 Zernikes in Cartesian coordinates

```
TableForm[zernikeXyList, TableHeadings -> {{}, {"#", "n", "m", "Polynomial"}}]
```

#	n	m	Polynomial
0	0	0	1
1	1	1	x
2	1	1	y
3	1	0	$-1+2\,(x^2+y^2)$
4	2	2	x^2-y^2
5	2	2	$2\,x\,y$
6	2	1	$-2\,x+3\,x\,(x^2+y^2)$
7	2	1	$-2\,y+3\,y\,(x^2+y^2)$
8	2	0	$1-6\,(x^2+y^2)+6\,(x^2+y^2)^2$
9	3	3	$x^3-3\,x\,y^2$
10	3	3	$3\,x^2\,y-y^3$
11	3	2	$-3\,x^2+3\,y^2+4\,x^2\,(x^2+y^2)-4\,y^2\,(x^2+y^2)$
12	3	2	$-6\,x\,y+8\,x\,y\,(x^2+y^2)$
13	3	1	$3\,x-12\,x\,(x^2+y^2)+10\,x\,(x^2+y^2)^2$
14	3	1	$3\,y-12\,y\,(x^2+y^2)+10\,y\,(x^2+y^2)^2$
15	3	0	$-1+12\,(x^2+y^2)-30\,(x^2+y^2)^2+20\,(x^2+y^2)^3$
16	4	4	$x^4-6\,x^2\,y^2+y^4$
17	4	4	$4\,x^3\,y-4\,x\,y^3$
18	4	3	$-4\,x^3+12\,x\,y^2+5\,x^3\,(x^2+y^2)-15\,x\,y^2\,(x^2+y^2)$
19	4	3	$-12\,x^2\,y+4\,y^3+15\,x^2\,y\,(x^2+y^2)-5\,y^3\,(x^2+y^2)$
20	4	2	$6\,x^2-6\,y^2-20\,x^2\,(x^2+y^2)+20\,y^2\,(x^2+y^2)+15\,x^2\,(x^2+y^2)^2-15\,y^2\,(x^2+y^2)^2$
21	4	2	$12\,x\,y-40\,x\,y\,(x^2+y^2)+30\,x\,y\,(x^2+y^2)^2$
22	4	1	$-4\,x+30\,x\,(x^2+y^2)-60\,x\,(x^2+y^2)^2+35\,x\,(x^2+y^2)^3$
23	4	1	$-4\,y+30\,y\,(x^2+y^2)-60\,y\,(x^2+y^2)^2+35\,y\,(x^2+y^2)^3$
24	4	0	$1-20\,(x^2+y^2)+90\,(x^2+y^2)^2-140\,(x^2+y^2)^3+70\,(x^2+y^2)^4$
25	5	5	$x^5-10\,x^3\,y^2+5\,x\,y^4$
26	5	5	$5\,x^4\,y-10\,x^2\,y^3+y^5$
27	5	4	$-5\,x^4+30\,x^2\,y^2-5\,y^4+6\,x^4\,(x^2+y^2)-36\,x^2\,y^2\,(x^2+y^2)+6\,y^4\,(x^2+y^2)$
28	5	4	$-20\,x^3\,y+20\,x\,y^3+24\,x^3\,y\,(x^2+y^2)-24\,x\,y^3\,(x^2+y^2)$
29	5	3	$10\,x^3-30\,x\,y^2-30\,x^3\,(x^2+y^2)+90\,x\,y^2\,(x^2+y^2)+21\,x^3\,(x^2+y^2)^2-63\,x\,y^2\,(x^2+y^2)^2$
30	5	3	$30\,x^2\,y-10\,y^3-90\,x^2\,y\,(x^2+y^2)+30\,y^3\,(x^2+y^2)+63\,x^2\,y\,(x^2+y^2)^2-21\,y^3\,(x^2+y^2)^2$
31	5	2	$-10\,x^2+10\,y^2+60\,x^2\,(x^2+y^2)-60\,y^2\,(x^2+y^2)-105\,x^2\,(x^2+y^2)^2+105\,y^2\,(x^2+y^2)^2+56\,x^2\,(x^2+y^2)^3-56\,y^2\,(x^2+y^2)^3$
32	5	2	$-20\,x\,y+120\,x\,y\,(x^2+y^2)-210\,x\,y\,(x^2+y^2)^2+112\,x\,y\,(x^2+y^2)^3$
33	5	1	$5\,x-60\,x\,(x^2+y^2)+210\,x\,(x^2+y^2)^2-280\,x\,(x^2+y^2)^3+126\,x\,(x^2+y^2)^4$
34	5	1	$5\,y-60\,y\,(x^2+y^2)+210\,y\,(x^2+y^2)^2-280\,y\,(x^2+y^2)^3+126\,y\,(x^2+y^2)^4$
35	5	0	$-1+30\,(x^2+y^2)-210\,(x^2+y^2)^2+560\,(x^2+y^2)^3-630\,(x^2+y^2)^4+252\,(x^2+y^2)^5$
36	6	6	$x^6-15\,x^4\,y^2+15\,x^2\,y^4-y^6$
37	6	6	$6\,x^5\,y-20\,x^3\,y^3+6\,x\,y^5$
38	6	5	$-6\,x^5+60\,x^3\,y^2-30\,x\,y^4+7\,x^5\,(x^2+y^2)-70\,x^3\,y^2\,(x^2+y^2)+35\,x\,y^4\,(x^2+y^2)$
39	6	5	$-30\,x^4\,y+60\,x^2\,y^3-6\,y^5+35\,x^4\,y\,(x^2+y^2)-70\,x^2\,y^3\,(x^2+y^2)+7\,y^5\,(x^2+y^2)$
40	6	4	$15\,x^4-90\,x^2\,y^2+15\,y^4-42\,x^4\,(x^2+y^2)+252\,x^2\,y^2\,(x^2+y^2)-42\,y^4\,(x^2+y^2)+28\,x^4\,(x^2+y^2)^2-168\,x^2\,y^2\,(x^2+y^2)^2+28\,y^4\,(x^2+y^2)^2$

41	6	4	$60 x^3 y - 60 x y^3 - 168 x^3 y (x^2 + y^2) + 168 x y^3 (x^2 + y^2) + 112 x^3 y (x^2 + y^2)^2 - 112 x y^3 (x^2 + y^2)^2$
42	6	3	$-20 x^3 + 60 x y^2 + 105 x^3 (x^2 + y^2) - 315 x y^2 (x^2 + y^2) - 168 x^3 (x^2 + y^2)^2 + 504 x y^2 (x^2 + y^2)^2 + 84 x^3 (x^2 + y^2)^3 - 252 x y^2 (x^2 + y^2)^3$
43	6	3	$-60 x^2 y + 20 y^3 + 315 x^2 y (x^2 + y^2) - 105 y^3 (x^2 + y^2) - 504 x^2 y (x^2 + y^2)^2 + 168 y^3 (x^2 + y^2)^2 + 252 x^2 y (x^2 + y^2)^3 - 84 y^3 (x^2 + y^2)^3$
44	6	2	$15 x^2 - 15 y^2 - 140 x^2 (x^2 + y^2) + 140 y^2 (x^2 + y^2) + 420 x^2 (x^2 + y^2)^2 - 420 y^2 (x^2 + y^2)^2 - 504 x^2 (x^2 + y^2)^3 + 504 y^2 (x^2 + y^2)^3 + 210 x^2 (x^2 + y^2)^4 - 210 y^2 (x^2 + y^2)^4$
45	6	2	$30 x y - 280 x y (x^2 + y^2) + 840 x y (x^2 + y^2)^2 - 1008 x y (x^2 + y^2)^3 + 420 x y (x^2 + y^2)^4$
46	6	1	$-6 x + 105 x (x^2 + y^2) - 560 x (x^2 + y^2)^2 + 1260 x (x^2 + y^2)^3 - 1260 x (x^2 + y^2)^4 + 462 x (x^2 + y^2)^5$
47	6	1	$-6 y + 105 y (x^2 + y^2) - 560 y (x^2 + y^2)^2 + 1260 y (x^2 + y^2)^3 - 1260 y (x^2 + y^2)^4 + 462 y (x^2 + y^2)^5$
48	6	0	$1 - 42 (x^2 + y^2) + 420 (x^2 + y^2)^2 - 1680 (x^2 + y^2)^3 + 3150 (x^2 + y^2)^4 - 2772 (x^2 + y^2)^5 + 924 (x^2 + y^2)^6$

2.2 OSC Zernikes

Much of the early work using Zernike polynomials in the computer analysis of interferograms was performed by John Loomis at the Optical Sciences Center, University of Arizona in the 1970s. In the OSC work Zernikes for n= 1 through 5 and the n=6, m=0 term were used. The n=m=0 term (piston term) was used in interferogram analysis, but it was not included in the numbering of the Zernikes. Thus, there were 36 Zernike terms, plus the piston term used.

3 Zernike Plots

A few sample plots are given in this section. More plots can be found at http://www.optics.arizona.edu/jcwyant/Zernikes/ZernikePolynomials.htm.

3.1 Density Plots

```
zernikeNumber = 8;

temp = zernikeXy[zernikeNumber];
DensityPlot[If[x^2 + y^2 ≤ 1, (Cos[2 π temp])^2, 1], {x, -1, 1}, {y, -1, 1},
  PlotLabel → "Zernike #" <> ToString[zernikeNumber], ColorFunction → GrayLevel, PlotPoints -> 150, Mesh -> False];
```

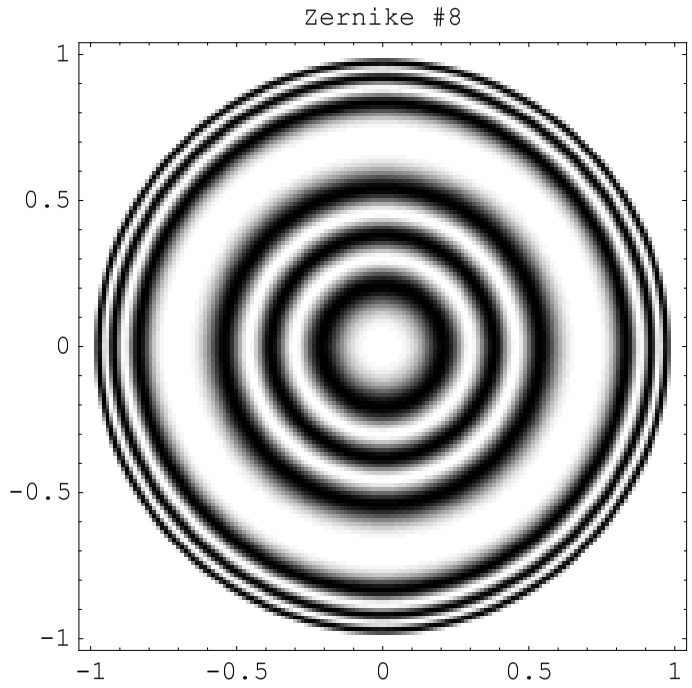

3.2 3D Plots

```
zernikeNumber = 8;

temp = zernikeXy[zernikeNumber]; Graphics3D[Plot3D[
  {If[x^2 + y^2 ≤ 1, temp, 1], If[x^2 + y^2 ≤ 1, Hue[temp, 1, 1], Hue[1, 1, 1]]}, {x, -1, 1}, {y, -1, 1}, PlotPoints → 40]];
```

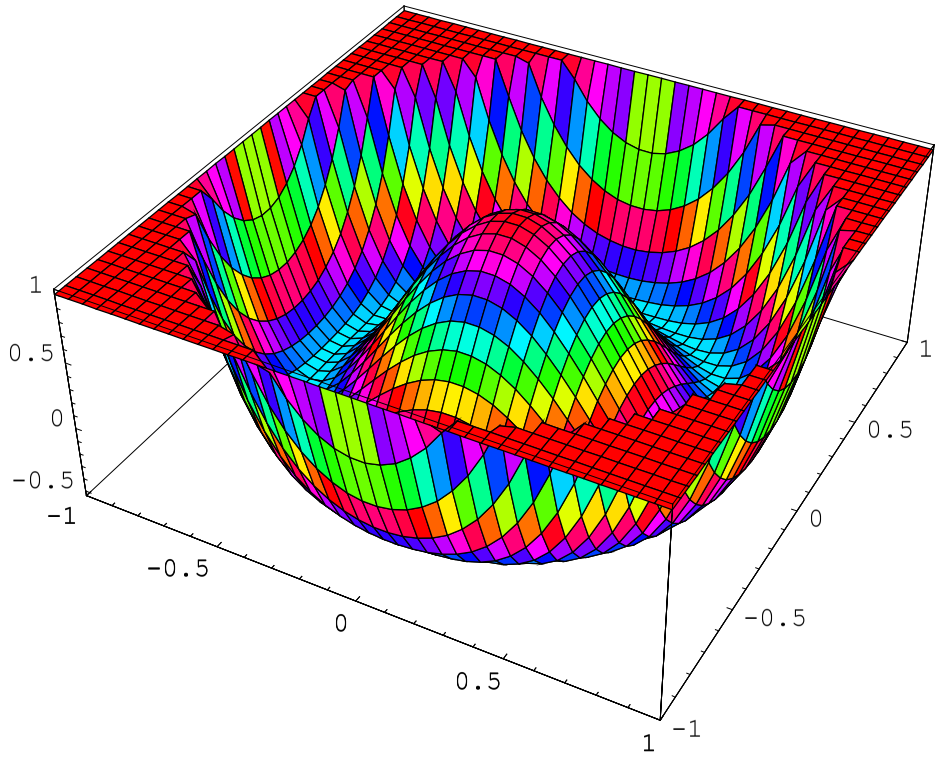

```
zernikeNumber = 8;

temp = zernikeXy[zernikeNumber];
Graphics3D[Plot3D[If[x^2 + y^2 ≤ 1, temp, 1], {x, -1, 1}, {y, -1, 1}, PlotPoints → 40,
    LightSources -> {{{1., 0., 1.}, RGBColor[1, 0, 0]},
     {{1., 1., 1.}, RGBColor[0, 1, 0]}, {{0., 1., 1.}, RGBColor[0, 0, 1]},
            {{-1., 0., -1.}, RGBColor[1, 0, 0]}, {{-1., -1., -1.}, RGBColor[0, 1, 0]},
     {{0., -1., -1.}, RGBColor[0, 0, 1]}}]];
```

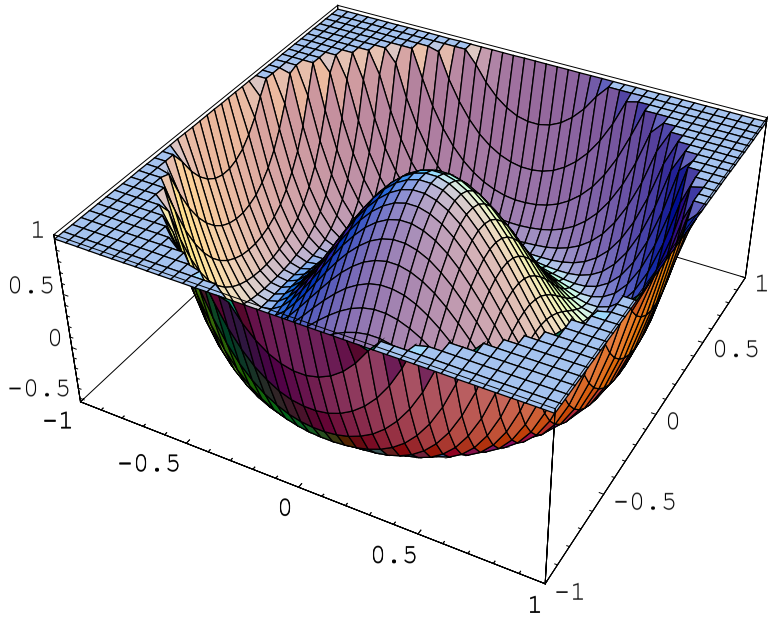

3.3 Cylindrical Plot 3D

```
zernikeNumber = 8;

temp = zernikePolar[zernikeNumber];
gr = CylindricalPlot3D[temp, {ρ, 0, 1}, {θ, 0, 2 π}, BoxRatios → {1, 1, 0.5}, Boxed → False, Axes → False];
```

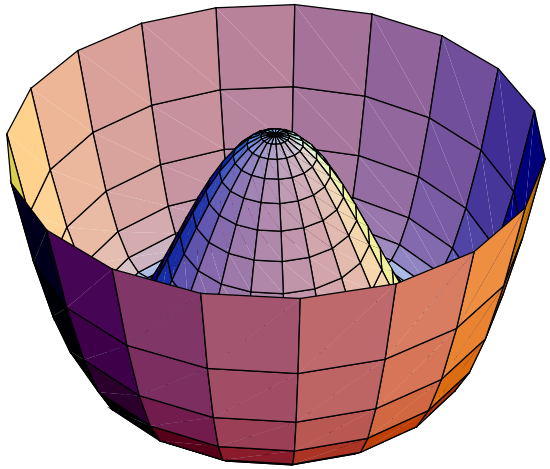

```
zernikeNumber = 5;

temp = zernikePolar[zernikeNumber];
gr = CylindricalPlot3D[{temp, Hue[temp]}, {ρ, 0, 1},
   {θ, 0, 2 π}, BoxRatios → {1, 1, 0.5}, Boxed → False, Axes → False, Lighting → False];
```

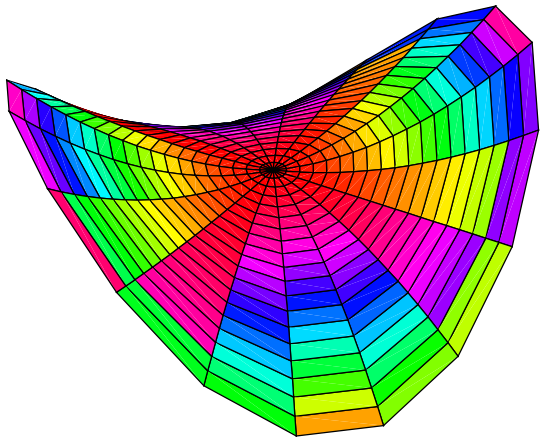

Can rotate without getting dark side

```
zernikeNumber = 5;

temp = zernikePolar[zernikeNumber];
gr = CylindricalPlot3D[temp, {ρ, 0, 1}, {θ, 0, 2 π}, BoxRatios → {1, 1, 0.5},
   Boxed → False, Axes → False, LightSources -> {{{1., 0., 1.}, RGBColor[1, 0, 0]},
     {{1., 1., 1.}, RGBColor[0, 1, 0]}, {{0., 1., 1.}, RGBColor[0, 0, 1]},
            {{-1., 0., -1.}, RGBColor[1, 0, 0]}, {{-1., -1., -1.}, RGBColor[0, 1, 0]},
     {{0., -1., -1.}, RGBColor[0, 0, 1]}}];
```

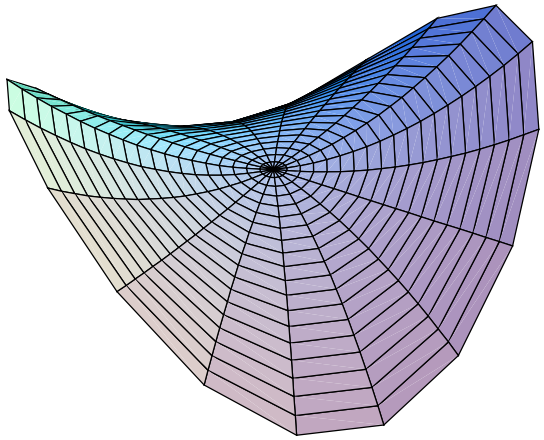

```
zernikeNumber = 16;

temp = zernikePolar[zernikeNumber];
gr = CylindricalPlot3D[temp, {ρ, 0, 1}, {θ, 0, 2 π}, BoxRatios → {1, 1, 0.5},
   Boxed → False, Axes → False, LightSources -> {{{1., 0., 1.}, RGBColor[1, 0, 0]},
     {{1., 1., 1.}, RGBColor[.5, 1, 0]}, {{0., 1., 1.}, RGBColor[1, 0, 0]},
           {{-1., 0., -1.}, RGBColor[1, 0, 0]}, {{-1., -1., -1.}, RGBColor[.5, 1, 0]},
     {{0., -1., -1.}, RGBColor[1, 0, 0]}}];
```

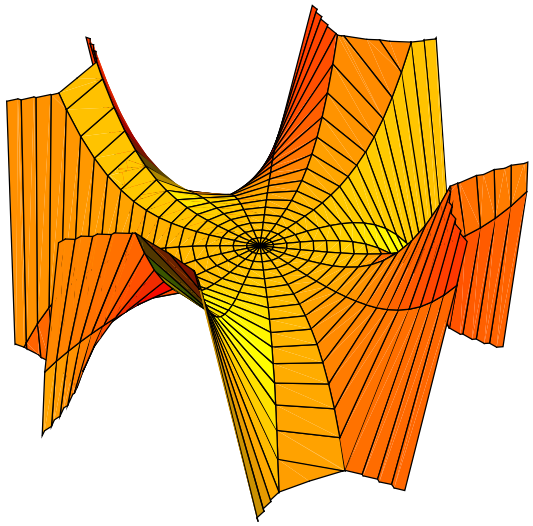

3.4 Surfaces of Revolution

```
zernikeNumber = 8;

temp = zernikePolar[zernikeNumber];
SurfaceOfRevolution[temp, {ρ, 0, 1}, PlotPoints → 40, BoxRatios → {1, 1, 0.5},
    LightSources -> {{{1., 0., 1.}, RGBColor[1, 0, 0]},
    {{1., 1., 1.}, RGBColor[.5, 1, 0]}, {{0., 1., 1.}, RGBColor[1, 0, 0]},
            {{-1., 0., -1.}, RGBColor[1, 0, 0]}, {{-1., -1., -1.}, RGBColor[.5, 1, 0]},
    {{0., -1., -1.}, RGBColor[1, 0, 0]}}];
```

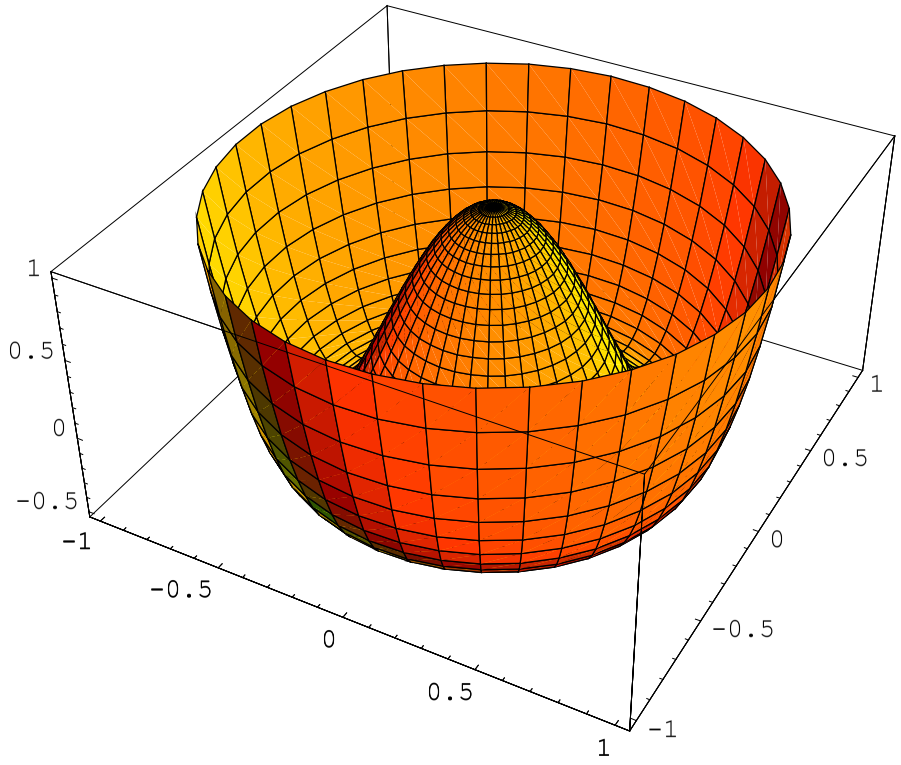

3.5 3D Shadow Plots

```
zernikeNumber = 5;

temp = zernikeXy[zernikeNumber];
ShadowPlot3D[temp, {x, -√(1 - y^2), √(1 - y^2)}, {y, -1, 1}, PlotPoints → 40];
```

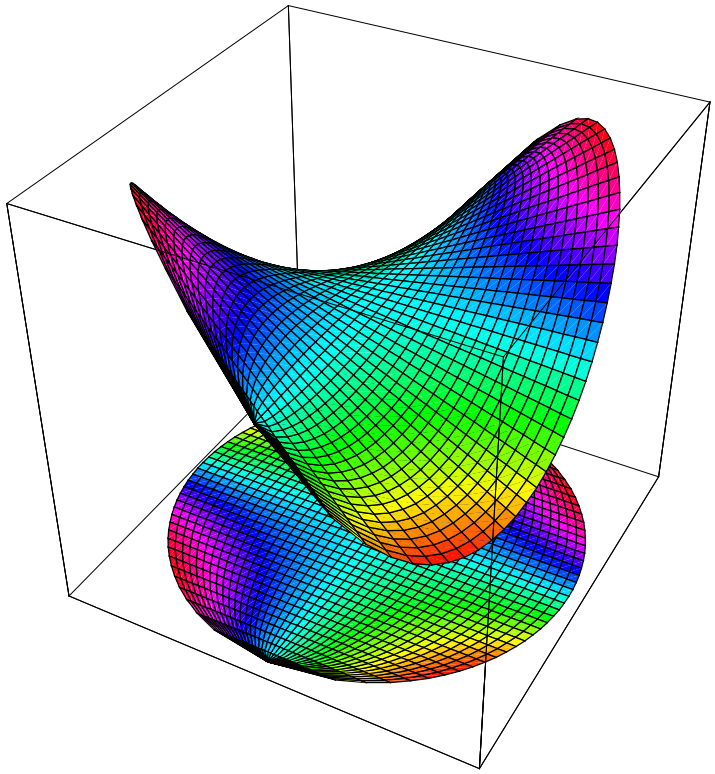

3.6 Animated Plots

3.6.1 Animated Density Plots

```
zernikeNumber = 3;

temp = zernikeXy[zernikeNumber];
MovieDensityPlot[If[x^2 + y^2 < 1, Sin[(temp + t y^2) π]^2, 1], {x, -1, 1}, {y, -1, 1},
  {t, -7, 4, 1}, PlotPoints → 100, Mesh -> False, FrameTicks -> None, Frame → False];
```

3.6.2 Animated 3D Shadow Plots

```
zernikeNumber = 5;

temp = zernikeXy[zernikeNumber];
g = ShadowPlot3D[temp, {x, -√(1 - y^2), √(1 - y^2)}, {y, -1, 1}, PlotPoints → 40, DisplayFunction → Identity];
SpinShow[ g, Frames -> 6,
  SpinRange -> {0 Degree, 360 Degree} ]
```

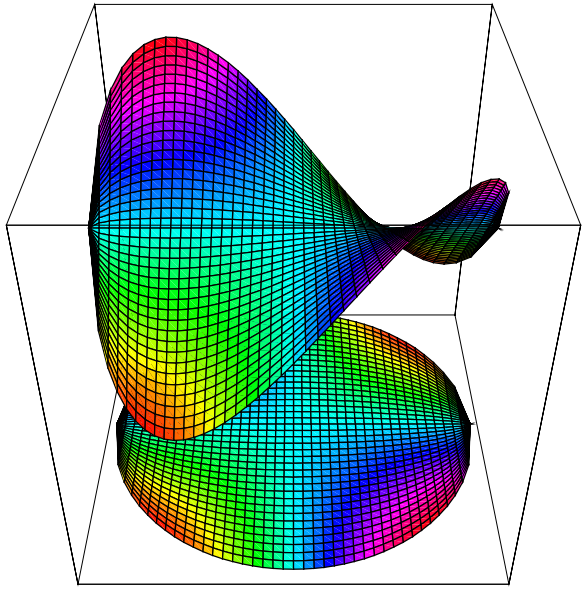

3.6.3 Animated Cylindrical Plot 3D

```
zernikeNumber = 5;

temp = zernikePolar[zernikeNumber];
gr = CylindricalPlot3D[{temp, Hue[Abs[temp + .4]]}, {ρ, 0, 1}, {θ, 0, 2 π},
   BoxRatios → {1, 1, 0.5}, Boxed → False, Axes → False, Lighting → False, DisplayFunction → Identity];
SpinShow[ gr, Frames -> 6,
  SpinRange -> {0 Degree, 360 Degree} ]
```

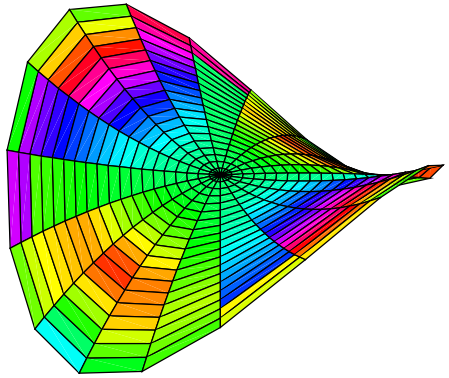

3.7 Two pictures stereograms

```
zernikeNumber = 8;

Print["Zernike #" <> ToString[zernikeNumber]];
ed = 0.6;
temp = zernikeXy[zernikeNumber];
f[x_, y_] := temp /; (x^2 + y^2) < 1
f[x_, y_] := 1 /; (x^2 + y^2) >= 1
plottemp = Plot3D[f[x, y], {x, -1, 1}, {y, -1, 1}, Boxed → False,
   Axes → False, DisplayFunction → Identity, PlotPoints → 50, Mesh -> False];
Show[GraphicsArray[{Show[plottemp, ViewPoint -> {-ed / 2, -2.4, 2.}, ViewCenter → 0.5 + {-ed / 2, 0, 0}],
    Show[plottemp, ViewPoint -> {ed / 2, -2.4, 2.}, ViewCenter → 0.5 + {ed / 2, 0, 0}]},
   GraphicsSpacing → 0], PlotLabel → zernikeXy[zernikeNumber]];
```

```
Zernike #8
```

$$1 - 6\,(x^2 + y^2) + 6\,(x^2 + y^2)^2$$

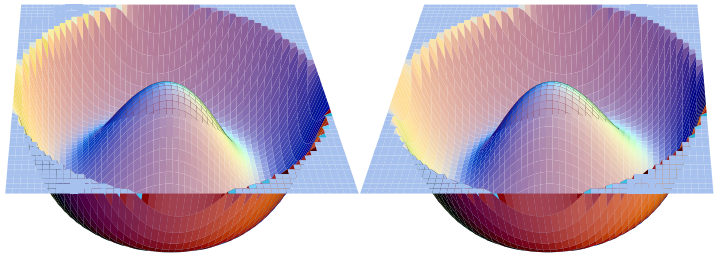

3.8 Single picture stereograms

```
zernikeNumber = 8;

temp = zernikeXy[zernikeNumber];
tempPlot = Plot3D[If[x^2 + y^2 < 1, temp, 1], {x, -1, 1}, {y, -1, 1}, PlotPoints → 400, DisplayFunction → Identity];
SIRDS[tempPlot];
Clear[temp, tempPlot];
```

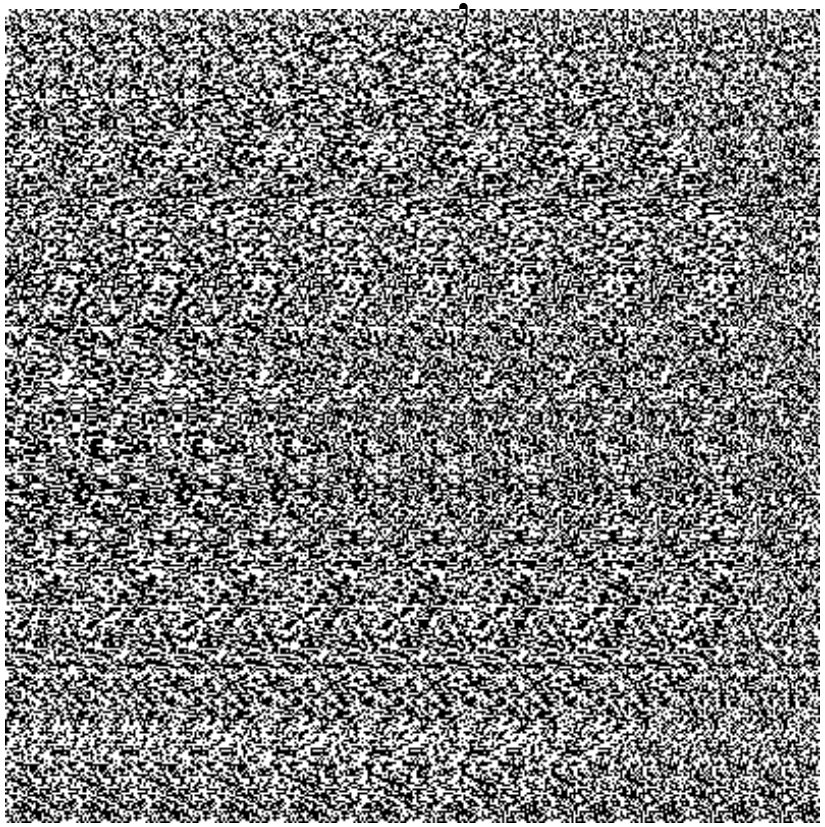

4 Relationship between Zernike polynomials and third-order aberrations

4.1 Wavefront aberrations

The third-order wavefront aberrations can be written as shown in the table below. Because there is no field dependence in these terms they are not true Seidel aberrations. Wavefront measurement using an interferometer only provides data at a single field point. This causes field curvature to look like focus and distortion to look like tilt. Therefore, a number of field points must be measured to determine the Seidel aberrations.

```
thirdOrderAberration = {{"piston", w00}, {"tilt", w11 ρ Cos[θ - αTilt]}, {"focus", w20 ρ^2},
   {"astigmatism", w22 ρ^2 Cos[θ - αAst]^2}, {"coma", w31 ρ^3 Cos[θ - αComa]}, {"spherical", w40 ρ^4}};

TableForm[thirdOrderAberration]
```

piston	w_0
tilt	$\rho \cos[\theta - \alpha_{Tilt}]\, w_{11}$
focus	$\rho^2\, w_{20}$
astigmatism	$\rho^2 \cos[\theta - \alpha_{Ast}]^2\, w_{22}$
coma	$\rho^3 \cos[\theta - \alpha_{Coma}]\, w_{31}$
spherical	$\rho^4\, w_{40}$

4.2 Zernike terms

First-order wavefront properties and third-order wavefront aberration coefficients can be obtained from the Zernike polynomials. Let the coefficients of the first nine zernikes be given by

```
zernikeCoefficient = {z0, z1, z2, z3, z4, z5, z6, z7, z8};
```

The coefficients can be multiplied times the Zernike polynomials to give the wavefront aberration.

```
wavefrontAberrationList = Table[zernikeCoefficient zernikePolarList[[Range[1, 9], 4]]];
```

We will now express the wavefront aberrations and the corresponding Zernike terms in a table

4.3 Table of Zernikes and aberrations

```
wavefrontAberrationLabels = {"piston", "x-tilt", "y-tilt", "focus", "astigmatism at 0 degrees & focus",
   "astigmatism at 45 degrees & focus", "coma and x-tilt", "coma and y-tilt", "spherical & focus"};

Do[
 {tableData[i, 1] = wavefrontAberrationLabels[[i]], tableData[i, 2] = wavefrontAberrationList[[i]]}, {i, 1, 9}]

TableForm[Array[tableData, {9, 2}], TableHeadings → {{}, {"Aberration", "Zernike Term"}}]
```

Aberration	Zernike Term
piston	z_0
x-tilt	$\rho \cos[\theta]\, z_1$
y-tilt	$\rho \sin[\theta]\, z_2$
focus	$(-1 + 2\rho^2)\, z_3$
astigmatism at 0 degrees & focus	$\rho^2 \cos[2\theta]\, z_4$
astigmatism at 45 degrees & focus	$\rho^2 \sin[2\theta]\, z_5$
coma and x-tilt	$\rho\, (-2 + 3\rho^2) \cos[\theta]\, z_6$
coma and y-tilt	$\rho\, (-2 + 3\rho^2) \sin[\theta]\, z_7$
spherical & focus	$(1 - 6\rho^2 + 6\rho^4)\, z_8$

The Zernike expansion above can be rewritten grouping like terms and equating them with the wavefront aberration coefficients.

```
wavefrontAberration = Collect[Sum[wavefrontAberrationList[[i]], {i, 9}], ρ]
```

$$z_0 - z_3 + \rho\,(\cos[\theta]\, z_1 + \sin[\theta]\, z_2 - 2\cos[\theta]\, z_6 - 2\sin[\theta]\, z_7) + \rho^3\,(3\cos[\theta]\, z_6 + 3\sin[\theta]\, z_7) + \rho^2\,(2 z_3 + \cos[2\theta]\, z_4 + \sin[2\theta]\, z_5 - 6 z_8) + z_8 + 6\rho^4 z_8$$

```
piston = Select[wavefrontAberration, FreeQ[#, ρ] &];

tilt = Collect[Select[wavefrontAberration, MemberQ[#, ρ ] &], {ρ, Cos[θ], Sin[θ]}];

focusPlusAstigmatism = Select[wavefrontAberration, MemberQ[#, ρ^2 ] &];
```

```
coma = Select[wavefrontAberration, MemberQ[#, ρ^3 ] &];

spherical = Select[wavefrontAberration, MemberQ[#, ρ^4 ] &];
```

4.4 zernikeThirdOrderAberration Table

```
zernikeThirdOrderAberration = {{"piston", piston}, {"tilt", tilt},
   {"focus + astigmatism", focusPlusAstigmatism}, {"coma", coma}, {"spherical", spherical}};

TableForm[zernikeThirdOrderAberration]
```

piston	$z_0 - z_3 + z_8$
tilt	$\rho\ (\text{Cos}[\theta]\ (z_1 - 2\ z_6) + \text{Sin}[\theta]\ (z_2 - 2\ z_7))$
focus + astigmatism	$\rho^2\ (2\ z_3 + \text{Cos}[2\ \theta]\ z_4 + \text{Sin}[2\ \theta]\ z_5 - 6\ z_8)$
coma	$\rho^3\ (3\ \text{Cos}[\theta]\ z_6 + 3\ \text{Sin}[\theta]\ z_7)$
spherical	$6\ \rho^4\ z_8$

These tilt, coma, and focus plus astigmatism terms can be rearranged using the equation
$a\ \text{Cos}[\theta] + b\ \text{Sin}[\theta] = \sqrt{a^2 + b^2}\ \text{Cos}[\theta - \text{ArcTan}[a, b]]$.

4.4.1 Tilt

```
tilt = tilt /. a_ Cos[θ_] + b_ Sin[θ] → Sqrt[a^2 + b^2] Cos[θ - ArcTan[a, b]]
```

$$\rho\ \text{Cos}[\theta - \text{ArcTan}[z_1 - 2\ z_6,\ z_2 - 2\ z_7]]\ \sqrt{(z_1 - 2\ z_6)^2 + (z_2 - 2\ z_7)^2}$$

4.4.2 Coma

```
coma = Simplify[coma /. a_ Cos[θ_] + b_ Sin[θ] → Sqrt[a^2 + b^2] Cos[θ - ArcTan[a, b]]]
```

$$3\,\rho^3\,\text{Cos}[\theta - \text{ArcTan}[z_6, z_7]]\,\sqrt{z_6^2 + z_7^2}$$

4.4.3 Focus

This is a little harder because we must separate the focus and the astigmatism.

```
focusPlusAstigmatism
```

$$\rho^2\,(2\,z_3 + \text{Cos}[2\,\theta]\,z_4 + \text{Sin}[2\,\theta]\,z_5 - 6\,z_8)$$

```
focusPlusAstigmatism = focusPlusAstigmatism /. a_ Cos[θ_] + b_ Sin[θ_] → Sqrt[a^2 + b^2] Cos[θ - ArcTan[a, b]]
```

$$\rho^2\left(2\,z_3 + \text{Cos}[2\,\theta - \text{ArcTan}[z_4, z_5]]\,\sqrt{z_4^2 + z_5^2} - 6\,z_8\right)$$

But $\text{Cos}[2\,\phi] = 2\,\text{Cos}[\phi]^2 - 1$

```
focusPlusAstigmatism = focusPlusAstigmatism /. a_ Cos[2 θ_ - θ1_] → 2 a Cos[θ - θ1/2]^2 - a
```

$$\rho^2\left(2\,z_3 - \sqrt{z_4^2 + z_5^2} + 2\,\text{Cos}\left[\theta - \frac{1}{2}\,\text{ArcTan}[z_4, z_5]\right]^2\sqrt{z_4^2 + z_5^2} - 6\,z_8\right)$$

Let

```
focusMinus = ρ^2 (2 z3 - Sqrt[z4^2 + z5^2] - 6 z8);
```

Sometimes $2\left(\sqrt{z_4{}^2 + z_5{}^2}\right)\rho^2$ is added to the focus term to make its absolute value smaller and then $2\left(\sqrt{z_4{}^2 + z_5{}^2}\right)\rho^2$ must be subtracted from the astigmatism term. This gives a focus term equal to

```
focusPlus = ρ^2 (2 z3 + Sqrt[z4^2 + z5^2] - 6 z8);
```

For the focus we select the sign that will give the smallest magnitude.

```
focus = If[Abs[focusPlus / ρ^2] < Abs[focusMinus / ρ^2], focusPlus, focusMinus];
```

It should be noted that most commercial interferogram analysis programs do not try to minimize the absolute valus of the focus term so the focus is set equal to focusMinus.

4.4.4 Astigmatism

```
astigmatismMinus = focusPlusAstigmatism - focusMinus // Simplify
```

$$2\,\rho^2\,\text{Cos}\left[\theta - \frac{1}{2}\,\text{ArcTan}[z_4,\,z_5]\right]^2\,\sqrt{z_4^2 + z_5^2}$$

```
astigmatismPlus = focusPlusAstigmatism - focusPlus // Simplify
```

$$-2\,\rho^2\,\text{Sin}\left[\theta - \frac{1}{2}\,\text{ArcTan}[z_4,\,z_5]\right]^2\,\sqrt{z_4^2 + z_5^2}$$

Since $\text{Sin}[\theta - \frac{1}{2}\,\text{ArcTan}[z_4,\,z_5]]^2$ is equal to $\text{Cos}[\theta - (\frac{1}{2}\,\text{ArcTan}[z_4,\,z_5] + \frac{\pi}{2})]^2$, astigmatismPlus could be written as

```
astigmatismPlus = -2 ρ^2 Cos[θ - (1/2 ArcTan[z4, z5] + π/2)]^2 Sqrt[z4^2 + z5^2];
```

Note that in going from astigmatismMinus to astigmatismPlus not only are we changing the sign of the astigmatism term, but we are also rotating it 90°.
We need to select the sign opposite that chosen in the focus term.

```
astigmatism = If[Abs[focusPlus / ρ^2] < Abs[focusMinus / ρ^2], astigmatismPlus, astigmatismMinus];
```

Again it should be noted that most commercial interferogram analysis programs do not try to minimize the absolute valus of the focus term and the astigmatism is given by astigmatismMinus.

4.4.5 Spherical

```
spherical = 6 z8 ρ^4
```

4.5 seidelAberrationList Table

We can summarize the results as follows.

```
seidelAberrationList := {{"piston", piston}, {"tilt", tilt},
   {"focus", focus}, {"astigmatism", astigmatism}, {"coma", coma}, {"spherical", spherical}};
```

```
seidelAberrationList // TableForm
```

piston	$z_0 - z_3 + z_8$
tilt	$\rho \text{Cos}[\theta - \text{ArcTan}[z_1 - 2 z_6, z_2 - 2 z_7]] \sqrt{(z_1 - 2 z_6)^2 + (z_2 - 2 z_7)^2}$
focus	$\text{If}\left[\text{Abs}\left[2 z_3 + \sqrt{z_4^2 + z_5^2} - 6 z_8\right] < \text{Abs}\left[2 z_3 - \sqrt{z_4^2 + z_5^2} - 6 z_8\right], \text{focusPlus}, \text{focusMinus}\right]$
astigmatism	$\text{If}\left[\text{Abs}\left[2 z_3 + \sqrt{z_4^2 + z_5^2} - 6 z_8\right] < \text{Abs}\left[2 z_3 - \sqrt{z_4^2 + z_5^2} - 6 z_8\right], \text{astigmatismPlus}, \text{astigmatismMinus}\right]$
coma	$3 \rho^3 \text{Cos}[\theta - \text{ArcTan}[z_6, z_7]] \sqrt{z_6^2 + z_7^2}$
spherical	$6 \rho^4 z_8$

4.5.1 Typical Results

```
seidelAberrationList //. {z0 → 0, z1 → 1, z2 → 1, z3 → 1, z4 → 3, z5 → 1, z6 → 1, z7 → 1, z8 → 2} // TableForm
```

piston	1
tilt	$\sqrt{2}\ \rho \text{Cos}[\frac{3\pi}{4} + \theta]$
focus	$\left(-10 + \sqrt{10}\right) \rho^2$
astigmatism	$-2 \sqrt{10}\ \rho^2 \text{Sin}[\theta - \frac{1}{2} \text{ArcTan}[\frac{1}{3}]]^2$
coma	$3 \sqrt{2}\ \rho^3 \text{Cos}[\frac{\pi}{4} - \theta]$
spherical	$12 \rho^4$

```
seidelAberration = Apply[Plus, seidelAberrationList][[2]];
```

```
seidelAberration //. {z0 → 0, z1 → 1, z2 → 1, z3 → 1, z4 → 3, z5 → 1, z6 → 1, z7 → 1, z8 → 2}
```

$$1 + \left(-10 + \sqrt{10}\right) \rho^2 + 12 \rho^4 + 3 \sqrt{2}\ \rho^3 \text{Cos}\left[\frac{\pi}{4} - \theta\right] + \sqrt{2}\ \rho \text{Cos}\left[\frac{3\pi}{4} + \theta\right] - 2 \sqrt{10}\ \rho^2 \text{Sin}\left[\theta - \frac{1}{2} \text{ArcTan}\left[\frac{1}{3}\right]\right]^2$$

5 RMS Wavefront Aberration

If the wavefront aberration can be described in terms of third-order aberrations, it is convenient to specify the wavefront aberration by stating the number of waves of each of the third-order aberrations present. This method for specifying a wavefront is of particular convenience if only a single third-order aberration is present. For more complicated wavefront aberrations it is convenient to state the peak-to-valley (P-V) sometimes called peak-to-peak (P-P) wavefront aberration. This is simply the maximum departure of the actual wavefront from the desired wavefront in both positive and negative directions. For example, if the maximum departure in the positive direction is +0.2 waves and the maximum departure in the negative direction is -0.1 waves, then the P-V wavefront error is 0.3 waves.

While using P-V to specify wavefront error is convenient and simple, it can be misleading. Stating P-V is simply stating the maximum wavefront error, and it is telling nothing about the area over which this error is occurring. An optical system having a large P-V error may actually perform better than a system having a small P-V error. It is generally more meaningful to specify wavefront quality using the rms wavefront error.

The next equation defines the rms wavefront error σ for a circular pupil, as well as the variance σ^2. $\Delta w(\rho, \theta)$ is measured relative to the best fit spherical wave, and it generally has the units of waves. Δw is the mean wavefront OPD.

$$\text{average}[\Delta w\_] := \frac{1}{\pi}\int_0^{2\pi}\int_0^1 \Delta w\, \rho\, d\rho\, d\theta;$$

$$\text{standardDeviation}[\Delta w\_] := \sqrt{\frac{1}{\pi}\int_0^{2\pi}\int_0^1 (\Delta w - \text{average}[\Delta w])^2\, \rho\, d\rho\, d\theta}$$

As an example we will calculate the relationship between σ and the mean wavefront aberrations for the third-order aberrations of a circular pupil.

$$\begin{aligned}
\text{meanRmsList} = \{&\{\text{"Defocus"}, \text{"}w_{20}\rho^2\text{"}, w_{20}\,\text{average}[\rho^2], w_{20}\,\text{N}[\text{standardDeviation}[\rho^2], 3]\},\\
&\{\text{"Spherical"}, \text{"}w_{40}\rho^4\text{"}, w_{40}\,\text{average}[\rho^4], w_{40}\,\text{N}[\text{standardDeviation}[\rho^4], 3]\},\\
&\{\text{"Spherical \& Defocus"}, \text{"}w_{40}\,(\rho^4-\rho^2)\text{"}, w_{40}\,\text{average}[(\rho^4-\rho^2)], w_{20}\,\text{N}[\text{standardDeviation}[(\rho^4-\rho^2)], 3]\},\\
&\{\text{"Astigmatism"}, \text{"}w_{22}\,\rho^2\ \text{Cos}[\theta]^2\text{"}, w_{22}\,\text{average}[\rho^2\,\text{Cos}[\theta]^2], w_{22}\,\text{N}[\text{standardDeviation}[\rho^2\,\text{Cos}[\theta]^2], 3]\},\\
&\Big\{\text{"Astigmatism \& Defocus"}, \text{"}w_{22}\rho^2\ (\text{Cos}[\theta]^2-\tfrac{1}{2})\text{"},\\
&\ w_{22}\,\text{average}\Big[\rho^2\left(\text{Cos}[\theta]^2-\frac{1}{2}\right)\Big], w_{22}\,\text{N}\Big[\text{standardDeviation}\Big[\rho^2\left(\text{Cos}[\theta]^2-\frac{1}{2}\right)\Big], 3\Big]\Big\},\\
&\{\text{"Coma"}, \text{"}w_{31}\rho^3\ \text{Cos}[\theta]\text{"}, w_{31}\,\text{average}[\rho^3\,\text{Cos}[\theta]], w_{31}\,\text{N}[\text{standardDeviation}[\rho^3\,\text{Cos}[\theta]], 3]\}, \Big\{\text{"Coma \& Tilt"},\\
&\ \text{"}w_{31}\,(\rho^3-\tfrac{2}{3}\rho)\ \text{Cos}[\theta]\text{"}, w_{31}\,\text{average}\Big[\left(\rho^3-\frac{2}{3}\rho\right)\text{Cos}[\theta]\Big], w_{31}\,\text{N}\Big[\text{standardDeviation}\Big[\left(\rho^3-\frac{2}{3}\rho\right)\text{Cos}[\theta]\Big], 3\Big]\Big\}\};
\end{aligned}$$

```
TableForm[meanRmsList, TableHeadings -> {{}, {"Aberration", "Δw", "$\overline{\Delta w}$", "RMS"}}]
```

Aberration	Δw	$\overline{\Delta w}$	RMS
Defocus	$w_{20}\,\rho^2$	$\frac{w_{20}}{2}$	$0.288675\,w_{20}$
Spherical	$w_{40}\,\rho^4$	$\frac{w_{40}}{3}$	$0.298142\,w_{40}$
Spherical & Defocus	$w_{40}\,(\rho^4-\rho^2)$	$-\frac{w_{40}}{6}$	$0.0745356\,w_{20}$
Astigmatism	$w_{22}\,\rho^2\,\text{Cos}[\theta]^2$	$\frac{w_{22}}{4}$	$0.25\,w_{22}$
Astigmatism & Defocus	$w_{22}\,\rho^2\,(\text{Cos}[\theta]^2-\frac{1}{2})$	0	$0.204124\,w_{22}$
Coma	$w_{31}\,\rho^3\,\text{Cos}[\theta]$	0	$0.353553\,w_{31}$
Coma & Tilt	$w_{31}\,(\rho^3-\frac{2}{3}\rho)\,\text{Cos}[\theta]$	0	$0.117851\,w_{31}$

If the wavefront aberration can be expressed in terms of Zernike polynomials, the wavefront variance can be calculated in a simple form by using the orthogonality relations of the Zernike polynomials. The final result for the entire unit circle is

$$\sigma = \sqrt{\sum_{n=1}^{nmax}\left(\frac{a[n]^2}{2n+1} + \frac{1}{2}\sum_{m=1}^{n}\frac{b[n,m]^2 + c[n,m]^2}{2n+1-m}\right)};$$

The following table gives the relationship between σ and the Zernike polynomials if the Zernike coefficients are unity.

```
zernikeRms = Table[If[zernikePolarList[[i, 3]] == 0, 1/Sqrt[2 zernikePolarList[[i, 2]] + 1],
    1/Sqrt[2 (2 zernikePolarList[[i, 2]] + 1 - zernikePolarList[[i, 3]])]], {i, Length[zernikePolarList]}];

zernikePolarRmsList = Transpose[Insert[Transpose[zernikePolarList], zernikeRms, 4]];

TableForm[zernikePolarRmsList, TableHeadings -> {{}, {"#", "n", "m", "RMS", "Polynomial"}}]
```

#	n	m	RMS	Polynomial
0	0	0	1	1
1	1	1	$\frac{1}{2}$	$\rho\,\text{Cos}[\theta]$
2	1	1	$\frac{1}{2}$	$\rho\,\text{Sin}[\theta]$
3	1	0	$\frac{1}{\sqrt{3}}$	$-1+2\,\rho^2$

4	2	2	$\frac{1}{\sqrt{6}}$	$\rho^2 \text{Cos}[2\theta]$
5	2	2	$\frac{1}{\sqrt{6}}$	$\rho^2 \text{Sin}[2\theta]$
6	2	1	$\frac{1}{2\sqrt{2}}$	$\rho\,(-2+3\rho^2)\,\text{Cos}[\theta]$
7	2	1	$\frac{1}{2\sqrt{2}}$	$\rho\,(-2+3\rho^2)\,\text{Sin}[\theta]$
8	2	0	$\frac{1}{\sqrt{5}}$	$1-6\rho^2+6\rho^4$
9	3	3	$\frac{1}{2\sqrt{2}}$	$\rho^3 \text{Cos}[3\theta]$
10	3	3	$\frac{1}{2\sqrt{2}}$	$\rho^3 \text{Sin}[3\theta]$
11	3	2	$\frac{1}{\sqrt{10}}$	$\rho^2\,(-3+4\rho^2)\,\text{Cos}[2\theta]$
12	3	2	$\frac{1}{\sqrt{10}}$	$\rho^2\,(-3+4\rho^2)\,\text{Sin}[2\theta]$
13	3	1	$\frac{1}{2\sqrt{3}}$	$\rho\,(3-12\rho^2+10\rho^4)\,\text{Cos}[\theta]$
14	3	1	$\frac{1}{2\sqrt{3}}$	$\rho\,(3-12\rho^2+10\rho^4)\,\text{Sin}[\theta]$
15	3	0	$\frac{1}{\sqrt{7}}$	$-1+12\rho^2-30\rho^4+20\rho^6$
16	4	4	$\frac{1}{\sqrt{10}}$	$\rho^4 \text{Cos}[4\theta]$
17	4	4	$\frac{1}{\sqrt{10}}$	$\rho^4 \text{Sin}[4\theta]$
18	4	3	$\frac{1}{2\sqrt{3}}$	$\rho^3\,(-4+5\rho^2)\,\text{Cos}[3\theta]$
19	4	3	$\frac{1}{2\sqrt{3}}$	$\rho^3\,(-4+5\rho^2)\,\text{Sin}[3\theta]$
20	4	2	$\frac{1}{\sqrt{14}}$	$\rho^2\,(6-20\rho^2+15\rho^4)\,\text{Cos}[2\theta]$
21	4	2	$\frac{1}{\sqrt{14}}$	$\rho^2\,(6-20\rho^2+15\rho^4)\,\text{Sin}[2\theta]$
22	4	1	$\frac{1}{4}$	$\rho\,(-4+30\rho^2-60\rho^4+35\rho^6)\,\text{Cos}[\theta]$
23	4	1	$\frac{1}{4}$	$\rho\,(-4+30\rho^2-60\rho^4+35\rho^6)\,\text{Sin}[\theta]$
24	4	0	$\frac{1}{3}$	$1-20\rho^2+90\rho^4-140\rho^6+70\rho^8$
25	5	5	$\frac{1}{2\sqrt{3}}$	$\rho^5 \text{Cos}[5\theta]$
26	5	5	$\frac{1}{2\sqrt{3}}$	$\rho^5 \text{Sin}[5\theta]$
27	5	4	$\frac{1}{\sqrt{14}}$	$\rho^4\,(-5+6\rho^2)\,\text{Cos}[4\theta]$
28	5	4	$\frac{1}{\sqrt{14}}$	$\rho^4\,(-5+6\rho^2)\,\text{Sin}[4\theta]$
29	5	3	$\frac{1}{4}$	$\rho^3\,(10-30\rho^2+21\rho^4)\,\text{Cos}[3\theta]$
30	5	3	$\frac{1}{4}$	$\rho^3\,(10-30\rho^2+21\rho^4)\,\text{Sin}[3\theta]$

31	5	2	$\frac{1}{3\sqrt{2}}$	$\rho^2 (-10 + 60 \rho^2 - 105 \rho^4 + 56 \rho^6) \mathrm{Cos}[2\theta]$
32	5	2	$\frac{1}{3\sqrt{2}}$	$\rho^2 (-10 + 60 \rho^2 - 105 \rho^4 + 56 \rho^6) \mathrm{Sin}[2\theta]$
33	5	1	$\frac{1}{2\sqrt{5}}$	$\rho (5 - 60 \rho^2 + 210 \rho^4 - 280 \rho^6 + 126 \rho^8) \mathrm{Cos}[\theta]$
34	5	1	$\frac{1}{2\sqrt{5}}$	$\rho (5 - 60 \rho^2 + 210 \rho^4 - 280 \rho^6 + 126 \rho^8) \mathrm{Sin}[\theta]$
35	5	0	$\frac{1}{\sqrt{11}}$	$-1 + 30 \rho^2 - 210 \rho^4 + 560 \rho^6 - 630 \rho^8 + 252 \rho^{10}$
36	6	6	$\frac{1}{\sqrt{14}}$	$\rho^6 \mathrm{Cos}[6\theta]$
37	6	6	$\frac{1}{\sqrt{14}}$	$\rho^6 \mathrm{Sin}[6\theta]$
38	6	5	$\frac{1}{4}$	$\rho^5 (-6 + 7 \rho^2) \mathrm{Cos}[5\theta]$
39	6	5	$\frac{1}{4}$	$\rho^5 (-6 + 7 \rho^2) \mathrm{Sin}[5\theta]$
40	6	4	$\frac{1}{3\sqrt{2}}$	$\rho^4 (15 - 42 \rho^2 + 28 \rho^4) \mathrm{Cos}[4\theta]$
41	6	4	$\frac{1}{3\sqrt{2}}$	$\rho^4 (15 - 42 \rho^2 + 28 \rho^4) \mathrm{Sin}[4\theta]$
42	6	3	$\frac{1}{2\sqrt{5}}$	$\rho^3 (-20 + 105 \rho^2 - 168 \rho^4 + 84 \rho^6) \mathrm{Cos}[3\theta]$
43	6	3	$\frac{1}{2\sqrt{5}}$	$\rho^3 (-20 + 105 \rho^2 - 168 \rho^4 + 84 \rho^6) \mathrm{Sin}[3\theta]$
44	6	2	$\frac{1}{\sqrt{22}}$	$\rho^2 (15 - 140 \rho^2 + 420 \rho^4 - 504 \rho^6 + 210 \rho^8) \mathrm{Cos}[2\theta]$
45	6	2	$\frac{1}{\sqrt{22}}$	$\rho^2 (15 - 140 \rho^2 + 420 \rho^4 - 504 \rho^6 + 210 \rho^8) \mathrm{Sin}[2\theta]$
46	6	1	$\frac{1}{2\sqrt{6}}$	$\rho (-6 + 105 \rho^2 - 560 \rho^4 + 1260 \rho^6 - 1260 \rho^8 + 462 \rho^{10}) \mathrm{Cos}[\theta]$
47	6	1	$\frac{1}{2\sqrt{6}}$	$\rho (-6 + 105 \rho^2 - 560 \rho^4 + 1260 \rho^6 - 1260 \rho^8 + 462 \rho^{10}) \mathrm{Sin}[\theta]$
48	6	0	$\frac{1}{\sqrt{13}}$	$1 - 42 \rho^2 + 420 \rho^4 - 1680 \rho^6 + 3150 \rho^8 - 2772 \rho^{10} + 924 \rho^{12}$

6 Strehl Ratio

While in the absence of aberrations, the intensity is a maximum at the Gaussian image point, if aberrations are present this will in general no longer be the case. The point of maximum intensity is called diffraction focus, and for small aberrations is obtained by finding the appropriate amount of tilt and defocus to be added to the wavefront so that the wavefront variance is a minimum.

The ratio of the intensity at the Gaussian image point (the origin of the reference sphere is the point of maximum intensity in the observation plane) in the presence of

aberration, divided by the intensity that would be obtained if no aberration were present, is called the Strehl ratio, the Strehl definition, or the Strehl intensity. The Strehl ratio is given by

$$\text{strehlRatio} := \frac{1}{\pi^2}\,\text{Abs}\left[\int_0^{2\pi}\int_0^{1} e^{i\,2\pi\,\Delta w[\rho,\theta]}\,\rho\,d\rho\,d\theta\right]^2$$

where $\Delta w[\rho, \theta]$ in units of waves. As an example

```
strehlRatio /. Δw[ρ, θ] → ρ^3 Cos[θ] // N
```

```
0.0790649
```

where $\Delta w[\rho, \theta]$ is in units of waves. The above equation may be expressed in the form

$$\text{strehlRatio} = \frac{1}{\pi^2}\,\text{Abs}\left[\int_0^{2\pi}\int_0^{1} (1 + 2\,i\,\pi\,\Delta w[\rho, \theta] - 2\,\pi^2\,\Delta w[\rho, \theta]^2 + \cdots)\,\rho\,d\rho\,d\theta\right]^2$$

If the aberrations are so small that the third-order and higher-order powers of $2\pi\Delta w$ can be neglected, the above equation may be written as

$$\begin{aligned}\text{strehlRatio} &\approx \text{Abs}\left[1 + i2\pi\,\overline{\Delta w} - \frac{1}{2}\,(2\pi)^2\,\overline{\Delta w^2}\right]^2\\ &\approx 1 - (2\pi)^2\left(\overline{\Delta w^2} - \overline{(\Delta w)^2}\right)\\ &\approx 1 - (2\pi\sigma)^2\end{aligned}$$

where σ is in units of waves.

Thus, when the aberrations are small, the Strehl ratio is independent of the nature of the aberration and is smaller than the ideal value of unity by an amount proportional to the variance of the wavefront deformation.

The above equation is valid for Strehl ratios as low as about 0.5. The Strehl ratio is always somewhat larger than would be predicted by the above approximation. A better approximation for most types of aberration is given by

```
strehlRatioApproximation := e^-(2 π σ)^2
```

$$\text{strehlRatioApproximation} \approx 1 - (2\pi\sigma)^2 + \frac{(2\pi\sigma)^4}{2} + \cdots$$

which is good for Strehl ratios as small as 0.1.

Once the normalized intensity at diffraction focus has been determined, the quality of the optical system may be ascertained using the Marechal criterion. The Marecha1 criterion states that a system is regarded as well corrected if the normalized intensity at diffraction focus is greater than or equal to 0.8, which corresponds to an rms wavefront error $<\lambda/14$.

As mentioned above, a useful feature of Zernike polynomials is that each term of the Zernikes minimizes the rms wavefront error to the order of that term. That is, each term is structured such that adding other aberrations of lower orders can only increase the rms error. Removing the first-order Zernike terms of tilt and defocus represents a shift in the focal point that maximizes the intensity at that point. Likewise, higher order terms have built into them the appropriate amount of tilt and defocus to minimize the rms wavefront error to that order. For example, looking at Zernike term #9 shows that for each wave of third-order spherical aberration present, one wave of defocus should be subtracted to minimize the rms wavefront error and find diffraction focus.

7 References

Born, M. and Wolf, E., (1959). Principles of Optics, pp. 464-466, 767-772. Pergamon press, New York.
Kim, C.-J. and Shannon, R.R. (1987). In "Applied Optics and Optical Engineering," Vol. X (R. Shannon and J. Wyant, eds.), pp. 193-221. Academic Press, New York.
Wyant, J. C. and Creath, K. (1992). In "Applied Optics and Optical Engineering," Vol. XI (R. Shannon and J. Wyant, eds.), pp. 28-39. Academic Press, New York.
Zernike, F. (1934), *Physica* **1**, 689.

8 Index

Wavefront Analysis Experiment F36 – Zernike gradients fit example

Version August 26, 2021

1. The python2 script f36_tests.py can be used as a template to fit your own measured Shack-Hartmann gradients with Zernike polynomial gradients.

2. Before modifying this script make a copy of the following directory: $HOME/F36examples/F36_task2_zernike_fit_script/cart_zernike/tests

3. Where ever you have placed this copy, go there and run the python script, e.g. python2 f36_tests.py

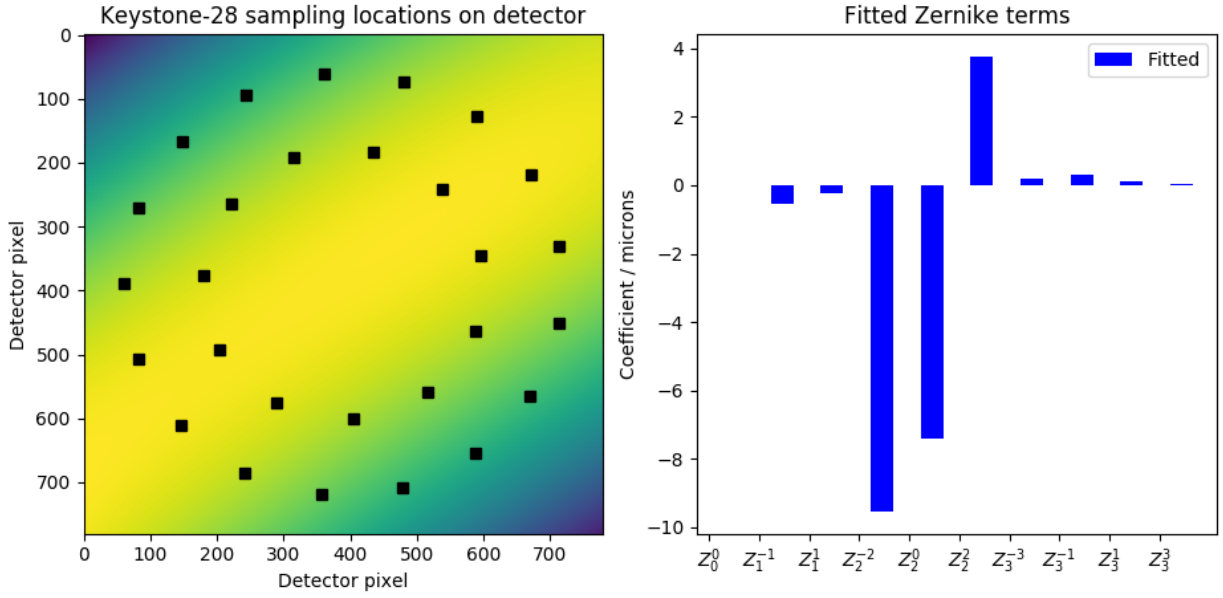

Figure 1 left: the black dots show the measured reference spots locations on the detector. The yellow/green/blue background shows the reconstructed wavefront from Zernike polynomials. The plot on the right, shows the reconstructed Zernike coefficients in units of microns.